UNIVERSITÉ DU QUÉBEC À CHICOUTIMI

MÉMOIRE PRÉSENTÉ À
L'UNIVERSITÉ DU QUÉBEC À CHICOUTIMI
COMME EXIGENCE PARTIELLE
DE LA MAÎTRISE EN INGÉNIERIE

PAR
SHAN LIN

A STUDY OF HOT TEARING IN WROUGHT ALUMINUM ALLOYS

26 février 1999

Bibliothèque
Paul-Émile-Boulet

UQAC
Université du Québec
à Chicoutimi

Mise en garde/Advice

Afin de rendre accessible au plus grand nombre le résultat des travaux de recherche menés par ses étudiants gradués et dans l'esprit des règles qui régissent le dépôt et la diffusion des mémoires et thèses produits dans cette Institution, **l'Université du Québec à Chicoutimi (UQAC)** est fière de rendre accessible une version complète et gratuite de cette œuvre.

Motivated by a desire to make the results of its graduate students' research accessible to all, and in accordance with the rules governing the acceptation and diffusion of dissertations and theses in this Institution, the **Université du Québec à Chicoutimi (UQAC)** is proud to make a complete version of this work available at no cost to the reader.

L'auteur conserve néanmoins la propriété du droit d'auteur qui protège ce mémoire ou cette thèse. Ni le mémoire ou la thèse ni des extraits substantiels de ceux-ci ne peuvent être imprimés ou autrement reproduits sans son autorisation.

The author retains ownership of the copyright of this dissertation or thesis. Neither the dissertation or thesis, nor substantial extracts from it, may be printed or otherwise reproduced without the author's permission.

RÉSUMÉ

La fissuration à chaud est un défaut important qui apparaît lors de la solidification des alliages. Alors qu'il existe beaucoup d'études visant à caractériser les alliages de fonderie selon leur susceptibilité à la fissuration à chaud, très peu de recherches ont été entreprises sur les alliages d'aluminium de corroyage. Puisque la fissuration à chaud se produit occasionnellement lors de la coulée de ces alliages, par le procédé D.C. (Direct Chill), une étude de ce phénomène devrait être faite pour cette série d'alliages.

Lors de la présente étude, des essais ont été faits, en utilisant la méthode C.R.C. (Constrained Rod Casting), afin de déterminer la susceptibilité à la fissuration à chaud des alliages de corroyage. Quatre alliages d'aluminium commerciaux et une série d'alliages binaires (Al-Si) furent utilisés. Il s'agit des alliages AA1050, AA3104, AA5182, AA6111, Al-0,5wt% Si, Al-1wt% Si, Al-1,5wt% Si, Al-2wt% Si et Al-3wt% Si. Afin d'évaluer leur susceptibilité à la fissuration à chaud, deux systèmes ont étés utilisés, soit H.T.S. (Hot Tearing Susceptibility) et F.C. (Footprint Chart). La méthode avec le moule C.R.C. fut efficace lors de l'évaluation des alliages d'aluminium. Il fut observé que la susceptibilité à la fissuration à chaud des alliages de corroyage et des alliages binaires avec silicium, pouvait se classer comme suit, en ordre croissant, pour les alliages de corroyage, AA1050, AA5182, AA3104, AA6111, et pour les alliages binaires, Al-0,5wt% Si, Al-1wt% Si, Al-1,5wt% Si, Al-2wt% Si, Al-3wt% Si.

Cet ordre, pour les alliages de corroyage, correspond bien aux observations typiques faites dans les centres de coulées industriels. Le classement des alliages binaires correspond aussi à quelques études antérieures faites en fonderie.

Une étude de la macrostructure et de la microstructure des échantillons coulés a permis de trouver une corrélation raisonnable entre les différentes structures et la susceptibilité à la fissuration à chaud. Le microscope métallographique, le microscope électronique à balayage, le spectromètre dispersif d'énergie, la dissolution de la matrice et la diffraction X, furent utilisés pour cette étude. Il fut observé que la zone de solidification des alliages, la quantité et la distribution de la phase eutectique, la grosseur de grain, la tension de surface, les phases secondaires, et les composés intermétalliques peuvent être des facteurs importants qui influencent la fissuration à chaud. Néanmoins, il fut constaté que le phénomène de fissuration à chaud ne pouvait être expliqués par un seul mécanisme pour tous les alliages observés.

L'affinage de grain a été fait pour les alliages de corroyage. La méthode d'interception linéaire fut utilisée pour déterminer la grosseur des grains. La méthode "C.R.C." et l'index "H.T.S." peuvent caractériser la sensibilité à la fissuration à chaud des alliages pour différents niveaux d'affinage de grain. L'analyse de la microstructure de l'alliage AA1050, avec ou sans affineur de grain, montre une relation directe entre la tendance à la fissuration à chaud et le degré d'affinage des grains.

Les résultats expérimentaux montrent aussi que l'affinage de grain peut réduire de beaucoup la susceptibilité à la fissuration à chaud des alliages à faible tendance comme les alliages AA1050 et AA5182. Néanmoins, l'affinage de grain n'est pas très efficace sur les alliages à tendance élevée à la fissuration à chaud, surtout pour l'alliage AA6111, même si les grains sont fins et de forme équiaxe. Ceci pourrait s'expliquer par le fait que ces derniers sont hautement alliés et possèdent déjà un grain fin.

L'analyse des surfaces des fissures fut faite pour les quatre alliages de corroyage. Les résultats pour les alliages AA1050, AA3104, et AA5182 démontrent clairement que le liquide eutectique restant, s'introduit dans la région de la fissure et recouvre les surfaces qui étaient séparées. Il fut observé que les surfaces des fissures de l'alliage AA6111, qui a la plus haute tendance à la fissuration à chaud, ne contiennent pas de phase eutectique. La composition des phases eutectiques des alliages est probablement le facteur le plus important lors de la fissuration à chaud des alliages. Il fut aussi

observé que l'alliage AA3104 est différent, seulement par le fait que l'on peut voir un relief de fracture ductile à l'endroit où les bouts de dendrites se rencontrent alors que l'alliage est dans un état "solide-liquide".

ABSTRACT

Hot tearing is an important defect that occurs during the solidification of aluminum alloys. While a number of studies exist in characterizing the hot tearing susceptibility of foundry alloys, very few investigations have been carried out on wrought aluminum alloys. Since hot tearing occasionally occurs during the DC casting process for the production of wrought aluminum alloys, it is important to conduct studies on hot tearing of this alloy group.

In this study, an investigation has been conducted using the Constrained Rod Casting (CRC) method to determine the susceptibility of hot tearing of wrought aluminum alloys. Four commercial aluminum alloys, AA1050, AA3104, AA5182 and AA6111, and a series of Al-Si binary alloys, Al-0.5wt%Si, Al-1.0wt%Si, Al-1.5%wtSi, Al-2.0%wtSi, and Al-3.0wt%Si have been examined. In order to measure the hot tearing susceptibilities of wrought aluminum alloys, two new rating systems, Hot Tearing Susceptibility (HTS) and Footprint Chart (FC), were evaluated. The CRC mold casting method has been found to be effective in evaluating and quantifying hot tearing susceptibility of aluminum alloys. It was found that the hot tearing susceptibility of the wrought aluminum alloys and the Al-Si binary alloys could be using the HTS ranked as:

AA1050 < AA5182 < AA3104 < AA6111, and

0.5wt%Si>1.0wt%Si>1.5wt%Si>2.0wt%Si>3.0wt%Si.

This ranking of these wrought aluminum alloys agrees well with observations in typical industrial casting practice. The ranking of the binary alloys is in agreement with foundry practice and previous investigations.

The CRC method and the HTS index are able to distinguish the hot-tearing sensitivity of alloys with and without grain refinement. The microstructural investigation of the grain-refined and

non-grain refined AA1050 alloy showed an inverse relationship between the degree of grain refinement and the hot tearing tendency. The experimental results also show that grain refinement dramatically reduced the hot tearing susceptibility of the alloys exhibiting lower hot tearing tendencies, i.e. AA1050, AA5182, and AA3104. However, grain refinement was not very effective in AA6111, which is an alloy exhibiting higher hot tearing tendency, despite the fact that the grains were fine and equiaxed. This may be explained partly by the fact that this alloy inherently yields a fine grain size.

Analyses of hot tear surfaces were conducted on the four wrought aluminum alloys. The results from AA1050, AA3104 and AA5182 alloys indicate that the eutectic liquid flows into a hot tear area and covered parts of the tear surfaces. It was observed that the hot tear surface of AA6111 alloy, which has the highest hot tearing tendency among the four wrought alloys, was only partially covered by the eutectic phase in certain areas. It was observed that the AA3104 alloy is uniquely different in that it exhibited ductile fracture at points where the dendrite tips met in the mushy state.

A study of macro-and microstructures of the castings was performed and a reasonable degree of correlation was found between the structures and hot tearing susceptibility. Optical Metallography (OM), Scanning Electron Microscopy (SEM), Energy Dispersive Spectrocopy (EDS), matrix dissolution and X-Ray Diffraction (XRD) were used in this investigation. It was found that freezing ranges of the alloys, grain size, second phases, and amount and distribution of eutectic phases may all be important factors to contributing hot-tearing susceptibility. However, it was seen that no single factor or mechanism could explain the hot tearing behavior in all of the alloys examined.

ACKNOWLEDGMENTS

I gratefully acknowledge the financial assistance of Alcan International Ltd., Natural Sciences and Engineering Research Council of Canada (NSERC), and of the Foundation of the University of Québec in Chicoutimi.

I would like to acknowledge my director Dr. Mihriban O. Pekguleryuz, director of the Alcan-UQAC Chair in Solidification and Metallurgy of Aluminium, and co-director Dr. Michel Bouchard, director of Department of Applied Science, for their excellent teaching and the entire supervision.

I would also like to acknowledge Mr. A.B. Innus and Mr. J. Langlais of Arvida Research and Development Center of Alcan International Ltd., for their active suport.

I would like to thank Mr. Celil Aliravci and Mr. Lin Zhang for their helpful advice and recommendations.

I would also like to thank Mr. Gilles Lemire for his excellent technical support in the laboratory.

Finally, I wish to acknowledge the encouragement and cooperation from a number of friends and colleagues, and my family.

TABLE OF CONTENTS

LIST OF FIGURES

LIST OF TABLES

CHAPTER I INTRODUCTION

1.1 A Description of Hot Tearing

Hot tearing is a casting defect that is caused when the tensile stresses developed during the solidification of a casting exceed the mechanical strength of the solid alloy. When a casting solidifies and contracts under conditions that hinder the free contraction of a part of the casting, hot tearing of the metal is likely to occur. Hot tearing is found in both ferrous and non-ferrous alloys; particularly, in steels and aluminum alloys. It is one of the most serious defects encountered in foundry practice.

Direct Chill (DC) casting is an important process in the production of aluminum ingots and billets. A major problem in this process is the occurrence of induced stresses and strains on the shell zone that can lead to defects during casting, especially, longitudinal hot tearing on the cast surface. If the longitudinal tears are severe enough, the ingots have to be scrapped. A typical hot-tear in DC cast ingots is shown in Figure 1.1, and an SEM photograph of a typical hot tear surface from a AA6111 casting is shown in Figure 1.2. They illustrate the characteristics of hot tearing on a macro and a micro-scale, respectively, and they show that hot tears are always inter-granular and exhibit free-dendritic features on tear surfaces.

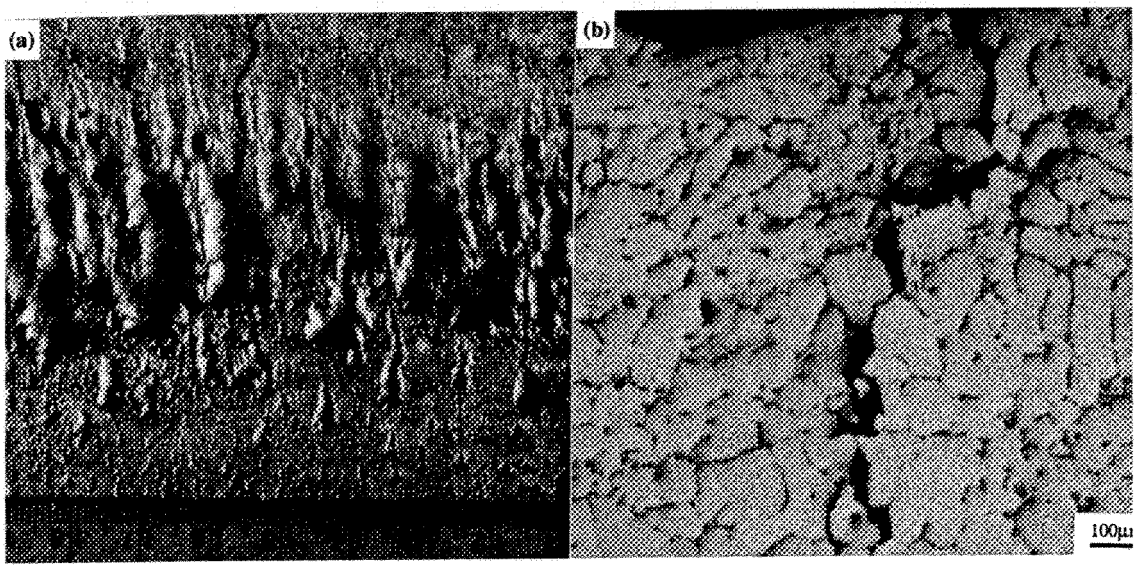

Figure 1.1. (a) Photograph of typical hot tears in DC cast ingot of AA6111 alloy; (b) Microstructure of DC cast ingot hot tears.

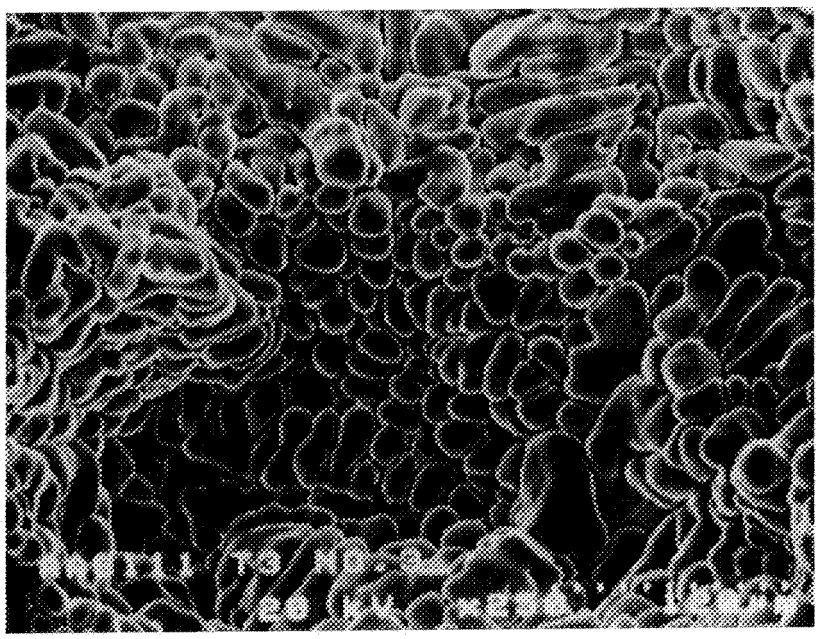

Figure 1.2. A SEM photo of a typical hot tear surface of cast AA6111 alloy showing the trips of free dendrite arms.

Over the decades, a great deal of research effort has been expended in an attempt to determine the principal variables that determine the development of hot tears. Hot tearing phenomenon, variously referred to as hot cracking, hot tearing, hot shortness, super solidus cracking, shrinkage brittleness, etc., has been the subject of previous studies [1-6]. However, it is important to note that hot tearing and hot cracking are different in their definitions; hot tearing is a fissure that develops during solidification when some liquid is still present, whereas hot cracking is a fracture occurring below the solidus temperature when the metal has completely solidified.

Hot tearing behavior has been empirically related to the freezing range of alloys and the related phase diagrams. The alloys with winder freezing range normally show low resistance to hot tearing, generally due to the in extended mushy ranges and its interaction with the geometry and the stresses of a particular casting configuration. Furthermore, if alloys have more low-melting point phases or inclusions segregated at the grain boundaries, the strength of the metal would be reduced because of the liquid film remaining at lower temperatures. The hot tear tendency is observed to be related to the amount of eutectic liquid present during the later stage of solidification. The presence of even a small amount of eutectic has been proven to aggravate the hot tearing tendency. When the eutectic increases to a critical amount, the maximum hot tearing susceptibility of alloys is obtained. With further increase in the amount of eutectics in alloys, hot tearing susceptibility starts to decrease. Grain refining or the presence of trace elements that alter growth kinetics and prevent early grain cohesion may be effective in reducing the susceptibility to hot tearing.

1.2 Objectives

The objectives of this study are planned in five phases as given below:

Phase 1: Use of an optimized mold-casting method to evaluate the hot tearing susceptibilities of aluminum alloys.

Phase 2: Development of a method to quantify hot tearing severity, quantitative measurement and prediction of hot tearing tendencies for cast houses.

Phase 3: Study of the interaction of the different factors and a fundamental understanding of the complex relationships between alloy compositions and other factors (such as grain refinement, second phases) that affect hot tearing susceptibility.

Phase 4: Observation of characteristics and possible mechanisms of hot tearing in various aluminum alloys.

1.3 Methodology

Various methods have been used to determine hot tearing susceptibilities of alloys. The test methods include the use of specifically designed molds allowing the metal to solidify under certain casting conditions, and mold constraints the assessment and calculation of the severity of tears formed in the castings. The specific mold design is to ensure the generation of a sufficient amount of stress (mold constraint) to initiate tears during solidification of castings.

In an attempt to adopt a successful mold casting method, the Constrained Rod Casting (CRC) mold was developed by Alcan Kingston Research & Development Center (KRDC). The cylindrical bars of different lengths are cast via a common sprue. Each bar has an enlarged filleted section at one end (which provides a hot spot) and a spherical riser flange at the other end. The risered ends hinder the contraction of the bar during and after solidification. Since long bars contract more than short ones, the strain imposed on long bars will be greater than that on short ones, and hence long bars tend to tear more readily. The extent of hot tears or cracks in each bar can be evaluated and used to rate the hot tear susceptibility of the alloys.

By using the CRC mold casting method, the following steps were performed in this present investigation:

- Typical wrought aluminum alloys with a wide range of hot tearing tendency (AA1050, AA3104, AA5182 and AA6111) were selected.
- Indices were developed to quantify the hot tearing susceptibilities of the alloys.
- Hot tearing susceptibilities of the alloys were evaluated/predicted; and experimental results were compared with the earlier observations encountered during industrial practices.
- The reproducibility of the mold casting tests was evaluated through the analysis of thirty samples per alloy. The standard deviation for the test results of the castings was calculated.

- The sensitivity of the mold to changes in grain refinement was evaluated by the addition of different levels of grain refiners to the alloys. The experimental results of the AA1050 alloy at different levels of Ti contents were compared.
- The reliability of the mold was evaluated by casting a series of wrought aluminum alloys with and without grain refinement.
- The surface of the hot tears and microstructure of the tear region were analyzed in order to characterize hot tearing of different alloys. The macro- and micro- structures of the alloys were related to hot tearing susceptibilities by means of optical microscopy, scanning electron microscopy, energy dispersive x-ray (EDX) analysis, as well as matrix dissolution and x-ray diffraction (XRD) analysis.
- A binary Al-Si system was investigated in order to shed more light on the understanding of the hot tearing phenomenon in aluminum alloys. Different levels of Si were added to commercial purity aluminum to study the mechanisms of hot tearing, and to understand the relationship between alloying elements and the properties that affect hot tearing susceptibilities (alloy composition, freezing range, and amount of eutectic) in binary alloys.
- Finally, the CRC mold casting method was globally evaluated and recommendations for the improvement of this method were given.

CHAPTER II THEORETICAL BACKGROUND AND LITERATURE REVIEW

Hot tearing is a common and serious defect that occurs during the solidification of liquid metals. This phenomenon, which is also referred to as hot cracking, hot shortness, super solidus cracking, and shrinkage brittleness, has been the subject of previous investigations. Hot tearing is the production of a macroscopic interface (a fissure) in a solidified part as a result of strains generated during freezing. The strains arise principally because of the volumetric shrinkage associated with the liquid-to-solid phase change in metals. This can also be made worse by thermal contraction in the solid state. The macrostructure of hot tearing is schematically illustrated in Figure 2.1 [7].

A number of metallurgical and mechanical factors determine whether or not tearing will actually occur when a critical temperature during of solidification is reached. This range which exists within a range between a temperature, in the solidification interval T_c, and the solidus temperature, T_s. this range is where hot tearing defects are likely to occur. Metallurgical factors such as freezing range, eutectic percentage, second phases that determine the strength and ductility of the alloy at semi-solid stage during solidification are primarily a function of metal composition. Variables which cause hot spots and contraction stresses are a function of casting geometry, mold material, and casting parameters.

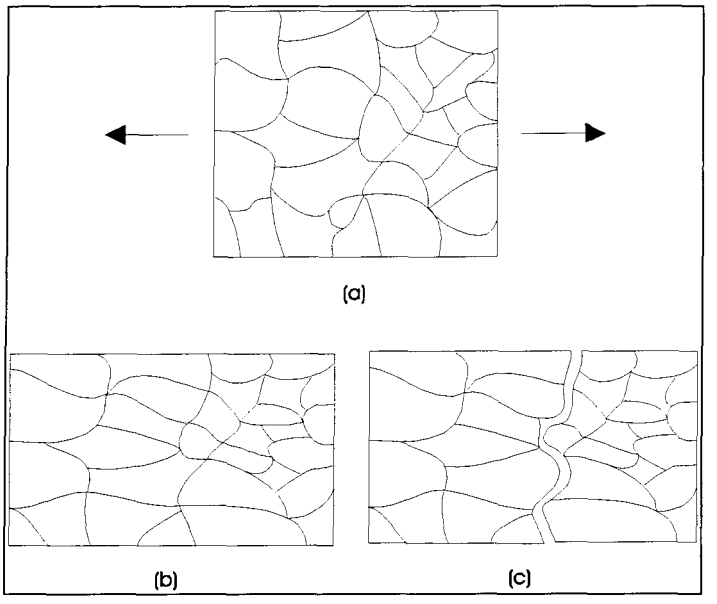

Figure 2.1. A schematic illustration of macro-structure of hot tearing, (a) stresses are formed during the solidification, (b) metal deformed without hot tears, and (c) metal deformed with hot tears [7].

Measurement of hot tearing susceptibility of aluminium alloys had been carried out in previous investigations by using various test methods. Casting methods [1, 2, 3, and 4] have been used with some success. However, these methods have certain limitations such as insufficient sensitivity to changes in alloy composition and to variation in grain refinement. Quantitative methods have also been investigated to predict hot tearing tendency. Some physical and mechanical methods [8, 9, 10, and 11] have been used to quantitatively measure and predict hot tearing susceptibility. Mathematical models for hot tearing [10,11] have also been developed for different casting conditions.

Even though theories have been developed to explain the mechanism of hot tearing, controversies still exist [12]. The fundamentals of hot tearing, and the parameters responsible for hot tearing need further investigation. In this chapter, a chronological review of hot tearing theories and a review of experimental methods are presented.

2.1 Theories of Hot Tearing: A Chronological Review

2.1.1 Early Theories of Hot Tearing Based on Stress and Strain

Hot tearing involves the formation of a macroscopic tear in a solidifying casting as a result of stress built up in the solidified metal. This stress arises principally because of the volume contraction, β, associated with the liquid to solid phase change in solidifying metals (usually $\beta \approx$ 6%), but it can be made worse by thermal contractions in the solid and/or by the constraints of the mold.

The first systematic study of the mechanism of formation of hot tears in cast metal was undertaken by k rber in 1928 [13]. Based on the experimental results, it was believed for years that hot tears were formed after the metal was completely solidified [14, 15, and 16]. The earliest theories [14 and 15] postulated that a brittle structure of low tensile strength existing within a temperature range somewhere below the solidus, was responsible for hot tearing. It was believed that when a casting contracted under conditions of restraint, the stresses induced might exceed the tensile strength of the material and cause tearing. In fact, at high temperature ranges solid metal

behaves in a ductile and plastic fashion. This ductile feature of the metal below the solidus cannot be explained by the previous theories.

An early theory called the *Brittleness Theory* was proposed by Vero [17] in 1936. It was postulated that hot tearing was caused by the contraction of the primary dendrites during the solidification of alloy. It was explained that at the semi-solid stage of alloys, while the primary dendrites grow and come into contact and form an interlocking or coherent network, the solidification contraction would set up stresses. The solidifying alloy will hence be restrained by the mold or by the cooling contraction of adjacent parts of the casting. If the stresses are high enough to separate the interlocking network dendrites and the remaining eutectic liquid is insufficient to feed into and heal the initial tears, hot tears will persist until the alloy is solidified.

An improvement of the brittleness theory was introduced later by Pumphrey [7]. It was explained that even though the strength of the metal increases following the solidification temperature drop, hot tearing still can take place when only a small amount of residual liquid remains. During this time, the metal possesses little ductility. Such a brittle property persists at a lower temperature until the residual liquid has completely solidified.

It was postulated that hot tearing occurs in a brittle temperature range between the temperature at which a coherent dendrite structure is first developed in the alloy and the effective solidus temperature under the relevant condition [7]. Hot tearing tendency is directly related to the duration extent within the brittle range, and upon contraction stresses during solidification as well as to other

external factors. Any factor that influences the extent of the brittle range may affect hot tearing susceptibility. The limit of the brittle temperature range is a function of the constitution of the alloy. The alloys with a more narrow brittle temperature range show higher resistance to hot tearing. This has been confirmed in Al-Si, Al-Si-Cu and Al-Mg-Si alloys with and without grain refinement [7].

The hot tearing susceptibility of the alloys can be affected during casting. Two important phenomena are associated with an alloy cooling through the brittle range: one is stress accommodation and the other is healing phenomenon. Both accommodation and healing can reduce the amount of hot tearing. In fact, a slight relative movement of crystals and some plastic deformation of primary dendrites to accommodate contraction stress always accompanied with the cooling of metals. When accommodation has proceeded as far as it is possible and the strength of metal cannot resist the tensile stresses developed during further cooling, hot tearing may occur [7]. If there is enough liquid remains to flow back to tears, the most tears may healed.

A theoretically derived relationship between the brittle-shrinkage range and the severity of hot tearing in different test conditions is shown in Figure 2.2 [7]. Curves under practical conditions show that the sensitivity of hot tearing can reach a maximum over a certain brittle range then it stabilises. The values of maximum hot tearing sensitivity were different due to different contraction stresses during solidification and other external factors under different test conditions.

Pellini et al [18] modified the previous theory. A liquid film concept was first introduced in their new theory. It was suggested that when the metal temperature is just above the solidus, there is a

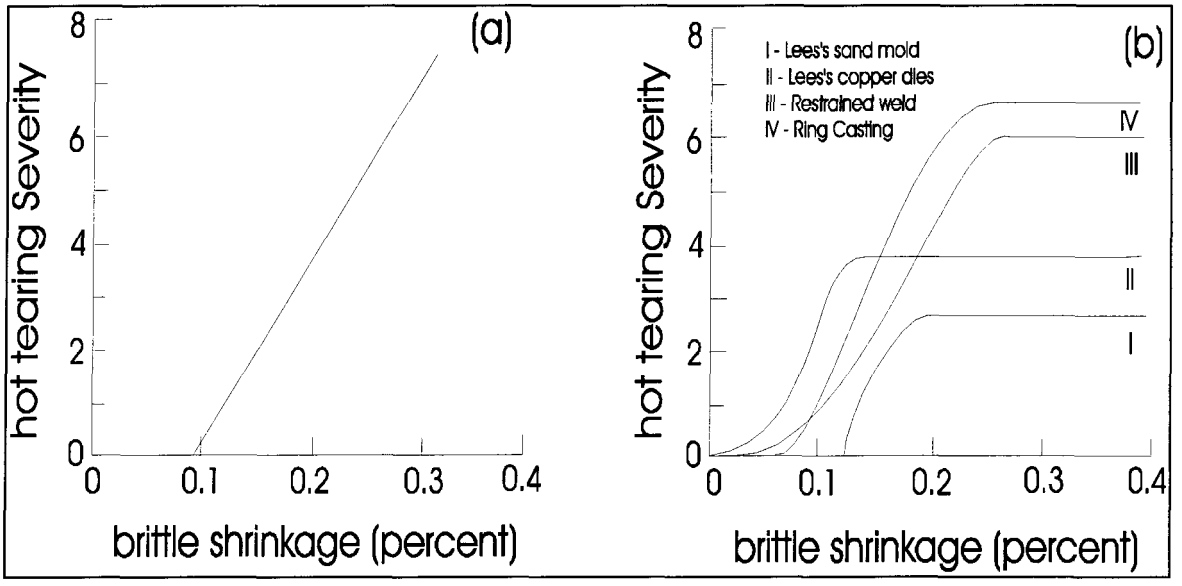

Figure 2.2. Relationship between the brittle-shrinkage range and hot tearing sensitivity: (a) in theoretical condition, (b) in practical test condition [7].

thin continuous liquid film that remains between the solidified dendrites. Highly concentrated stresses can build up in the liquid film region and result in hot tearing. But this still could not explain the fact that hot tearing occurred at temperatures below the solidus in some of their test

results [19]. The *Strain Theory* proposed by Pellini [20], with the hypothesis that the hot tearing temperatures of metals was slightly higher than the solidus has eventually been accepted by most scientists today.

Pellini [20] developed his *Strain Theory* of hot tearing based on a concept of liquid films existing at grain boundaries at temperatures above the solidus. Tearing is a strain controlled phenomenon, which occurs when the strain accumulated within the hot spot reaches a critical value. At a later stage, the liquid film is thinner and the overall extension is concentrated in these hot zones to

produce a high unit strain. Tensile stress caused by contraction is highly concentrated in these liquid film areas, To the extent that it may be sufficient to cause hot tearing. If the liquid film is thick or there is no liquid film in the interdendritic regions, the strain is essentially uniform and it is insufficient to cause a tear. The strain distributions resulting from the extension of the hot zone at various stages of solidification is shown in Figure 2.3 [20].

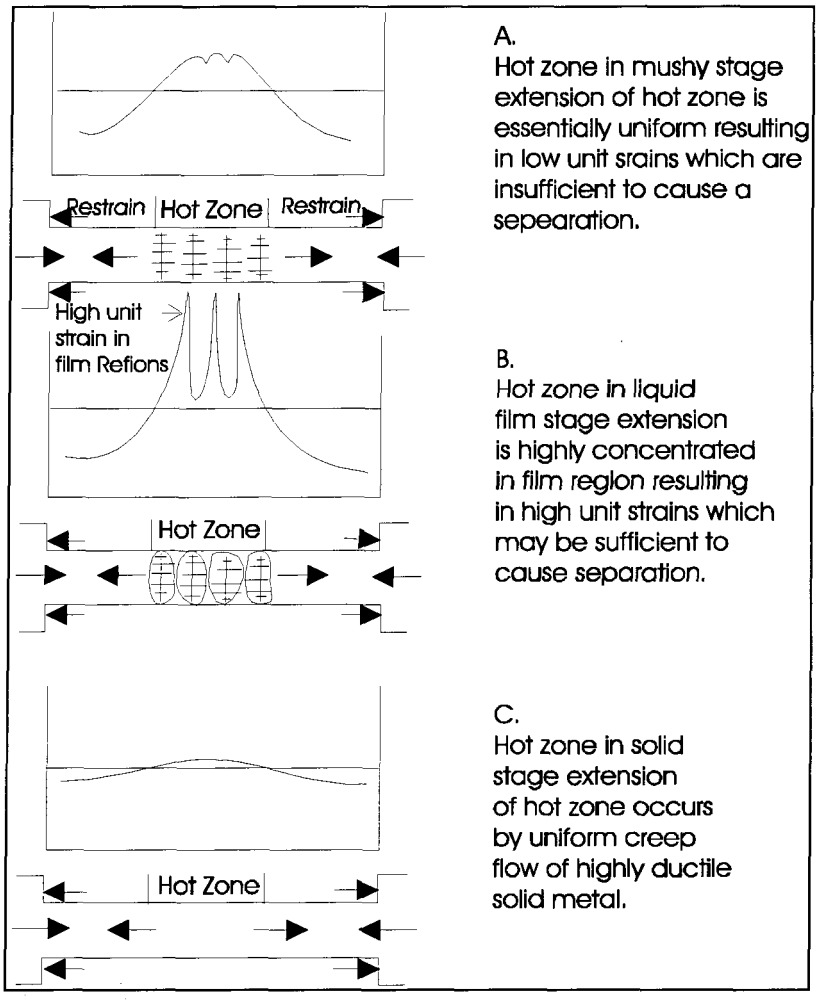

Figure 2.3. Diagrams showing the nature of strain distribution at various stages of solidification [20].

The strain accumulated within the hot spot is a function of the strain rate and time duration in which the metal passes through the film stage is schematically illustrated in Figure 2.4. It can be seen that the amount and rate of strain concentrated in the liquid film determines the development of hot tearing in castings.

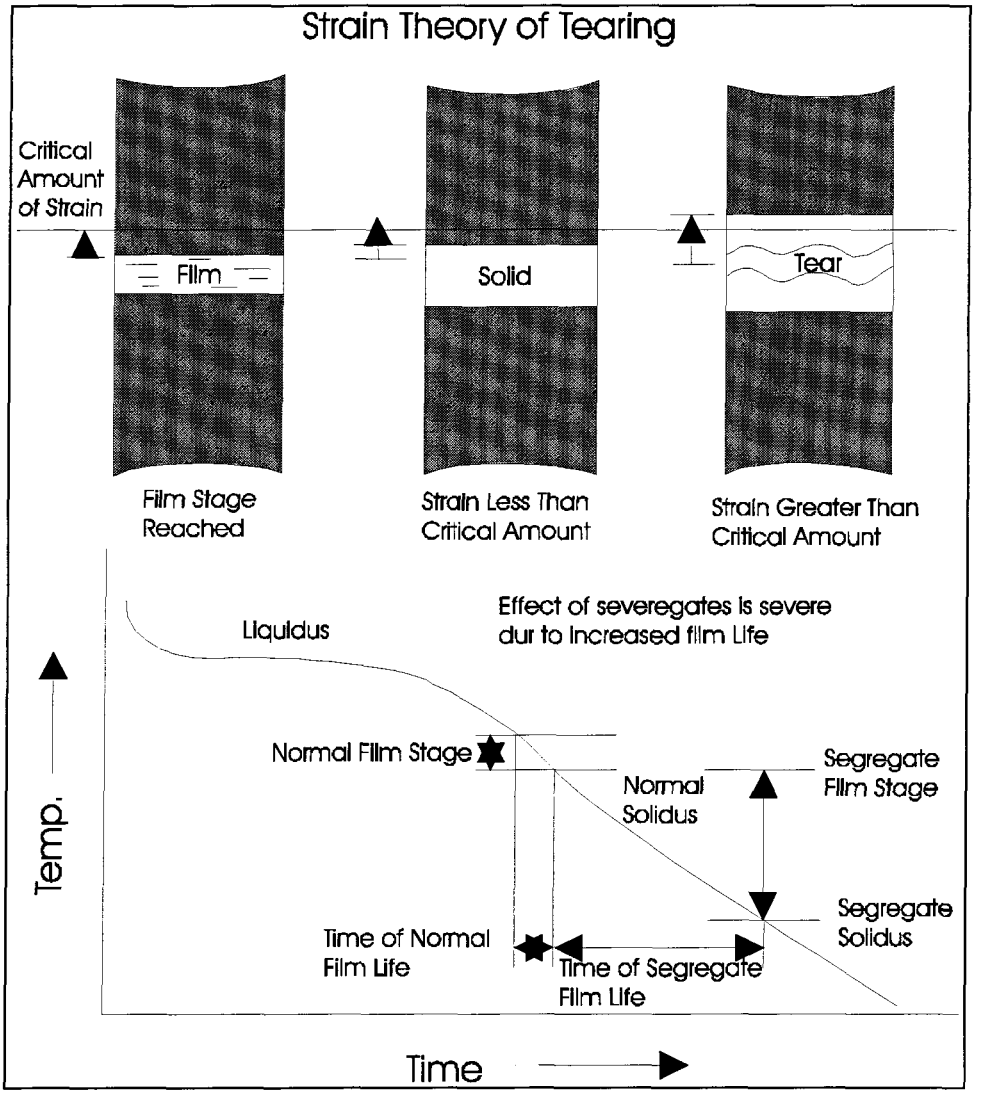

Figure 2.4. An illustration of the effects of stain rate and time of film life to hot tearing [20].

The rate of extension of the film region under going contraction may vary widely due to a number of factors, including size and cooling rate of the region, and width of the hot spot. If casting has wide regions of contraction, faster cooling rate, and a narrow hot spot, which contribute to a higher strain rate, it may have higher hot tearing tendency. A casting may have a higher strain rate, but if the alloys have a very short time to maintain it liquid film stage. It may exhibit low hot tearing tendency. Pellini tested the effect of high sulphur content on promoting hot tearing in steel castings on the basis of the reasons. It was confirmed that high sulphur contents can produce a longer liquid film stage and provide a further opportunity for strain to accumulate extension in the liquid film regions, thus causing an increase in hot tearing tendency (Figure 2.5) [21].

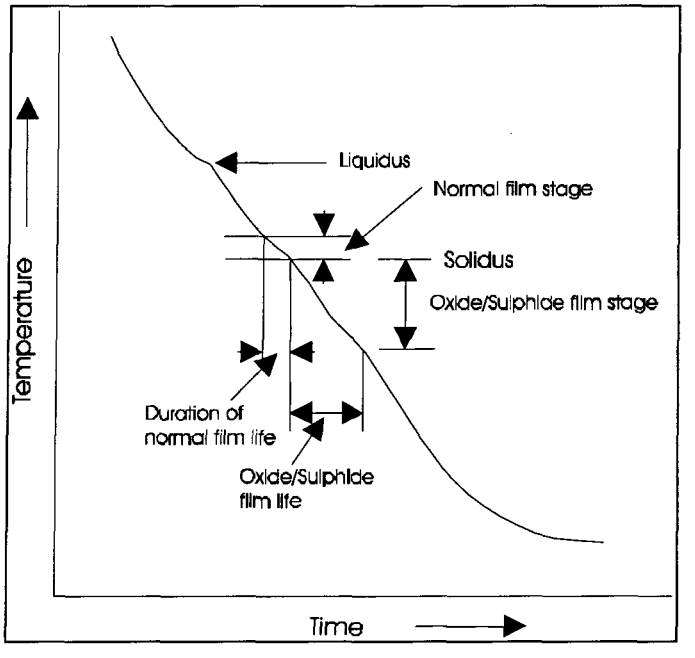

Figure 2.5. The effect of high sulphur content in the alloys on hot tearing as explained by the liquid-film hypothesis [21].

Because of the theory that the hot tearing temperature is higher than the solidus of an alloy, the temperature interval for hot tearing has become important and is considered to be significant for hot tearing [22]. This interval has been termed *Effective Interval of Crystallisation*, *Hot Shortness Temperature Range*, *Brittleness Stage*, or *Critical Solidification Range* (CSR) [1, 2, 7, 20, and 22]. It is regarded as the temperature range between the solidus and a temperature higher than but close to the solidus (Figure 2.6) [22].

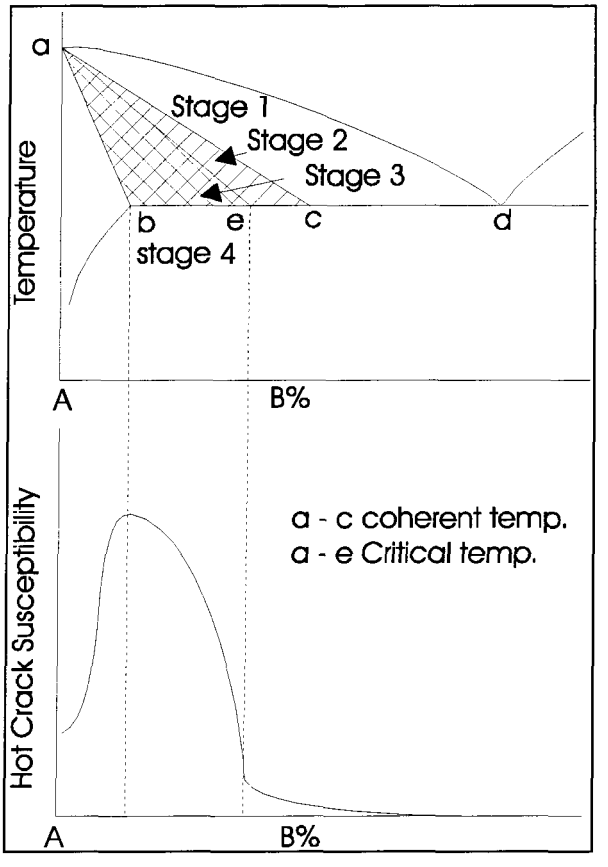

Figure 2.6. Critical temperature range of hot tearing in a binary system [22].

In this temperature range, many characteristics of the solidifying metal are different than for other stages of solidification. When an alloy solidifies through its freezing range, the solid grains will form dendritic interlock. The temperature at which the solid crystals form this semi-continuous network is called the coherency temperature. The remaining liquid surrounds the solid dendrites as thin films. In the presence of interlocking dendrites, the feeding of the interdendritic regions and the accommodation of deformation of solid metal are impeded, giving rise to hot tears in the solidifying structure. At this stage, The relative movement of liquid and solid is increasingly difficult with increasing solid fraction.

Recently, the confirmation of hot tearing temperature was conducted with the Acoustic Emission (AE) technique by Oya et al [8] using an Al-7wt%Si alloy. It was found that the AE signals of hot tearing had high peak voltage values and were always detected in the later stage of solidification at temperatures higher than the solidus. AE signals of hot tearing in an Al-7wt%Si alloy under non-directional solidification conditions are show in Figure 2.7 [8].

In industrial practice, most materials used for castings are not pure metals. Low-melting phases, and second phases, etc. are always concentrated at grain boundaries under non-equilibrium freezing conditions. The microstructural segregation always arises during solidification of castings at very low cooling rates. Therefore, the solidus temperature in non-equilibrium conditions is lower than that it is in equilibrium conditions. It is not difficult to understand that even some experimental results can exhibit hot tearing temperatures which are lower than the equilibrium-solidus temperature. Hot tearing should not be confused with hot cracking that

occurs after the metal has completely solidified.

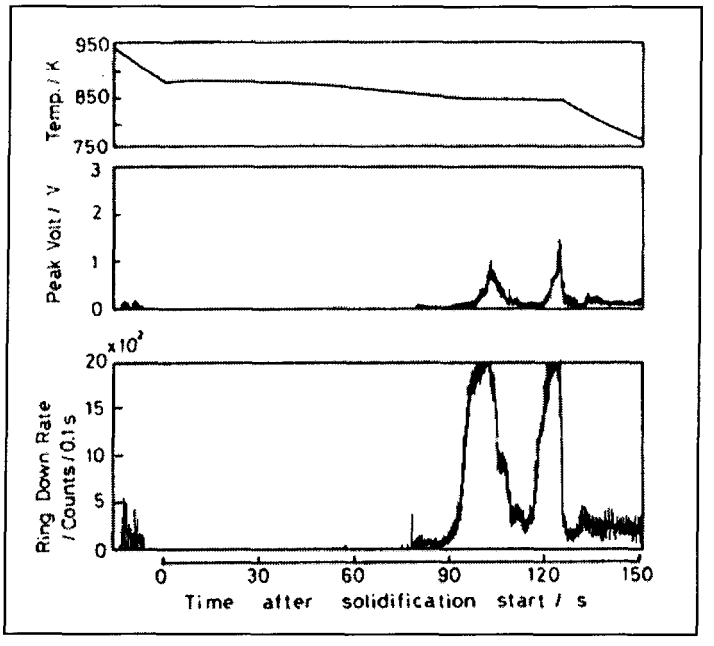

Figure 2.7. AE signals of hot tearing in a non-directionally solidified Al-7%Si alloy and its solidification cooling curve [8].

If hot tearing is related to a critical temperature range, it means that alloys in that temperature range may have low strength and ductility, as well as a particular structure that makes hot tears possible. Flinn [23] suggested that solidification could be classified into five stages according to metal properties.

Stage I - Completely liquid. It is impossible for hot tearing occur.

Stage II - Liquid with some solid. Hot tears can be initiated. Hot tears can be healed by a flow of liquid into the gaps in the interdendritic region since there is sufficient liquid present

at this time.

Stage III - Liquid films are present in the solidifying metal. Solid crystals grow and contact each other to form an interlocking structure. Since contraction strains are developed during cooling, hot tearing may be initiated, and since in this stage the movement of both the liquid and solid is greatly impeded, hot tearing cannot easily heal.

Stage IV- Solid metal is in the *plastic range*. The ductility of the alloy is high and metal flow takes place at low stress. The stresses can be relieved by plastic flow (this is similar to the *hot forging range* in which hot working operations are performed on wrought alloys).

Stage V- Solid metal is in "the elastic range". The important characteristic of this range is that if a stress is applied below the yield strength, elastic strain develops instead of rapid relief of the stress by creep.

The stress-strain curves for the different temperature ranges are summarised and schematically shown in Figure 2.8.

To summarise the essential feature of the hot tearing phenomenon as deduced from the casting process, the ductility and strength of the alloy in passing through the solidification process were also investigated by Apblett and Pellini [21]. Thermal analysis and radiography methods were used to simultaneously determine the onset of hot tearing. It was demonstrated that the metal consisted of a dendritic structure separated essentially by continuous films of liquid. Tensile tests were also used to measure the strength and ductility of the metal during solidification. The results are shown in Figure 2.9 [21]. It can be noted from this illustration that the metal possesses a lower strength and

ductility at the late liquid film stage.

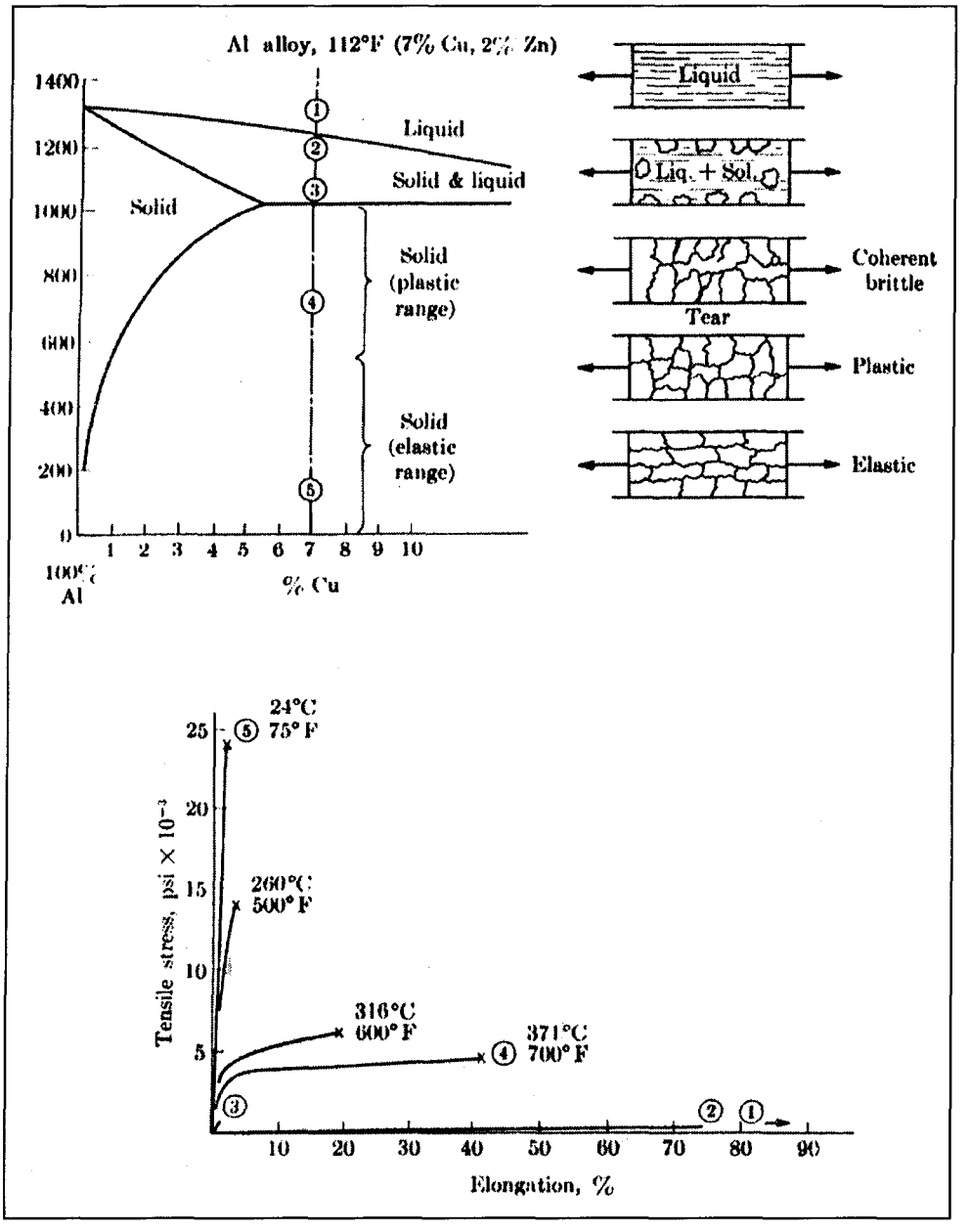

Figure 2.8. An example of strength and ductility of metals at different temperature ranges during solidification [23].

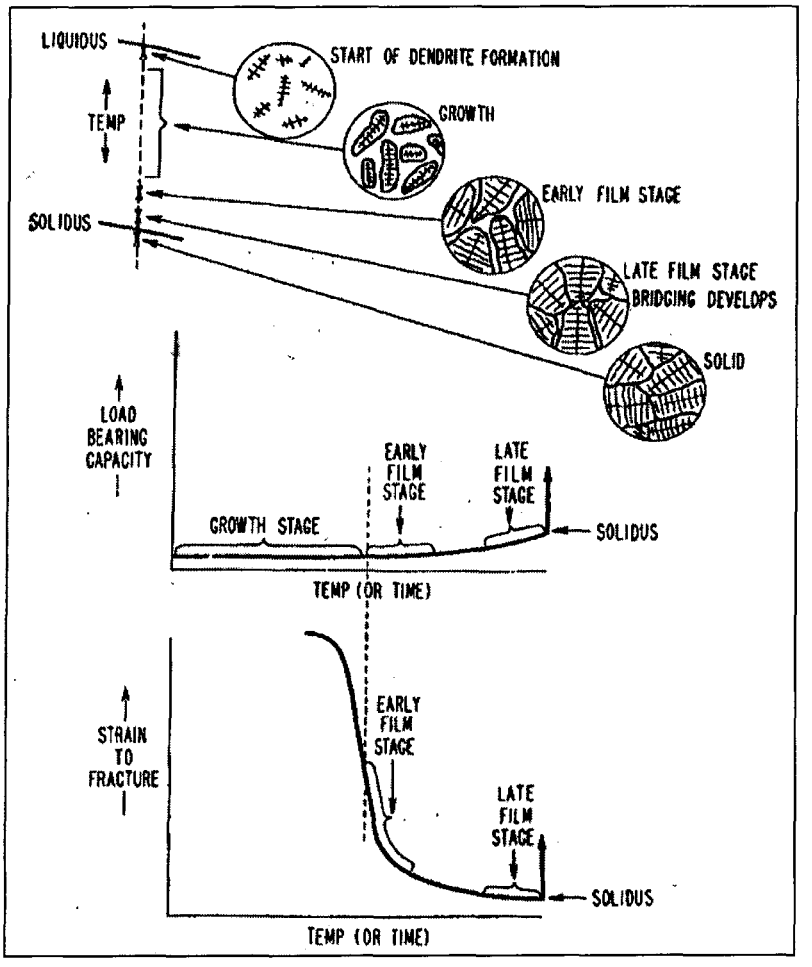

Figure 2.9. Strength and ductility of metal as deduced from casting studies [21].

The fact that both strength and ductility of alloys are low at the critical temperature range has been confirmed with some experiments [17 and 24]. Tensile and bending strengths of Al-Si alloys at higher temperatures were tested and plotted in Figures 2.10(a) and (b), respectively.

Actually, the *Later Liquid Film Stage* and *Brittleness Temperature Range* theories were put forward with different points of view. The former was from a metallurgical point of view and it considered more the microstructural characteristics of alloys during cooling and solidification. The

latter concentrated on the mechanical properties of the metal during its solidification process. The temperature range for both is almost the same. In fact, hot tearing is a combination of metallurgical and mechanical interaction. If a metal can have free contraction, and that is not restrained by a mold, it will not tear even if the alloy has very poor mechanical properties during solidification. In addition, if the feeding of the interdendritic regions of a solidifying alloy is facilitated throughout the freezing range, healing of hot tears may occur.

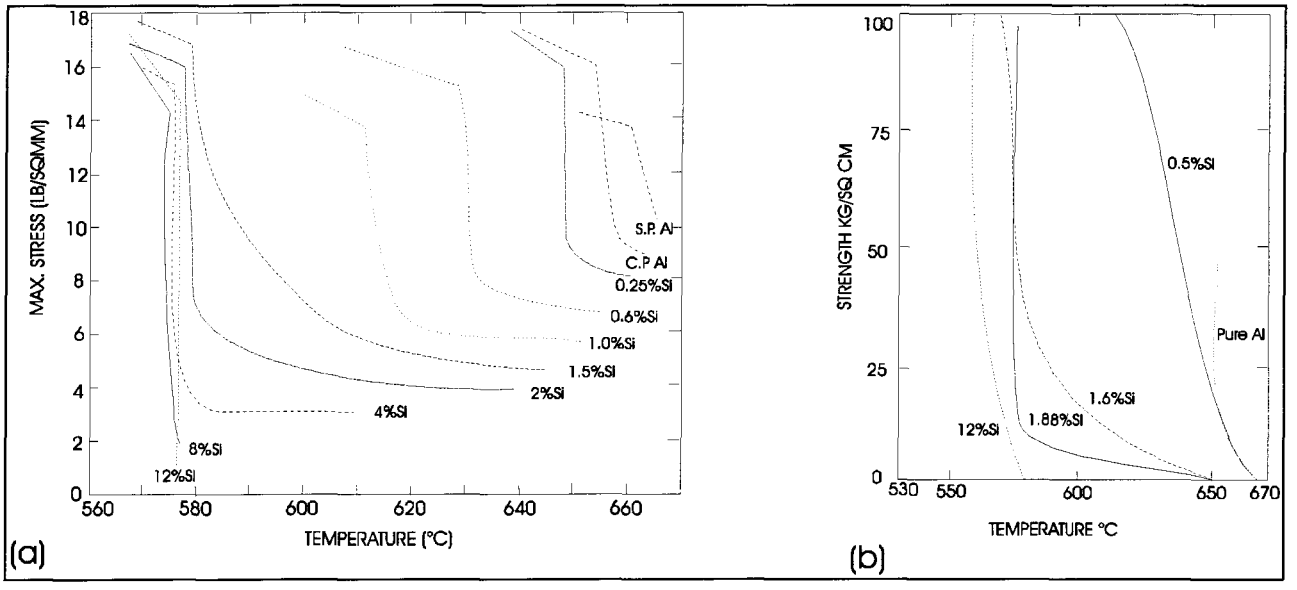

Figure 2.10. Properties of Al-Si alloys at high temperatures, (a) tensile strength tested by Singer and Cottrell [24], (b) bending strength tested by Verö [17].

2.1.2 Surface Tension Theory

Saveiko [25] presented a new hot tearing theory based on interdendritic liquid-film concepts. The

linear shrinkage of volume, deformation of the solid metallic matrix, and the surface tension at liquid film conditions were investigated for this theory. For simplification, it is assumed that grains are cubic in shape as shown in Figure 2.11 and the force is unidirectional and relatively perpendicular to the liquid film layer. When the extension is high enough to reach the deformation limit in the AB direction, hot tearing may occur along one of the liquid films. If hot tearing forms,two new surfaces must be formed and this necessitates the system to overcome the molecular adhesion force. In this system, the force applied at right angles separated the liquid film. The force required to separate the liquid film is given by the author as,

$$P = \frac{2\alpha F}{1000gb} kg \tag{2.1}$$

where α is surface tension of the liquid (erg/cm^2); F is the area of contact between the plates and liquid (cm^2); b is the thickness of the liquid layer between the plates (cm); and g is gravitational acceleration constant (cm/s^2).

According to the surface tension theory, the surface tension of an alloy, α, the thickness of the liquid film, b, and the area of contact between liquid and solid, F, are considered as the most important factors for hot tearing formation in alloys. Since the film thickness varies to a greater extent than the surface tension with a change in grain size of the alloys, film thickness may even more important than the surface tension. The impact of variation of the surface tension of liquid film and of grain size on hot tearing resistance of alloys is summarised in Table 2-1 [25].

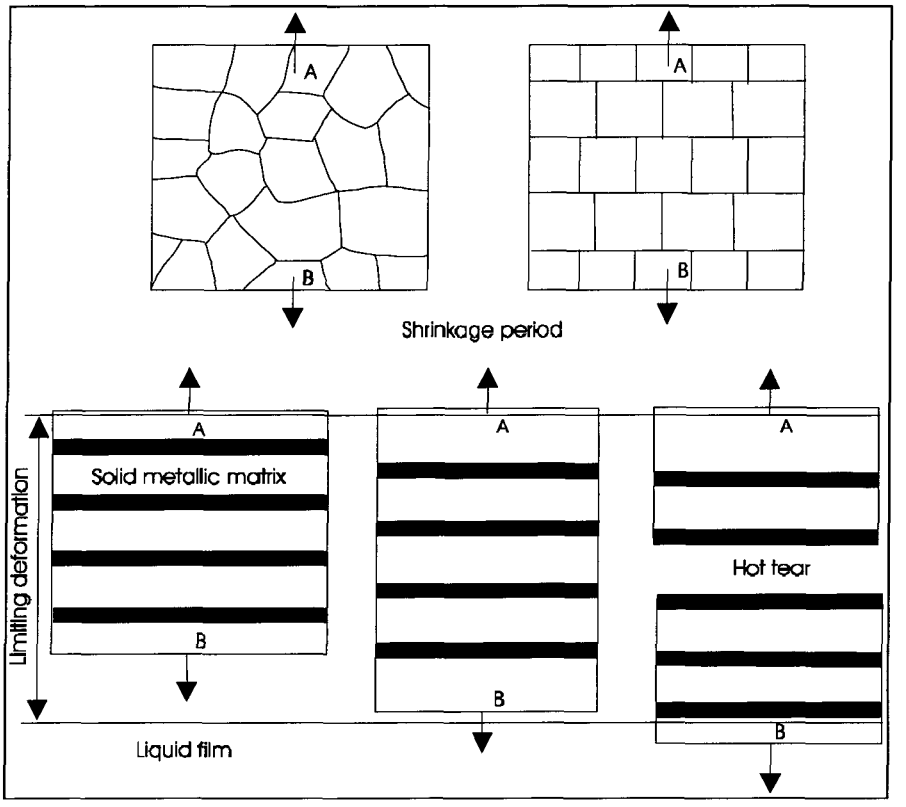

Figure 2.11. A simple model of solidifying metals and the formation of hot tears based on an interdendritic liquid film concept [25].

Table 2-1 Relationship of Hot Tearing Resistance to Surface Tension and Grain Size [25]

Surface Tension	Grain Size	Hot Tearing Resistance
Increases	Unaffected	Increases
Decreases	Unaffected	Decreases
unchanged	Plasticity increases or grain size decreases	Increases
unchanged	Plasticity decreases or grain size increases	Decreases
increases	Plasticity increase or grain size decreases	Increases considerably
Decreases	plasticity decreases and grain size increases	Decreases considerably
Increases	Plasticity decreases and grain size changes	Increase or decrease
Decreases	Plasticity increases and grain size changes	Increase or decrease

Experimental results [25] showed that various elements can affect surface tension. There is a close relationship between surface tension and hot tearing susceptibility (Figure 2.12). It seems that the maximum tear resistance of an alloy is associated with a maximum surface tension of the interdendritic liquid. However, this investigation did not explain how those values of surface tension of the interdendritic liquid were determined.

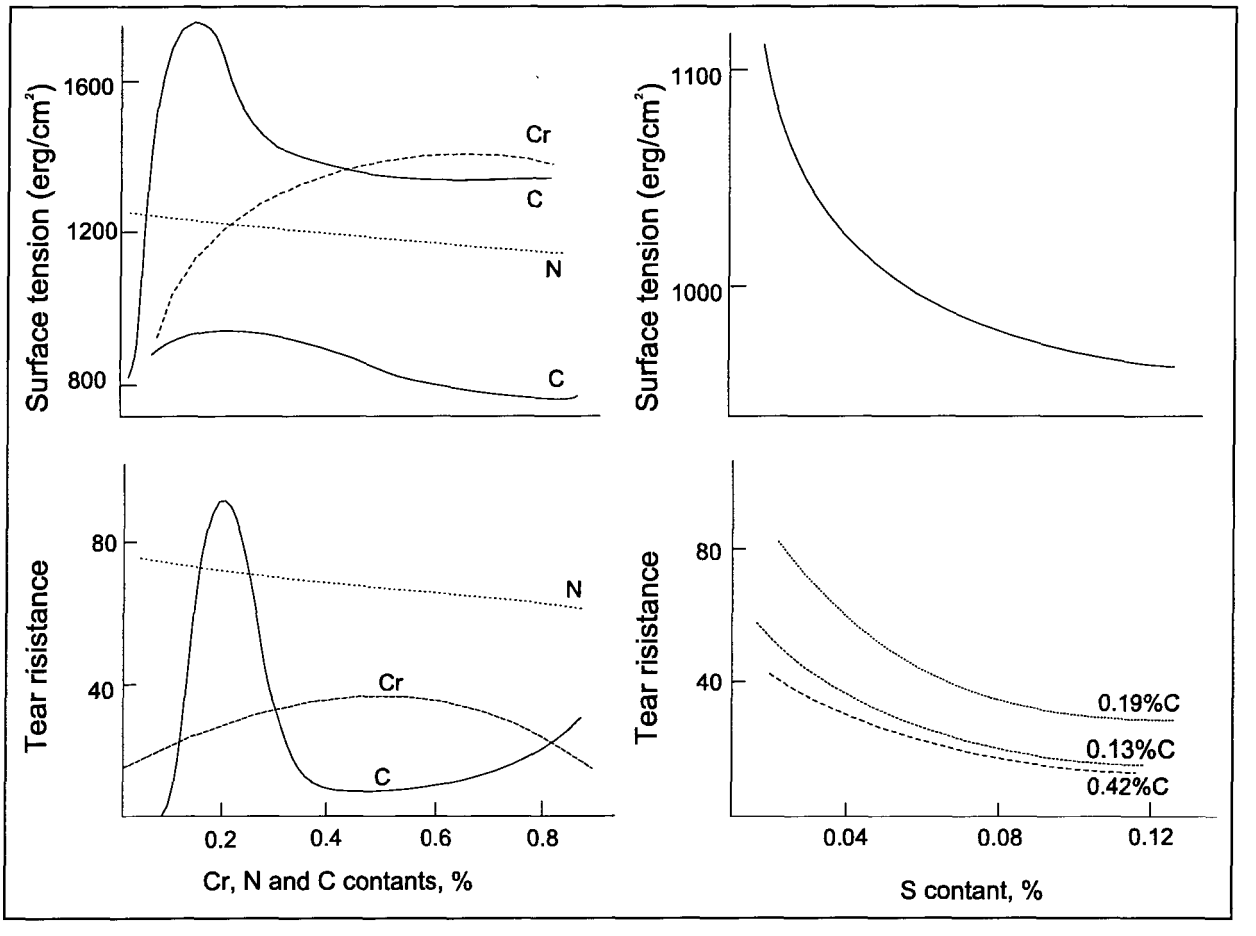

Figure 2.12. The relationship between surface tension and hot tearing susceptibility for steel alloys.

2.1.3 Generalised Liquid Film Theory

The *Generalised Liquid Film Theory* of Borland [22] explains the effect of quantity and distribution of liquid film on hot tearing susceptibility. It was suggested that the ratio of the inter-phase (solid-liquid) and inter-crystalline boundary energies determine the distribution of liquid film. If an alloy has a lower ratio of inter-phase energy, it tends to develop liquid films to cover both the grain faces and the edges. The grains are almost completely surrounded by the liquid film that makes the alloy to be more vulnerable to hot tearing (based on the strain theory). Conversely, if an alloy has a high ratio of the inter-phase energy, the remaining liquid tends to be confined to edges and corners of grain boundaries; and most grain faces can connect to each other leaving the alloys being more integral and able to accommodate the thermal stresses created during cooling. Therefore, the alloy can have a higher resistance to hot tearing. It can be seen that this explanation of Borland's is in contradiction with Equation 2.1 in Surface Tension Theory. According to that equation, the larger the surface covered by liquid film, the higher the force that would be required to separate the liquid film to form hot tears.

The distribution of liquid during solidification is related to the physical properties of alloys. Particularly, it is very important to establish a relationship between the interfacial energies of alloys and the liquid distribution at the grain boundaries. The relationship between grain boundary energy and the shape and distribution of micro-constituents has been discussed by Smith [28]. The interface and grain boundary energy is related to a dihedral angle which is expressed as:

$$\frac{\gamma_{SL}}{\gamma_{SS}} = \frac{1}{2\cos(\theta/2)} \tag{2.2}$$

where γ_{SL} is the interface (solid/liquid) energy, γ_{SS} is the grain boundary energy, θ is the dihedral angle. The dihedral angle is zero for $\tau \leq 0.5$. It was explained that if the ratio τ is ≤ 0.5 ($\theta=0°$), liquid progressively occupies the grain faces. The liquid will extend less along the grain boundary edges, and spread over larger areas of the solid. The cohesion between adjacent grains is reduced and the metal is therefore more likely to have hot tearing. Again, in contradiction with the surface tension theory, for values of $\tau \geq 0.57$, the liquid will progressively accumulate at the grain corner and will extend less along the grain boundary edges as τ increases. The relation between the dihedral angle and τ, for $\tau > 0.4$ is shown in Figure 2.13. The effect of dihedral angle on the distribution of liquid phase on grain corners, edges, and faces in three dimensions is shown in Figure 2.14 and discussed elsewhere [29, 30, and 31].

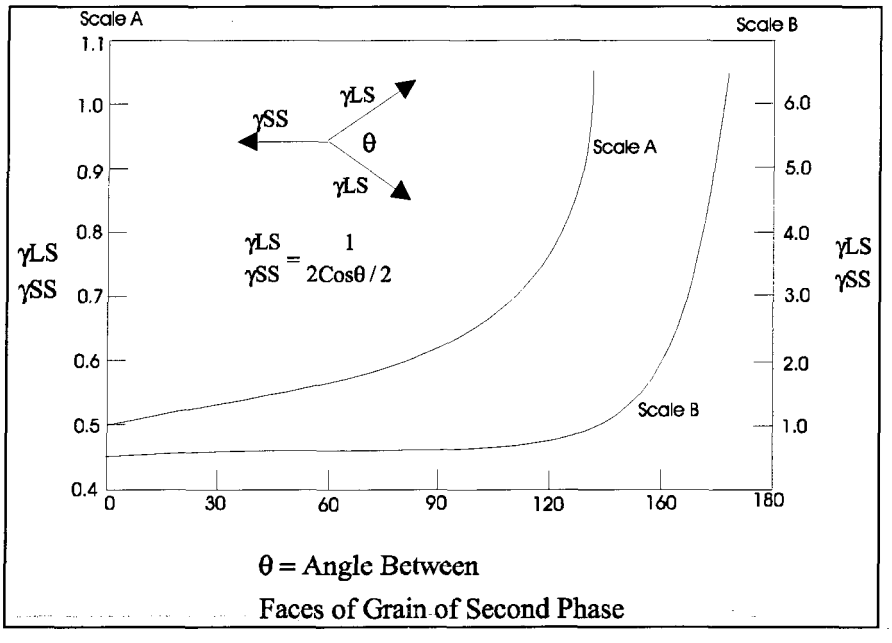

Figure 2.13. Ratio of inter-phase boundary tension and grain boundary tension as a function of dihedral angle of second phase [22].

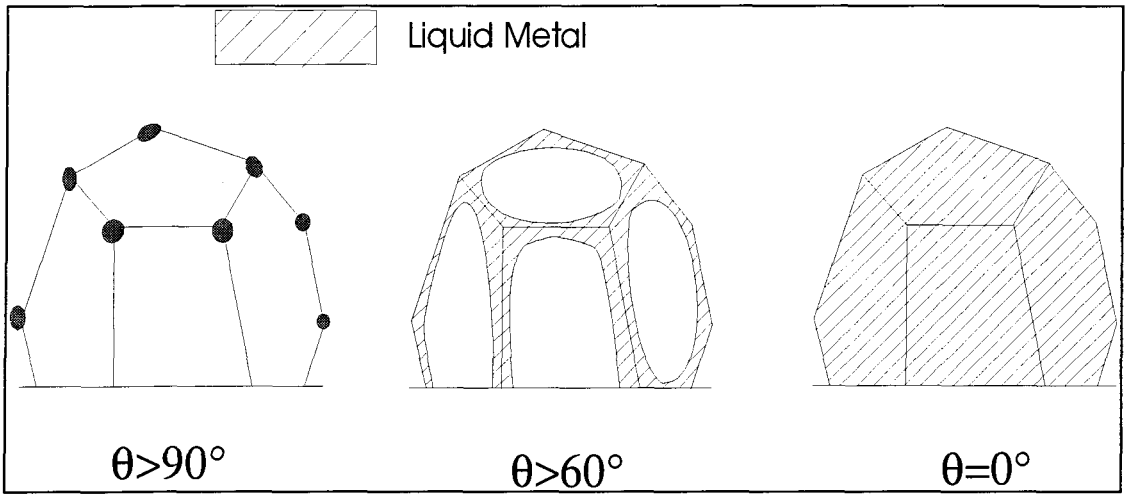

Figure 2.14. The distribution of liquid phase on grain boundaries, (a) $\theta>90°$ liquid at corner, (b) $\theta>60$ liquid at edge, and (c) $\theta=0$ liquid at face [22].

It should be mentioned that no agreement has been reached on the precise mechanism of hot tearing. These preliminary theories are far from explaining the behaviour observed in multiphase alloys. From the study of the mechanics of hot tearing, we can understand that there are two main factors that contribute to the initiation of hot tears: the inherent metal characteristics and external mold characteristics. Hot tearing defects are caused by a number of complex interrelated variables. An alloy may or may not have hot tearing depending on the design of the casting and the constraints of the mold. These factors basically control the rate of extension imposed on the weakened region during solidification. A rigid mold and wild regions undergoing contraction usually promote hot tearing. The phenomenon of hot tearing is usually studied by keeping the influence of the external factor constant and varying the inherent properties [32].

2.2 Factors of Hot Tearing

2.2.1 Alloy Constitution

2.2.1.1 Binary Alloys

A majority of the studies [26, 33, and 34] had dealt solely with variations in alloy composition. The evidence obtained in these previous investigations indicates that the most important feature of the alloy constitution is the amount of eutectic. Hot tearing tendency is observed to be related to the amount of eutectic liquid present during the later stages of solidification. The presence of only a small amount of eutectic was observed to aggravate hot tearing tendency. However, when the eutectic content increase in beyond a certain value, hot tearing decreased with continued increasing eutectic content. It was explained by the Brittleness Theory [7] that stress accommodation and healing phenomena are more significant with increase amount of eutectic.

Other investigators [35, 36] supported a similar assumption. They suggested that the reduction of severity of hot tearing should coincide with the first appearance of eutectic (widest freezing range) in non-equilibrium conditions, and further reduction in the severity of tearing should be accompanied by an increase in the amount of eutectic present. It was noted that an addition of a second alloying component resulted in an increase in hot tearing sensitivity. It was observed [35] that the maximum Hot Cracking Sensitivity (HCS) in base systems corresponded to a eutectic content of 0-0.15vol%.

Experimental results with Al-Cu and Al-Sn alloy systems have shown that the alloys had minimum resistance to hot tearing when liquid eutectic was sufficient to completely surround the solid [29, 37]. An Al-Sn (0.5 wt%Sn) system with higher wettability was found to have the primary dendrites covered by the eutectic liquid more easily than those in an Al-Cu (0.5wt% Cu) system. For the Al-Sn system, only 0.5% eutectic liquid was needed to completely cover the primary dendrites. The Al-Cu system, however, needed 12% eutectic liquid. Consequently, the Al-Sn alloy with higher wettability exhibited much lower hot tearing resistance than the Al-Cu alloy [29]. The experimental results of hot tearing susceptibility of an Al-Sn and Al-Cu alloys with different Sn and Cu content are shown in Figure 2.15.

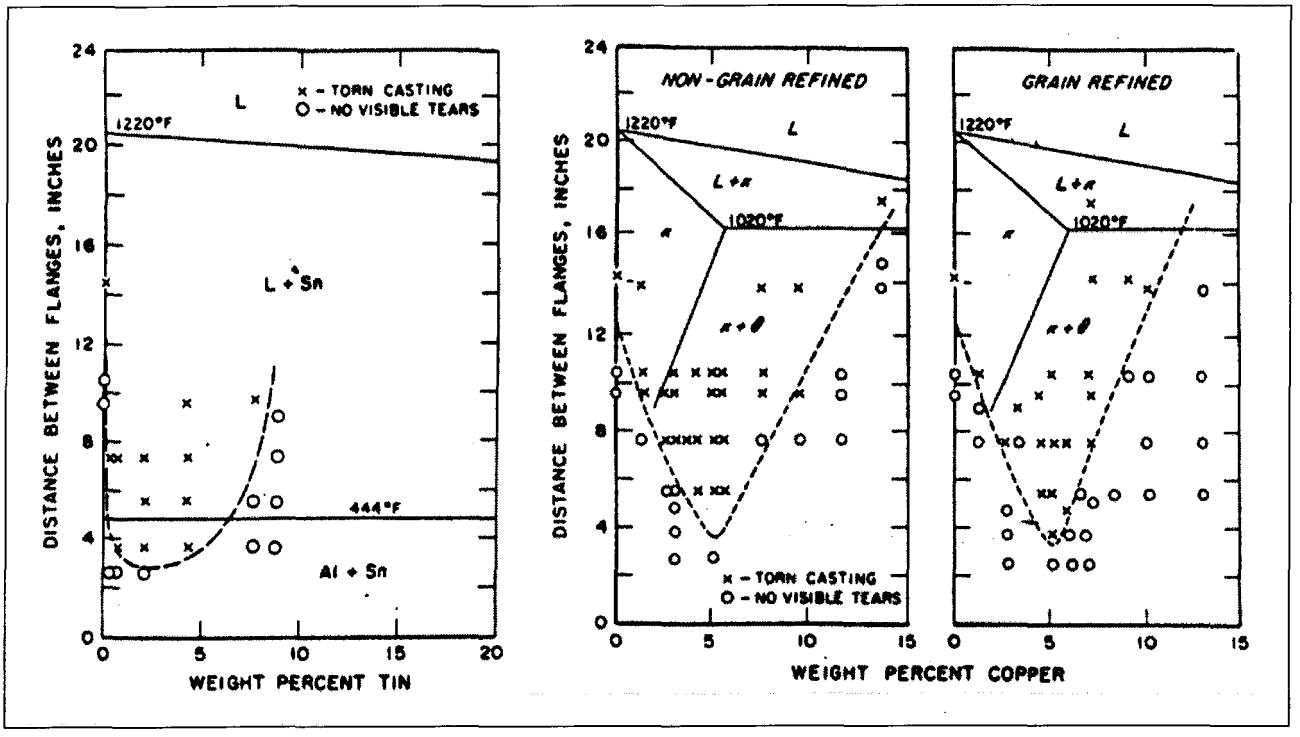

Figure 2.15. Hot tearing of Restrain Bar Test in binary aluminium systems. (a) Al-Sn, and (b) Al-Cu [29].

By analysing hot tearing severity and the amount of eutectic in the alloys, it was noticed that the amount of eutectic concentrated at grain boundaries was variable under different test conditions. Pumphrey and Jennings [7] discovered an approximately linear relationship between the low proportions of eutectic and the average cooling rate over the solidification range for an Al-Si alloy. The most favourable condition with regard to a low hot tearing tendency would exist at an infinitely slow rate of cooling. It was believed that the lower the cooling rate, the smaller the amount of residual eutectic that was required to compensate for hot tearing.

2.2.1.2 Multi-Phase Alloys

Few investigations have been carried out with multi-phase aluminium alloys. An investigation of hot tearing susceptibility of Al-Cu-Mg ternary alloys was conducted by Pumphrey and Jennings [7] using Ring Casting and Restrained Weld methods which had previously been used for binary aluminium alloys. They conducted the investigation by increasing magnesium percentage in the alloy while maintaining a constant copper content, or increasing the addition of copper to the alloy and keeping the magnesium content constant. The severity of hot tearing over the whole field was investigated and the experimental results of the two systems were presented by means of contour maps as shown in Figure 2.16 [7].

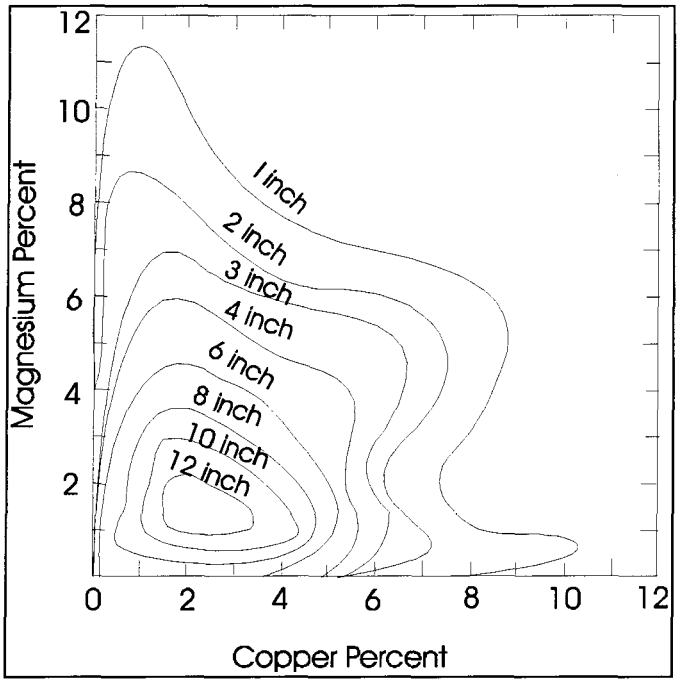

Figure 2.16. The contour of hot tearing susceptibility of an Al-Cu-Mg ternary system measured with Ring Casting method [7].

By using the system of Nishimura [38], Pumphrey and Jennings concluded that there was a close relationship between the form of the tearing phase diagram and the ternary constitution diagram [7]. From the complete ternary constitutional diagram, the maximum the solidus-to-liquidus temperature interval (freezing range) occurs at an alloy content of approximately 3.5%Cu and 2.5%Mg. The alloy content for maximum hot tearing in the experiment were slightly lower than these values, with 1.5-2.5% copper and 1-2% magnesium. The author explained that this was probably due to the difference in the extent of metastability of the phases in the alloy under non-equilibrium Ring Casting conditions.

The hot tearing susceptibilities of ternary Al-Cu-Mg aluminium alloys was also been investigated with the Annular Casting method [39]. It was concluded that hot tearing depended on the type of transformation during the final stage of solidification. Monovariant transformation resulted in high susceptibility to hot tearing and nonvariant transformation resulted in low susceptibility to hot tearing. The hot tearing susceptibility and polythermal sections of the aluminium corner of the Al-Cu-Mg system with different copper contents are shown in Figure 2.17 [39].

2.2.2 Type and Size of Grain

A fine equiaxed grain structure is normally desired in aluminium castings. The type and size of grains are determined by the composition of the master alloys (grain refiners) containing intermetallic particles which provide sites for heterogeneous nucleation. A simple and easy way to control the grain size is the addition of grain refiners. Grain size is a function of the type and amount of grain refiners added. The most widely used grain refiners are master alloys of titanium, or of titanium and boron with aluminium [40].

Matsuda et al [41] examined the solidification cracking susceptibility of an Al-Zn-Mg alloy with different additions of elements, such as Ti + B, Ti, Zr, Fe, Mn, Si, Be, Ni, Cr, etc. As expected, Cu was seen to have detrimental effects. The scatter in solidification tearing susceptibility was evaluated by using the Ring Casting method, and the results of the preliminary evaluation showed that Ti+B, Ti, and Zr drastically reduced the tear tendency among the 13 elements added. Based on

these results, they explored, in depth, the effect of varying additions of Ti +B, Ti and Zr. The results are shown in Figure 2.18.

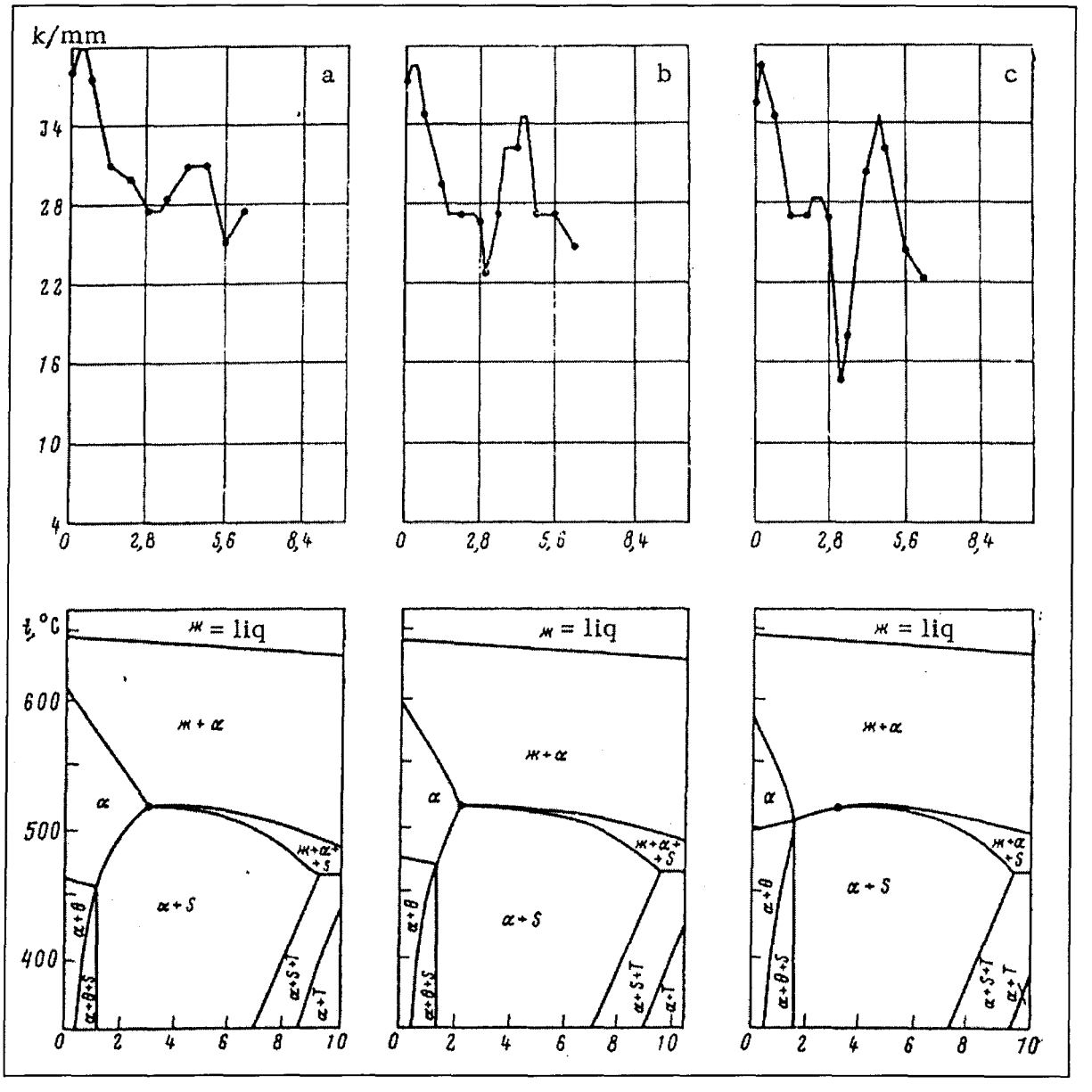

Figure 2.17. Polythermal sections of the Al-Cu-Mg systems and hot tearing susceptibilities of alloys with different Cu content. (a) 2.8%, (b) 3.5%, and (c) 2.9% [39].

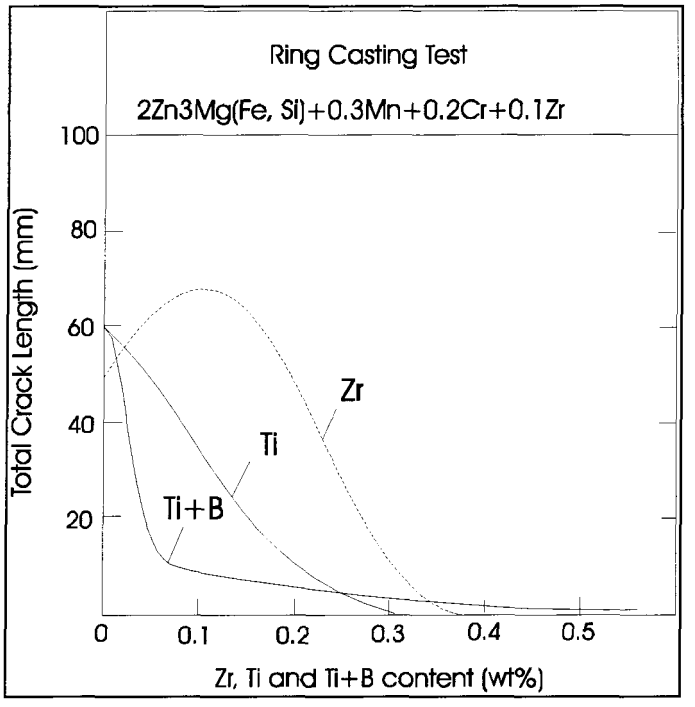

Figure 2.18. Effects of Ti+B, Ti and Zr additions on total crack length of Al-2%Zn-3%Mg synthesised-weld-metal alloy [41].

It can be observed that grain size was very important in determining the hot tearing behaviour of the alloy. Their examined results show that coarse columnar grained material was invariably more prone to tearing than fine equiaxed grained casting. It was explained that the size of the grain was important as it affected the mode of eutectic distribution. When the eutectic was present at the grain boundaries, it had the maximum effect on permitting free movement of the grains to accommodate the contraction of the casting. Consequently, hot tearing tendency was reduced. The finer the size of the primary grains, the greater was the probability of eutectic being present at their boundaries and, hence, the more likely it was for the thermal contraction to be accommodated by a slight general movement of the grains.

However, grain refinement is not always effective in reducing hot tearing susceptibility. Warrington and McCartney [42] have studied the effect of grain refiners Al-Ti and Al-Ti-B in 7010 and 7050 alloys. Without grain refining additions, columnar grain structures formed in both alloys which exhibited high tearing susceptibility. But, a high tearing susceptibility was still observed in both alloys even though an equiaxed grain structure was formed by using an Al-5wt%Ti-1wt%B grain refining master alloy. Similar results were obtained in Al-Mg alloy [9]. An increased cracking tendency over a narrow range of Ti contents was noted despite the fact that the grain structure was much finer and equiaxed (Figure 2.19).

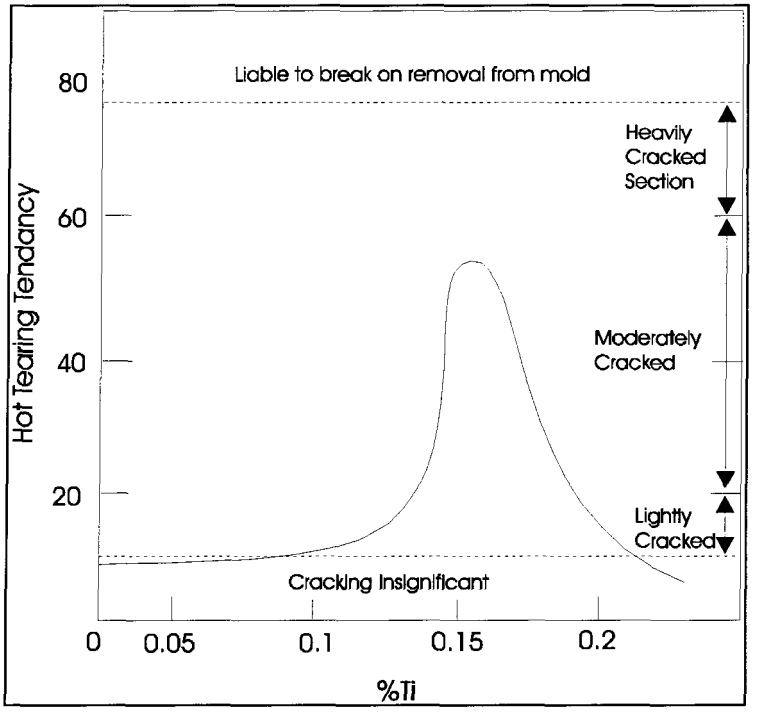

Figure 2.19. Hot tearing susceptibility versus Ti contents for Al-2wt%Mg alloy [9].

It has been recognised that some alloys that possess very fine and equiaxed grains still have much higher hot tearing susceptibility than other alloys that have coarse and columnar grains. One explanation was that grain refinement improved resistance to hot tearing not by making a casting "stronger" but by making it better to be able to accommodate local strains without formation of defects. If alloys have very low strength and ductility during the critical temperature range of solidification, grain refinement may not be sufficient to prevent hot tearing. Another explanation given was that many factors were related to hot tearing resistance of alloys, such as amounts of eutectic, second phases, etc., and their effect should also be considered with variation of the amount of grain refiners.

2.2.3 Metal Segregation and Second Phases

Small amounts of impurities may form low-melting eutectics with the base metal, which extends the life of the film stage. A classic example of such a case is that solidification tearing in steels is frequently associated with micro-segregation of certain elements [37, 43, 44, and 45], such as P and S. Both of them have relatively low partition coefficients in steel and tend to produce segregated interdendritic phases of low melting point. When the sulphur or phosphorus contents in plain carbon steel exceed the solid solubility limit, the hot tearing susceptibility of the alloys increases markedly.

Pumphrey and Lyons [36] carried out experiments to study cracking during both welding and

casting by using Ring Casting (RC) and Constrained Welding methods (CW) in six aluminium alloys. They found that for Al-Mn and Al-Fe binary systems, even though they had very similar phase diagrams with very short solidification intervals, Al-Mn alloys showed higher hot tearing tendency, while Al-Fe alloys exhibited very low hot tearing tendency using the RC method. This could be explained by means of microstructural analysis. The structure of the Al-Mn alloys was found to contain a second phase of $MnAl_6$ along the dendrites, it could weaken the boundaries and cause tearing [6].

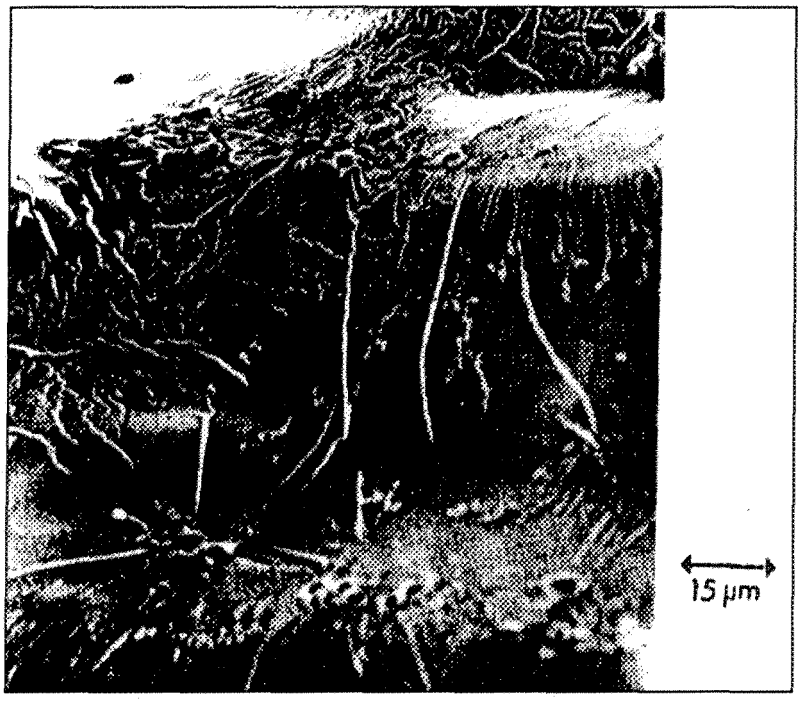

Figure 2.20. Fracture surface of an Al-0.05%Sn casting showing the decoration by tin-rich segregate [46].

Small additions of many alloying elements or impurities reduce the tearing resistance of pure metals by lowering strength and ductility of the semi-solid casting. This occurs because lower melting segregates form at the grain boundaries [46]. Figure 2.20 shows a fracture surface from an Al-0.05%Sn alloy casting. It can be seen that the surface is decorated with agglomerates of segregate materials, which were shown by microanalysis to be formed by almost pure tin. This segregate material was in the form of a thin liquid film at the time when interface separation took place. The role of micro-segregation in concentrating low melting-point material into the interdendritic region is further illustrated in Figure 2.21.

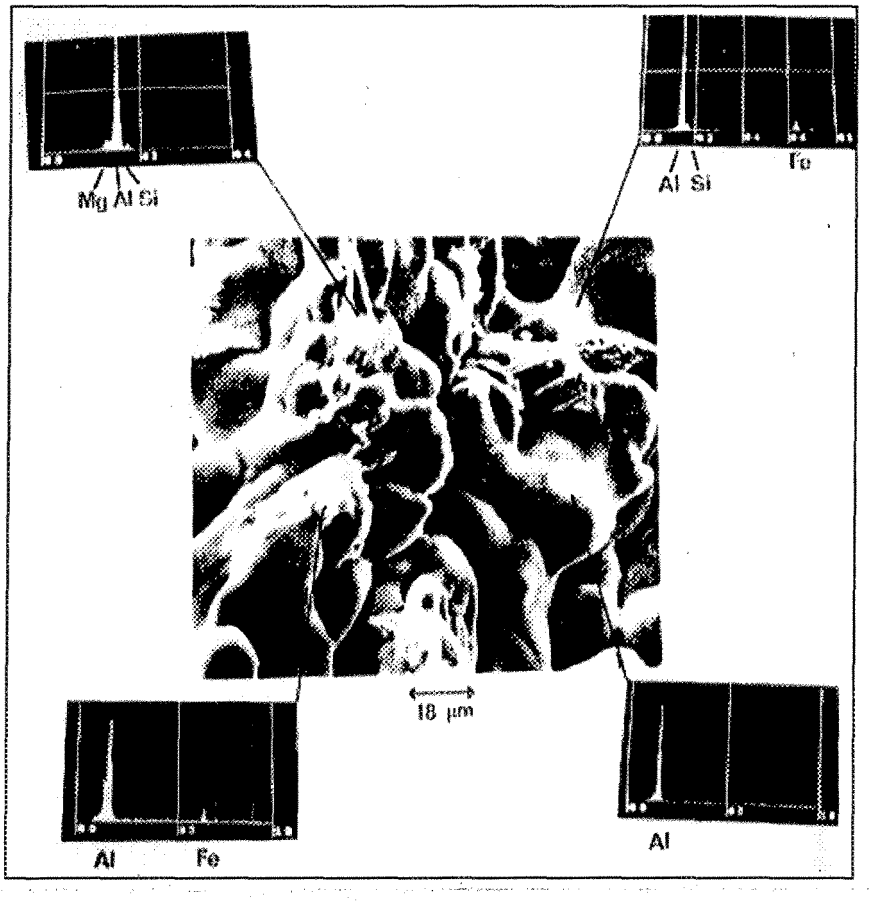

Figure 2.21. Fracture surface of an Al-3.0%Mg casting with the, X-ray analysis showing the segregates to be rich in Fe, (Mg+Si) and (Si+Fe) [46].

A higher concentration of solute is frequently found near the chill surface of DC cast ingot, which is commonly, called *inverse segregation* [47, 48]. Inverse segregation is a kind of micro/macro-segregation that has been to be caused by solidification contraction. Many experimental and theoretical studies have been performed on the formation of inverse segregation. A model for inverse segregation and porosity formation in directionally solidified aluminium alloys was given by Pousset et al [49]. It was found from their study that the fluid flow of solute-rich liquid in the mushy zone caused by solidification shrinkage is the main driving force for the formation of inverse segregation.

2.2.4 Gas Content

The effect of gas content has been studied using commercial alloy 424 and binary Al-Cu alloys which contain 4%Cu and 6% Cu [50]. Only the 424 alloy was found to have its hot tearing tendency to be evidently affected by the gas content in the melt in table 2-2. The explanation is that hydrogen rejected from solution during solidification sets up an internal pressure sufficient to force liquid eutectic into incipient tears to heal them. The gas bubbles that expand easily can also provide a volume change to compensate for solidification or contraction shrinkage, and reduce the development of stresses that could otherwise result in hot tearing.

An investigation [51] showed the two-fold effect of gas content in metals. It can improve the hot tearing resistance of alloys by driving residual liquid into tear gaps, and on the other hand, it can increase pinhole porosity in castings. Since excessive gas porosity can result in disadvantageous properties of castings, such as low strength, poor ductility, poor surface finish, etc., the use of increased porosity to reduce hot tearing is seldom used in the foundry practice [51].

Table 2-2. Result of Porosity and Hot Tearing Susceptibility of 424 Alloy with Different Gas Contents [50]

Gas Content	Void % (Copper die)	Void % (Sand Cast Test)	Hot Tearing Tendency
Nil	0.1	0.8	Torn
Moderate	1.1	1.7	Non
High	1.9	2.6	Non

2.2.5 Melt Superheat

It should be noted that process parameters, such as superheat, could influence the extent of tearing for a given composition. Clyne and Davies [9] utilised Electrical Resistance measurements to establish a relationship between the degree of tearing and melt superheat. Their results on Al-Mg alloys with different degrees of superheat are shown in Figure 2.22. It can be observed that when the superheat is high, the maximum value in hot tearing susceptibility curve is raised and moves to lower magnesium contents. The result indicates that hot tearing susceptibility is dependent both on composition and superheat of the metal.

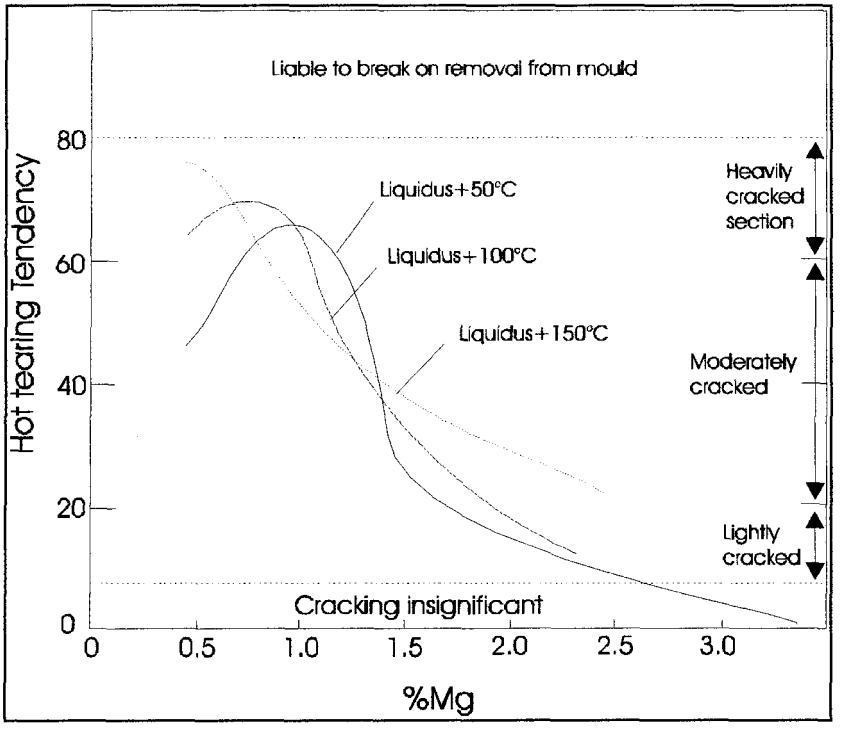

Figure 2.22. The variation of hot tear susceptibility of Al-Mg alloys with different super-heat [9].

Investigators [44, 52, and 53] declare that a higher superheat can increase the temperature gradients during solidification and result in the promotion of columnar dendritic growth. It has been discussed before that the alloys with columnar structures have higher hot tearing tendency than the alloys with equiaxed structures in normal situations. Therefore, higher superheat should be associated with a higher hot tearing tendency. However, the effects of superheat will really change with different test methods. Other factors in the casting process like metal fluidity, cooling rate, presence of grain refiners, and healing phenomena, etc., should also be considered. In order to understand how the metallurgical factors affect hot tearing susceptibility in different aluminium alloys. These factors are summarised in Table 2-3.

Table 2-3 A Summary of Factors that Affect Hot Tearing

Factor	Effects
Freezing Range	Low hot tearing tendency alloys usually have shorter freezing range, and high hot tearing tendency alloys usually have longer freezing range. However, high hot tearing susceptibility could occur in some shorter freezing range alloys because of other factors for hot tearing.
Type of Grain	Alloys with coarse columnar grains are usually more prone to hot tearing than the those with fine equiaxed grains. However, this is largely alloy dependent. Grain refinement can reduce hot tearing tendency of alloys. However, it is not always effective.
Amount and Distribution of Eutectic	Since stress accommodations and healing phenomena are more significant with increasing amount of eutectic, hot tearing tendency decreases with increasing amount of eutectic. If a small amount of eutectic were to extensively cover the solidifying grains, the alloy would obtain high hot tearing susceptibility because the thin liquid film weakens the grain boundaries during the solidification.
Metal Segregation and Second phases	Low-melting second phases could weaken grain boundaries by depressing the solidus temperature of the metal and prolonging liquid film life. Small additions of alloying elements or impurities reduce the tearing resistance of pure metals by lowering strength and ductility of semi-solid metal.
Melt Superheat	High superheat can promote columnar dendritic growth and result in high hot tearing susceptibility of alloys, however, it may also yield the opposite result because of variations of the other factors in the castings.
Gas content	Increasing gas content in the melt can reduce hot tearing susceptibility by facilitating interdendritic liquid infiltration or resistance to contraction, but is not used in practice.

2.3 Hot Tearing Tests

Various methods have been used to assess the hot tearing susceptibility of different alloys. A new classification scheme, subdivided according to the criteria used in each individual test facilitates

their comparability:

- Tests using visual techniques;
- Tests using mechanical techniques;
- Tests using physical methods; and
- Tests using mathematical modelling.

In this review, some discussions on possible developments of a global integrated evaluation technique for hot tearing are provided.

2.3.1 Tests Using Visual Techniques

Hot tearing which is formed during solidification from the residual liquid phase can extend to the surface of the solidified metal. It can be detected, as a rule, with a magnifying glass or sometimes with the naked eye. Tests using common visual techniques to detect hot tearing are:

- Ring Casting Test (RC) [1];
- Flanged Bar Test [6];
- Cylindrical Bar Casting Test [3];
- Ball-Bar Casting Test [55];
- I-Beam Casting Test [56];
- Chilled-Casting Test [42,57];
- C-bar Casting Test [58,59];
- "U" Casting [5].

The Ring casting test is one of the most simple and classic hot tearing test methods. It was introduced by a research group about fifty years ago [1]. It was adopted by many researchers for ferrous and non-ferrous alloys [60, 61, and 62]. The Ring mold used by Singer [1] was designed as shown in Figure 2.23. It consisted of a ring cavity in an open cast-iron mold made of a flat plate on which rested concentrically a ring and a core. The annular space between the ring and the core was used to cast the sample. The molten metal was poured readily into the mold to a height of about ¾ inch, and tensile stresses were set up by contraction of the cast metal ring around the core, which caused hot tearing to occur in the ring casting. Since the top of the mold is open, the whole process of solidification can be observed visually.

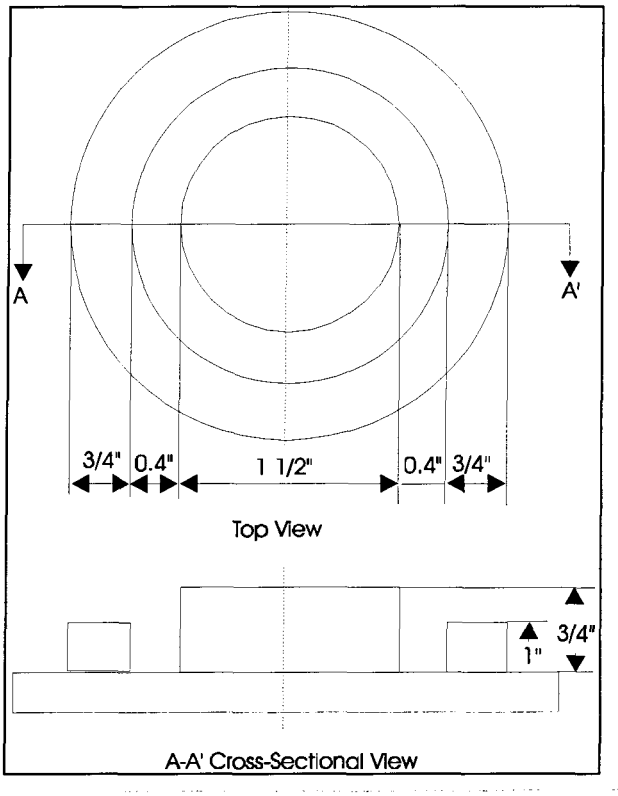

Figure 2.23. The design of Ring Casting mold [1].

The severity of hot tearing was evaluated numerically as the total length of cracks on the surface of the castings. This procedure has a disadvantage in that the width or depth of the cracks is not taken into account, but it has the merit of simplicity and appears to work quite well. Today, the Ring Casting method is still used in casting-houses and research projects.

Most tests are based on a version of the *Strain Theory* that the strain arising from the solid contraction of a portion of the casting is concentrated in a narrow hot spot. The hot spot may be localised at the junction of a runner (also riser or sprue) of the casting, or, more commonly, at the junctions of different cross sections of the castings. The majority of these tests do not, however, allow an easy alteration of the strain applied to the hot spot, and it is necessary to assess the severity of tearing by visual estimation of the length, width and extent of the tears.

From purely theoretical considerations, there are some opinions that Halls' tests [6] are the best according to the strain theory. The mold used in this test is a sand mold which employs flanged bars of different lengths containing a hot spot of constant dimensions in the middle of the bar. The solid contraction of the bar (the extent of which is determined by its length) is restricted by the flanges, and the resulting strain concentrated in the hot spot may or may not cause cracking. The minimum length of bar required to cause cracking is a measure of the hot shortness. It is true that the reliability of this is upset if ramming density, sand composition, etc., cannot be held constant [63].

A modification of Halls' design is an attractive and simple method developed by researchers at the MIT and it appears to work well [3]. The test pattern consists of a long thin cylindrical bar joined to

a heavier cylindrical section. The ends of the test pattern are restrained by flanges. Lengths of the thin cylindrical bars are increased or decreased in a series of tests so as to vary the severity of hot tearing, and the hot tearing tendency of each alloy is rated as the maximum length of test casting that can be made free of tears. The greater the length of the sound bar, the higher is the resistance to tearing. The design of the cylindrical-bar casting test is shown in Figure 2.24 [3]. As the thinner section cools below the temperature where it develops strength, it begins to contract. This will result in a strain at the point where the thin sections join the thick section. When the metal can no longer mass feed to the hot spot, the contraction strains pull the solid dendrites apart at this point, and the tears occur. The longer the bar where the tear occurred, the greater is the resistance of the alloy to hot tearing. The length of the bar without hot tearing can be used to measure hot tearing susceptibility.

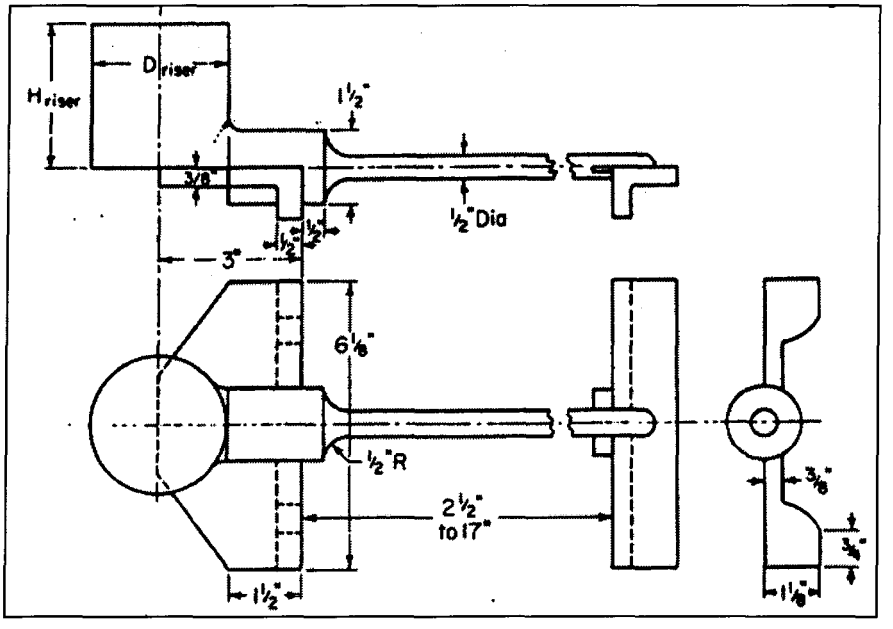

Figure 2.24. A schematic illustration of a Constrained Bar Casting mold [3].

There are other similar methods [55, 57, and 64], such as the Ball-Bar test and the I-Beam casting method. They also use the maximum length free from hot tearing to rate hot tearing susceptibility. The Ball-Bar Test Pattern and the I-Beam Casting mold are illustrated in the Figures 2.25 and 2.26 [55 and 56].

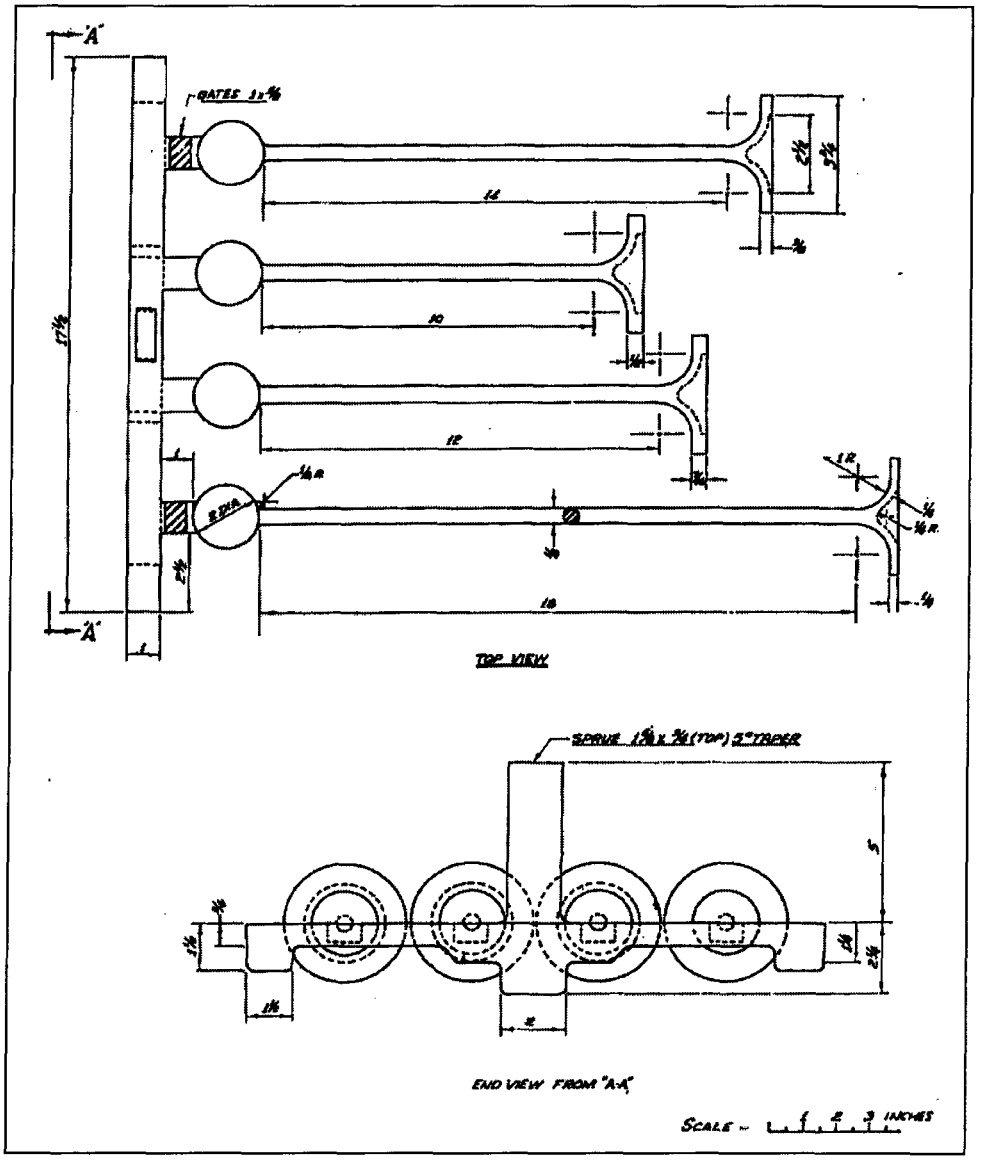

Figure 2.25. Ball-bar hot-tearing test pattern [55].

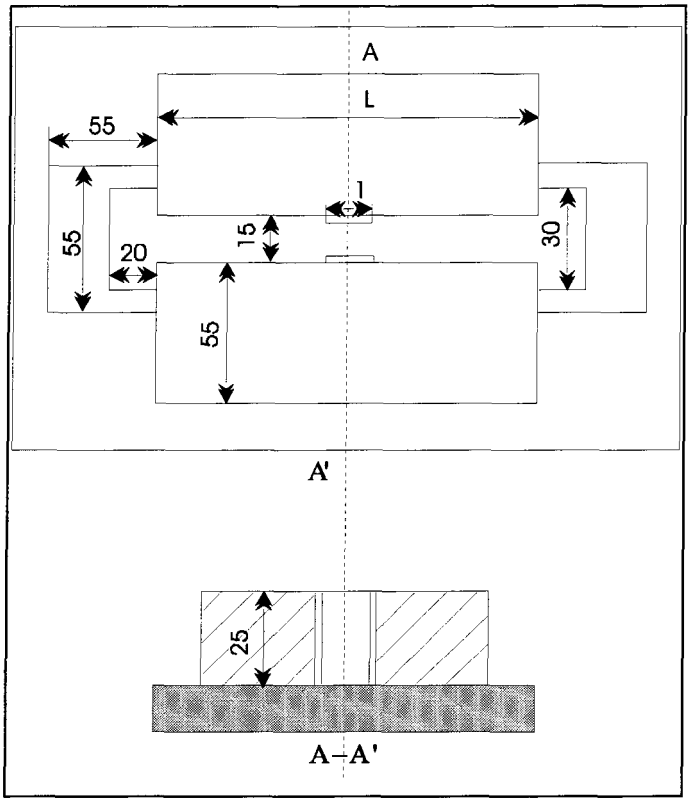

Figure 2.26. I-Beam Casting mold [56].

A method that can simulate DC casting is the Chilled Casting test [42 and 57]. The experimental conditions are reproducible and can be carefully controlled. The cooling rates in the test are similar to those in the shell zone of a DC-cast aluminium ingot. The test is likely to be particularly relevant to study the problem of shell zone hot tearing. It consists of an internally tapered steel crucible held in an open-ended tube furnace together with a separate water-cooled copper chill with a tapered conical portion as shown in Figure 2.27 [42]. The molten alloy under investigation is poured into the crucible and held at the desired temperature, then the chill is inserted into the melt to a pre-determined depth. Solidification occurs in a direction approximately

perpendicular to the chill surface. When freezing is complete the chill ingot is removed from the furnace. The cracking susceptibility is given by the maximum length of crack as a function of the test variables.

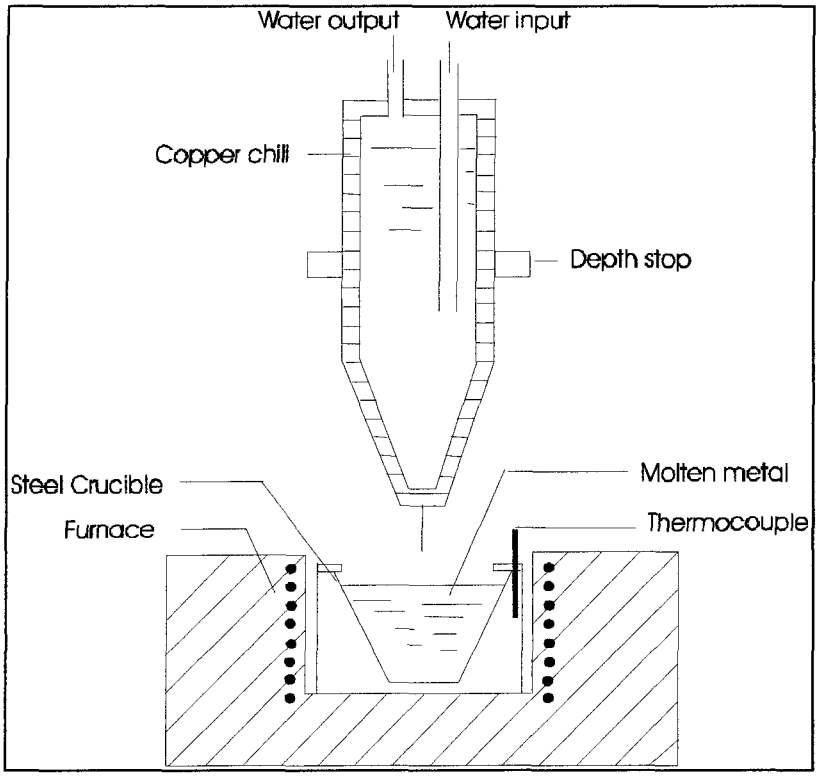

Figure 2.27. Schematic illustration of Chilled Casting test system [42].

Since so many factors can affect hot tearing susceptibility, quantitative measurement of hot tearing susceptibility is very difficult. Some early test techniques, such as the Ring Casting test [1], rely on the measurement of total crack length irrespective of crack severity. In Rosenberg's tests [4], numerous samples of different dimensions were cast and the susceptibility was measured in terms

of the maximum sample length cast without visible tears. It also has limitations such as its index for hot tearing sensitivity is not an absolute value and the results cannot be easily compared with those of other researchers.

E. J. Gamber [5] used a simple and reproducible test which is termed "U" casting to determine relative resistance to hot tearing of aluminium and magnesium alloys. A schematic representation of the casting is shown in Figure 2.28. He described the test as being capable of assessing a wide range of hot tearing susceptibilities, and that it possessed excellent sensitivity to small differences in hot tearing tendency. The test method is based on the fact that the probability for hot tearing to occur is the greatest at a sharp internal angle, and diminishes as fillet radius increases.

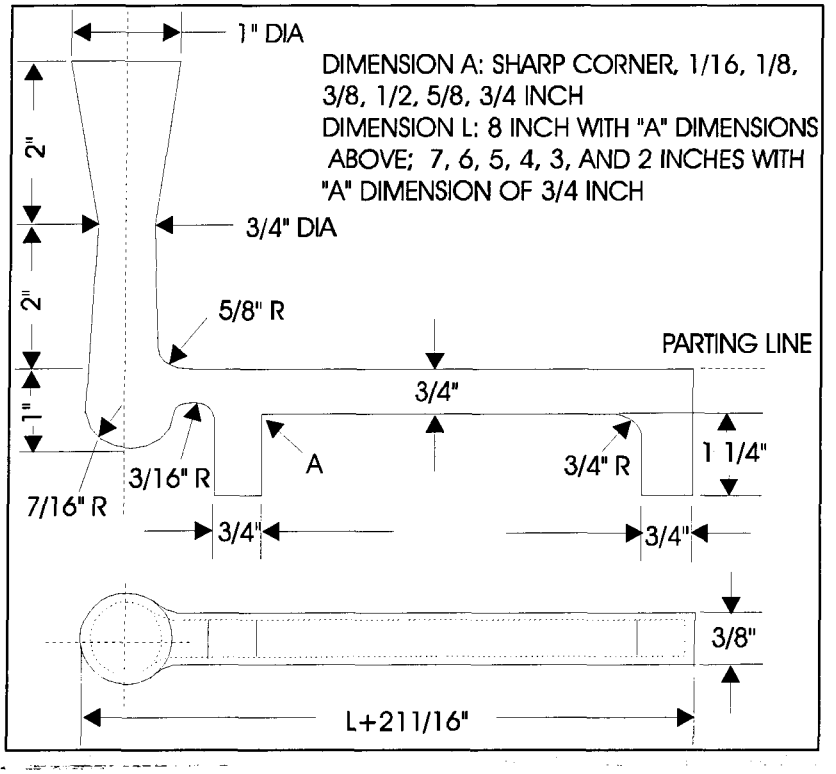

Figure 2.28. The design of the "U" Casting [5].

The rectangular cross section is 3/4 inch thick and 3/8 inch wide, and the length of the casting can be varied from 2 to 8 inches. Fillet radius is 3/4 inch at one end and varied at the other from 3/4 inch to a sharp corner. The severity of the test depends on both fillet radius and the length of the casting. The tendency to tear is more pronounced with smaller radius and greater length. The relationship between fillet radius, stress concentration and castability of L junctions is shown in Figure 2.29.

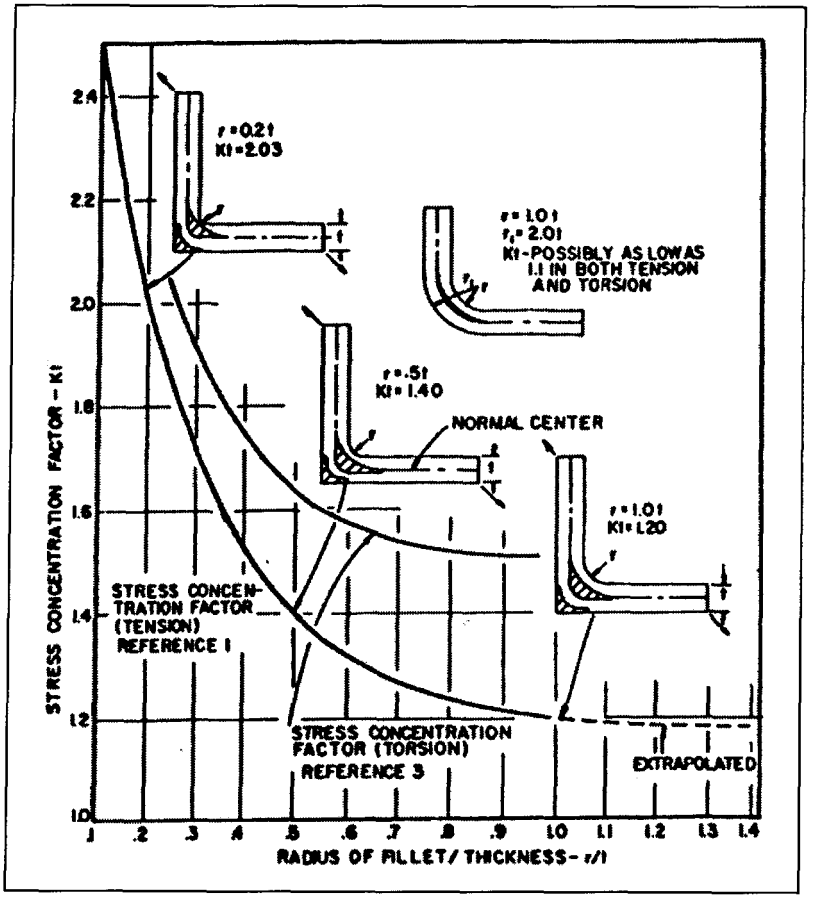

Figure 2.29. Relationship between fillet radius, stress concentration and castability of L junctions. Shaded areas at the fillets represent liquid metal pools [19].

A numerical rating system (Table 2-4) [19] was adopted in this test to eliminate the necessity of specifying length and radius dimensions in reporting test results. The rating indicating resistance to hot tearing is assigned to the alloys on the basis of the most severe condition tolerated without cracking. Higher hot tearing resistance of alloys is rated with a small value of Hot Cracking Rating which is characterised by longer bars of sharp corners exhibiting no tears under the casting conditions.

Table 2-4 Hot Tearing Rating System of "U" Casting [19]

Smallest Fillet Radius Not Cracked (inch)	Span Length, (inch)	Hot Cracking Rating
Sharp Corner	8	1.0
1/16	8	2.0
1/18	8	3.0
1/4	8	4.0
3/8	8	4.5
1/2	8	5.0
5/8	8	5.5
3/4	8	6.0
3/4	7	6.3
3/4	6	6.6
3/4	5	7.0
3/4	4	7.3
3/4	3	7.6
3/4	2	8.0
¾ Cracked	2	9.0

2.3.2 The Tests that Use Mechanical Techniques

From the previous section, it can been seen that visual measurements used in hot tearing tests have certain limitations. The severity of hot tearing is measured only by its length, and other parameters like the width and the depth of the tear are usually ignored. Furthermore, various test methods were developed by different researchers and hot tearing tendency was quantified by their own subjective indices or rating systems. This makes the comparison of the results of hot tearing tendency from different test methods an impossible task.

Researchers to study hot tearing, hence, used another approach. From the definition of solidification hot tearing, it is obvious that mechanical properties at temperatures within the freezing range are of great relevance to hot tearing susceptibility. If precise strength and strain of alloys can be measured at hot tearing temperatures instead of at room temperature, this would contribute to the development of a global integrated hot tearing test method. Such measurements are difficult to perform in general, but still many studies have been carried out to measure the mechanical properties of alloys at higher temperature ranges [34, 66, 67, and 68]. Four representative methods are:

- Tensile Test at Higher Temperature [24];
- Direct Chill Casting Tensile Test [68];
- Stress and Strain Measurement in "C" Shape Casting [58,59];
- Variable Tensile Strain Test [69].

Tensile properties of Al-Si alloys at temperature regions between the liquidus and solidus have been investigated using the apparatus shown in Figure 2.30 [24]. A Hounsfield tensile-meter was fixed with a motor drive for tensile tests. An eight-inch long resistance-tube furnace (isolated tube) was constructed so as to slide on the horizontal supporting columns of the tensile-meter and to enable the test pieces to be kept at high temperatures during testing. The mechanical test was carried out when the temperature of the test piece was higher than the solidus temperature. Traction was applied to the grips until the test piece was completely broken. The maximum strength of the test piece at the temperature above the solidus was read directly from the tensile-meter. From the tests, it was found that the strengths of the alloys were low at temperatures slightly above the solidus, and the brittle property of the metal at that temperature was also confirmed by the analysis of the fracture surface of the test pieces.

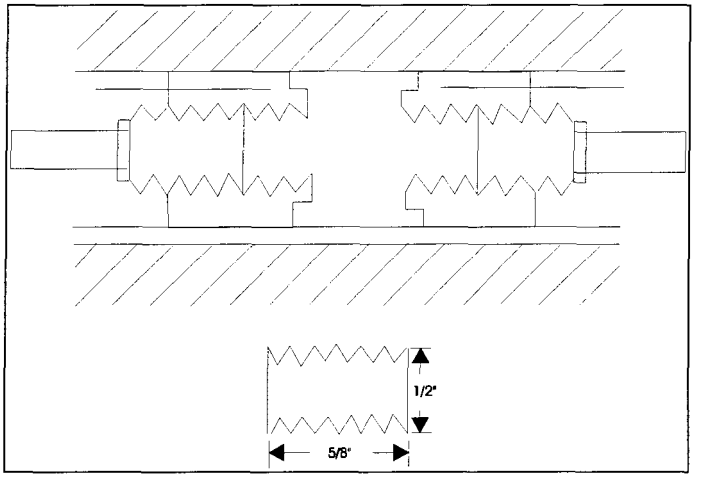

Figure 2.30. Apparatus of the tensile test of Singer and Cottrell [24].

Tensile tests needs to be performed on specimens which are simultaneously and continuously cooled and strained simultaneously to better simulate actual solidification conditions. A tensile test on direct chilled castings (Figure 2.31) [68] was carried out with Al-Si alloys. The metals were placed in the mold cavity and pulled at a series of temperatures during solidification. At the centre of the casting mold, a cylindrical core was placed to provide a slow cooling rate. Stainless steel bolts were inserted into each end of the mold cavity and fastened to components of the tensile testing machine. Chilling was provided by copper plates, which were placed around the top of the bolts. One thermocouple was inserted into the melt for temperature control. According to the results of tensile strength of alloys for different temperatures, hot tearing temperature of

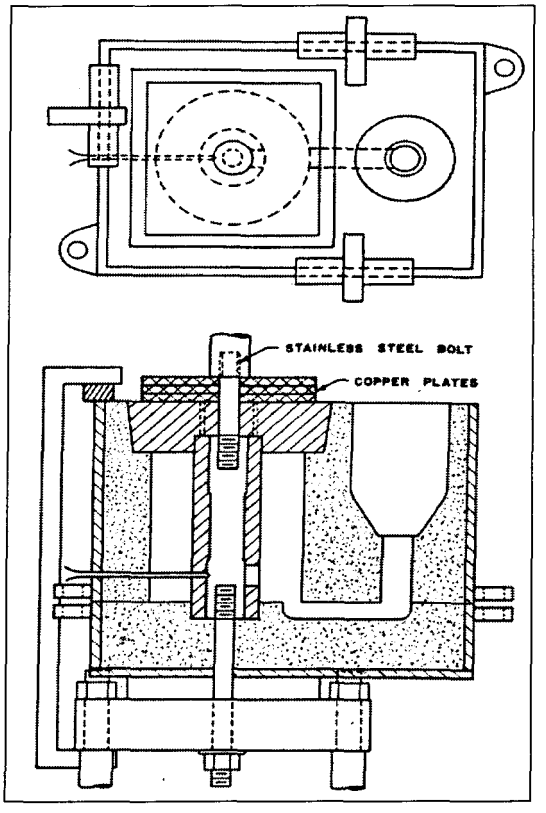

Figure 2.31. The design of direct cooling casting tensile test [68].

different alloys was determined. The tensile strengths of alloys in the hot tearing temperature range were determined using the maximum load on the metals. The experimental results showed that the ultimate strength values in the hot tearing temperature range varied consistently with phosphorus and other alloying contents.

A new test method [59] was declared to allow simultaneous measurement of stress (for a restrained casting) or strain (for a relaxed casting) of contraction during solidification. The apparatus is shown in Figure 2.32. It includes two components, a "C" shaped casting mold and a load unit. The mold consists of two copper arcs, A and B, which are hinged in the centre. The loads are produced in the restrained casting by the contraction which cause the movement of slit A-B. The loads are measured by strain gauges arranged in a Wheatstone Bridge and transferred to the load unit by the hinge at end between the two bars E and D. Using this equipment, the strain of metal during solidification can also be measured in a unrestrained casting by removing the C nut . A linear potentiometer between the two bars E and D can be measured, and the displacement of the bars can also be calculated.

Research had been carried out to study the interaction of strain rate and holding time of augmented strain by using a tensile strain test method (Figure 2.33) [69]. It was found that there was a minimum strain rate for crack initiation, and that the holding time of strain was more effective than the strain rate. It was also found that the crack length decreased with a decrease in holding time of strain and then reached a constant value. A qualitative explanation of the relationship between the strain rate and length of cracks in weld metals are shown in Figure 2.34 [69].

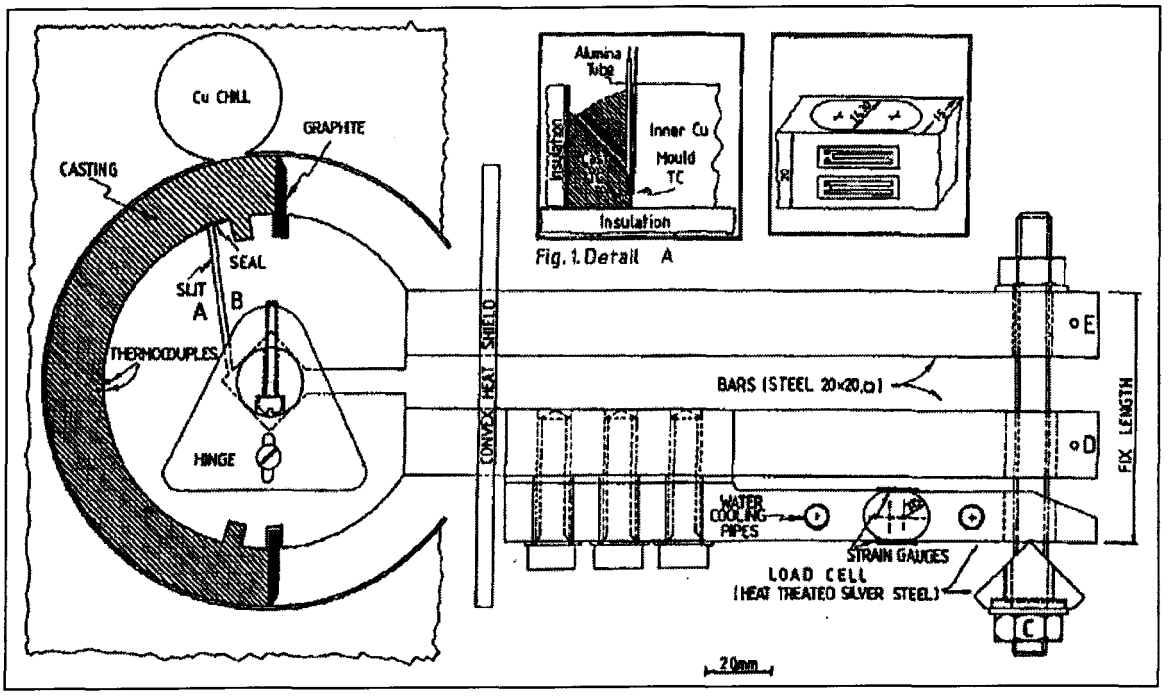

Figure 2.32. "C" shape casting mold and load unit [59].

2.3.3 The Tests Using Physical Methods

Basically, the subsurface hot tearing cannot be observed using visual methods, but can be detected with some physical methods. A casting is normally required to be crack free, that is, no cracks are to be detected using both visual and other physical methods. A few physical methods were used to measure hot tearing susceptibility. These are:

- Electrical Resistance Test [9 and 46] and
- Acoustic Emission Technique [8, 69, 70, and 71].

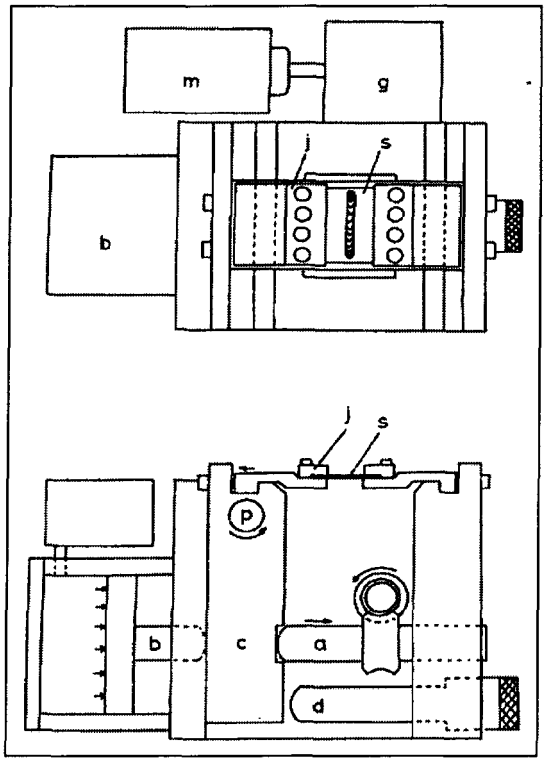

Figure 2.33. The tensile strain apparatus of hot tearing test in welding [69].

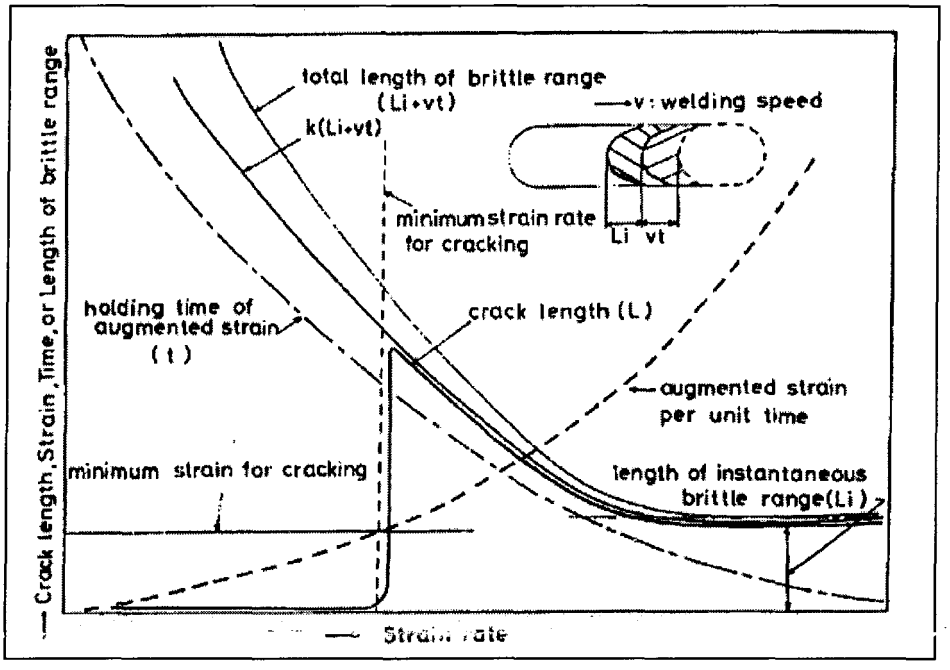

Figure 2.34. Qualitative explanation for strain rate dependence of crack length [69].

Electrical Resistance method involves the measurement of total cracks on the surface and subsurface (Figure 2.35) [9 and 46]. It measures the resistance across different locations on a cast sample. A steel mold which is water-cooled at both ends is placed beneath an inductively heated graphite crucible that contains the alloy to be cast. The experimental arrangement is shown in Figure 2.35 [9] and the lay-out for the resistance measurement is shown in Figure 2.36 [9].

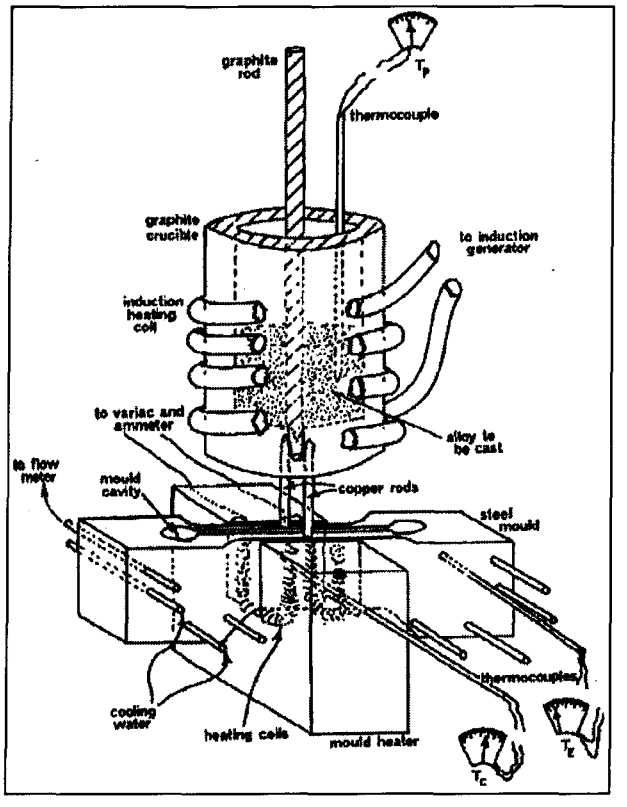

Figure 2.35. The experimental set-up of Electrical Resistance test [9].

The reduction in cross-sectional area from the initial value to the final value due to cracking, expressed as fractional area of cracking, X_{cr}, is related to the measured resistance. It can be expressed as

$$X_{cr} = 1 - \frac{R_{40}^{av}}{2\left(R_{100}^{av} - 2R_{40}^{av}\right)} \tag{2.3}$$

where R_{100}^{av} and R_{40}^{av} are the average resistance readings for the 100 mm and 40 mm lengths, respectively. This gives $X_{cr} = 0$ for a completely uncracked section and $X_{cr} = 1$ for a completely cracked section. Thus, the electrical measurement can be considered to be a sensitive measurement of cracking susceptibility. Clyne and Davies [9] have used this method to measure hot tearing tendency in Al-Mg alloys. The results were broadly in agreement with those reported by Pumphrey and Lyons [36] obtained using the Ring Casting tests.

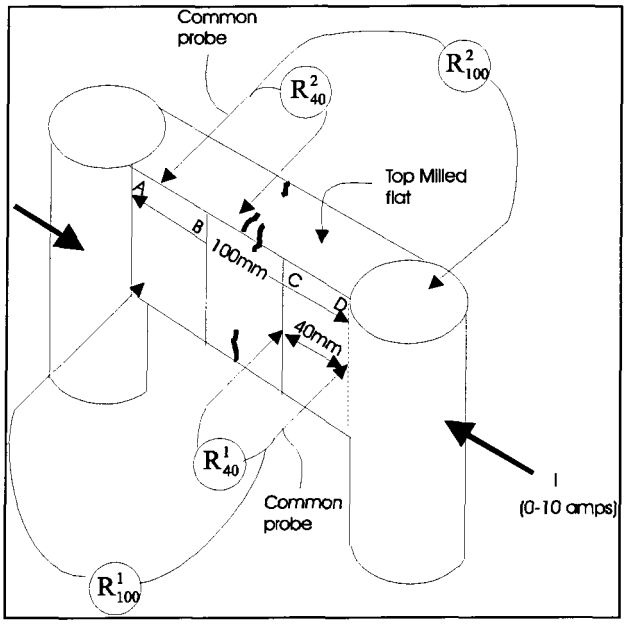

Figure 2.36. The layout of the measurement of electrical resistant [9].

Acoustic Emission (AE) [8, 69, 70, and 71] is a term describing a phenomenon in materials where transient elastic waves are generated by a rapid release of stored energy. These waves can be generated by a localised source, and are transmitted through the material and detected by a transducer that converts the waves to a voltage. Recently, AE techniques have been used in solidification studies and metal casting to detect casting defects such as hot tearing and hot cracking.

The apparatus for AE measurement used by Oya et al, is shown in Figure 2.37 [8]. The I-Beam Casting mold was used in this investigation. Purvis et al also used AE techniques to study the crack formation in a restrained bar casting of 319 aluminium alloy [71]. This casting mold had been previously used by Rosenberg et al. [4] for the investigation of hot tearing in a number of alloys. AE signals were obtained with a highly sensitive test apparatus. The characteristic of the AE signal being investigated is the Root Mean Square (RMS) voltage value. A typical result obtained from their investigation is displayed in Figure 2.38 [71]. In this figure, there could be seen a sharp increase in the RMS voltage value during the expected time of a hot tearing formation, as well as smaller peaks during primary Al and eutectic solidification. The RMS value can be further quantified for correlation with the energy released upon solidification and formation of other defects.

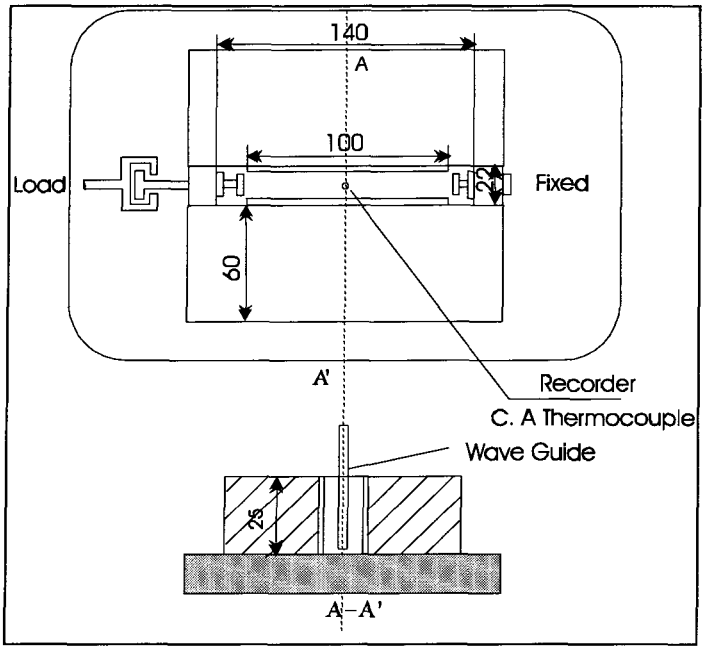

Figure 2.37. Schematic representation of the test apparatus for obtaining Acoustic Emission signals used by Oya et al [8].

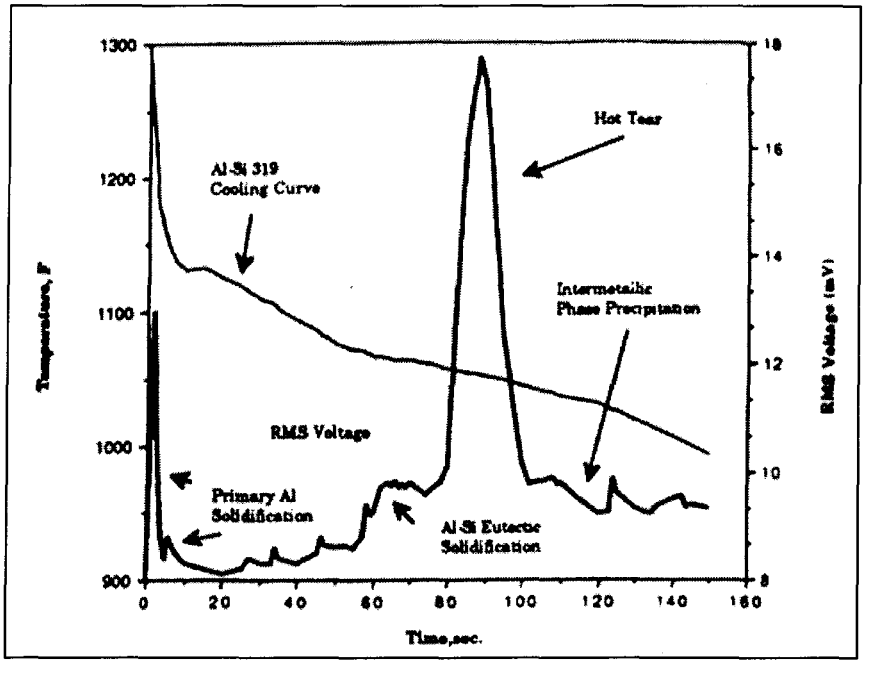

Figure 2.38. An example of the results obtained from the RMS voltage of the Acoustic Emission signals plotted by Purvis et al [71].

2.3.4 Mathematical Modelling of Hot Tearing

Computer simulation of casting processes has begun to play an increasing role in assisting foundry engineers in the cost-effective selection of design and process parameters. Most casting simulation programs contain modules for mold filling and solidification. They can assist in the prediction and elimination of porosity, shrinkage cavity, and inverse segregation, as well as hot tear and hot crack defects [72, 73, and 74]. Some mathematical and computer models have been used to predict hot tears and hot cracks in different casting processes. These are:

- Mathematical Model for Prediction of Hot Tears in Castings [10];
- Mathematical Model for Hot Cracking of Aluminium Alloys during DC Casting [11];
- Model Simulating the Formation of Thermal Stresses in DC Casting of Al Alloy [75];
- Model Simulating the Formation of Thermal Stresses in DC Casting of Aluminium Slabs: Application of a Finite Element Model [76].

Based upon experimental investigations, theories have been proposed to explain the occurrence of hot tears in castings. Based on Pellini's strain theory [20], a Finite Element (FE) based computer simulation method and a mathematical model for the prediction of hot tears in castings have been developed [10]. There are two major parts in this approach: (1) prediction of grain size and thickness of the liquid film around solid grains at various stages of solidificaion; (2) development of a stress model based on hot tear or fracture criterion. A hot tearing susceptilibility coeffficient was given as:

$$CSC = \frac{t_v}{t_r} \tag{2.4}$$

where t_v is the vulnerable time period for cracks to spread, and t_r is the time available for stress relaxation. Cambell [77] modified this original criterion, and developed a mathematical model for the susceptibility to hot tearing as given below:

$$CSC_b = \frac{\alpha \Delta T L a t_v}{l^2 t_r} \tag{2.5}$$

where ΔT is the solidification interval, L is the overall length of the casting, a is the grain size, α is the coefficient of thermal expansion, l is the length of the hot spot measured in the direction of strain for a one dimensional case, t_v is the vulnerable time period for cracks to spread, and t_r is the time available for stress relaxation mechanisms such as liquid and mass feeding.

A mathematical model to calculate the hot tearing tendencies during DC casting was given by Katgerman [11]. The model combines a new simplified thermal model for DC casting with the theoretical considerations of Feurer [78] and of Clyne and Davies [46]. The combination of both concepts with DC casting process of aluminium alloys makes it possible to calculate hot tearing tendency as a function of casting speed, ingot diameter, and alloy composition. In order to determine solidification time and fraction solid as a function of the distance along the ingot, a simplified heat flow model was developed as given below:

$$\frac{\delta T}{\delta t} = \alpha V^2 T - v_c \frac{\delta T}{\delta z} = 0 \tag{2.6}$$

where z is the distance along the axis of the ingot (m), T is the temperature of the ingot (°C), v_c is casting rate (m/s), and v is the volume of the ingot (m^3).

Applying this heat flow model to the DC casting process, Katgerman [11] defined a hot cracking index as the ratio of the time intervals during which interdendritic separation occurs. The hot tearing index can be expressed as

$$H.C.=\frac{(z_{99}-z_{90})}{(z_{90}-z_{40})} \tag{2.7}$$

where Z_{99}, Z_{90} and Z_{40} are the distances (m) along the ingot axis. When after feeding is considered, the vulnerable time proportionality changes from (Z_{99} -Z_{90}) to (Z_{99} - Z_{cr}), a hot tearing index can be defined as:

$$H.C.=\frac{(z_{99}-z_{cr})}{(z_{90}-z_{40})} \tag{2.8}$$

where Z_{cr} is the distance after which feeding is inadequate.

To make it more agreeable with experiments, the model was improved to take into account the coherence temperature. The hot tearing index can then be written as:

$$H.C.=\frac{(z_{99}-z_{cr})}{(z_{90}-z_{coh})} \tag{2.9}$$

where Z_{coh} is the distance along the axis of the ingot.

A hot tearing index can be calculated by using the three equations (Eqs. 2.7, 26, and 2.9) given above. Relative to Equation (2.9) hot tearing tendencies of binary Al-Mg alloys were obtained. The results are shown in Figure 2.39 together with experimental results.

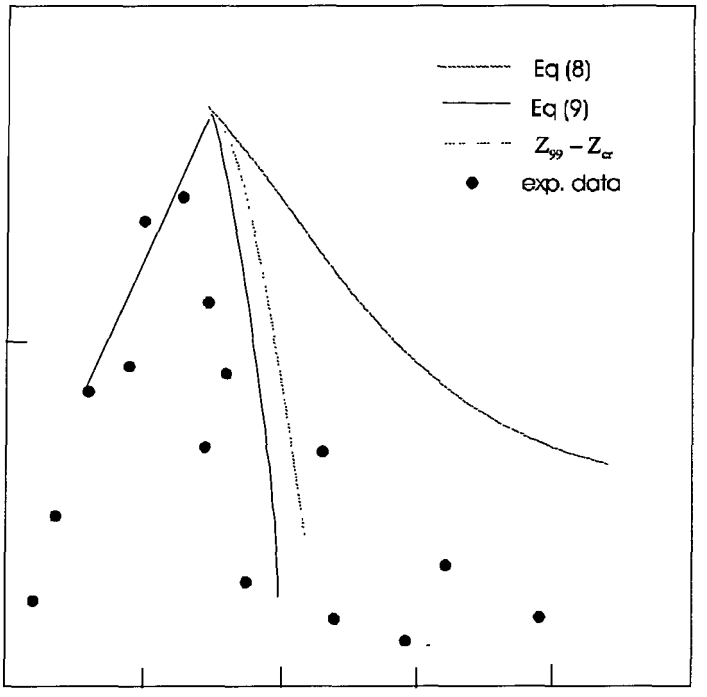

Figure 2.39. The calculated and experimental results of hot tearing tendency of Al-Mg alloys [11].

Moriceau [75] studied thermal stresses in DC casting of Al alloys by a finite difference method with an elastic-plastic model. Figure 2.40 show the temperature isotherms and computed stresses in an ingot of 2014 alloy [75]. It can be seen that highest stress occurred during solidification at the surface of the ingot.

Thermal stresses in DC-cast aluminium ingots had been studied using a Finite Element Method (FEM) [76]. The calculated deformation of the ingot was found to be in good agreement with experimental measurements. The location of the maximum computed principle stress gives a good indication of the position in the ingot where hot tears are likely to occur. A conclusion was also drawn that hot tears usually occur at the chill surface of DC cast ingots.

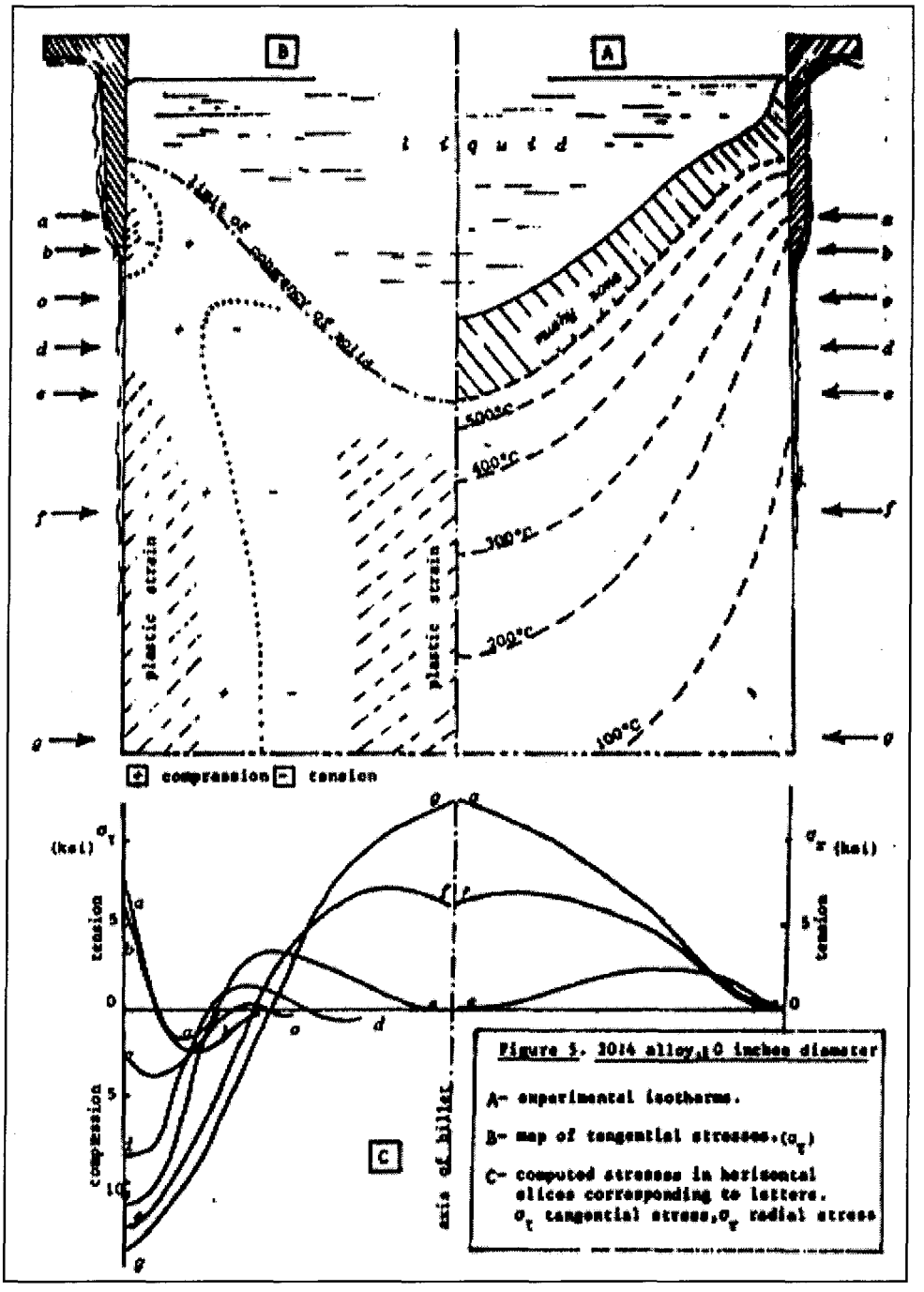

Figure 2.40. The temperature isotherms and computed stresses in an ingot of 2014 alloy [76].

CHAPTER III EXPERIMENTAL PROCEDURE

3.1 Materials

3.1.1 Commercial Wrought Aluminum Alloys

Four commercial wrought aluminum alloys from four different series, 1xxx, 3xxx, 5xxx, and 6xxx were selected for this present investigation (Table 3-1). The choice was made based on the observations of hot tearing behavior of these alloys in the industry. This was based on the fact that, in DC-casting of aluminum ingots, the alloy AA6111 exhibits a high tendency of hot tearing while the AA1050 alloy has a low susceptibility to hot tearing. The 3xxx and the 5xxx series alloys are noted to exhibit intermediate hot tearing susceptibility. All the aluminum alloys used in this work were supplied by Alcan International Limited. The chemical compositions of the materials are given in Table 3-1.

Table 3-1 The Chemical Compositions of the Alloys (Non-Grain Refined)*

Alloy	Cu	Fe	Mg	Mn	Ni	Si	Ti	Zn
AA1050	0.004	0.32	0.01	0.017	0.002	0.08	0.012	0.0025
AA3104	0.039	0.22	0.1	0.35	0.006	0.08	0.015	0.004
AA5182	0.039	0.22	4.87	0.34	0.006	0.09	0.014	0.004
AA6111	0.7	0.22	0.69	0.19	0.001	0.59	0.098	0.001

3.1.2 Grain Refiner

It has been proven that alloys solidifying with different grain sizes may have different hot tearing susceptibilities. Some experiments were, therefore, carried out with the four alloys in the grain refined condition.

A master alloy supplied to Alcan by KB Alloys Inc. was used in this investigation. The composition of the master alloy is shown in Table 3-2. Addition levels of grain refiners ranging from 0.001 to 0.01wt%Ti were employed for the AA1050 alloy (Table 3-3). Other alloys were tested with a single addition level of 0.01% Ti (Table 3-3).

Table 3-2 The Chemical Composition of the Master Alloy

Element	Ti	B	V	Si	OE (each)	OE (total)	Al
Master alloy	5.1	1.0	0.01	0.18	0.03	0.10	rem

Table 3-3 The Addition Ti Levels and Ti Contents in Gran refined Alloys

Alloy	Target Grain Refinement Addition	Actual Ti Content after Grain Refinement
AA1050	0.001% Ti 0.002% Ti 0.01%Ti	0.0035% Ti 0.0045% Ti 0.012% Ti
AA3104	0.01%Ti	0.014% Ti
AA5182	0.01%Ti	0.014% Ti
AA6111	0.01%Ti	0.011% Ti

3.1.3 Al-Si Binary Alloys

In order to investigate the hot tearing susceptibility of a binary alloy, experiments were carried out on pure aluminum with different levels of silicon additions. The compositions of the Al-Si binary alloys used are given in Table 3-4. The alloys were prepared using commercial purity, aluminum (99.7%) supplied by Alcan International Ltd. and commercial purely Si supplied to Alcan by SKW Canada.

Table 3-4 The Chemical Composition of Al-Si Binary Alloys

Al + Si%	Cu	Fe	Mg	Mn	Ni	Si	Ti	Zn
0.5%Si	0.002	0.06	0.001	0.001	0.001	0.055	0.002	0.001
1%Si	0.001	0.05	0.001	0.001	0.001	0.99	0.002	0.001
1.5%Si	0.001	0.06	0.000	0.001	0.001	1.5	0.002	0.001
2.0%Si	0.001	0.06	0.000	0.001	0.001	1.94	0.002	0.001
3.0%Si	0.001	0.06	0.000	0.001	0.001	2.89	0.002	0.001

3.2 Constrained Rod Casting Method

3.2.1 The Constrained Rod Casting (CRC) Mold

The CRC mold used in this study was designed at the Alcan International Ltd. Kingston Research & Development Center (KRDC). It is a permanent mold made of cast iron (Figure 3.1). The mold cavity is capable of producing four cylindrical constrained rods with the lengths of 2″ (bar A), 3.5″ (bar B), 5″ (bar C), and 6.5″ (bar D) and 0.5″ diameter. The bars are constrained at one end by a sprue and at the other end by a spherical riser (feeder) of 0.75″ in diameter. The cylindrical

rods are separated from each other by a distance of 1.5″ center to center. The melt is fed to the rods through a 7″ long sprue.

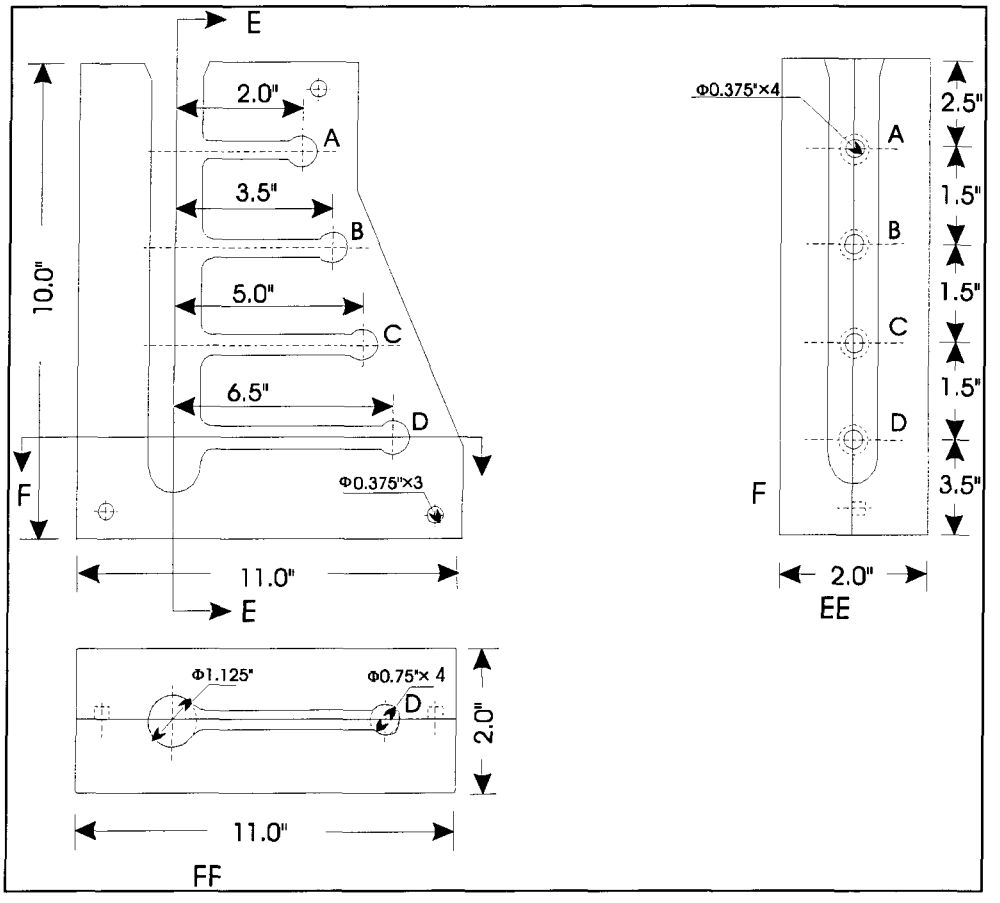

Figure 3.1. A schematic illustration of the CRC mold.

Preliminary experiments were carried out with the CRC mold placed vertically during casting. The test samples did not exhibit good reproducibility. In order to ensure that the mold cavities were well filled, and to reduce casting defects such as filling shortages, shrinkage cavity, gas

porosity, or inclusions in the constrained bars, the mold was set up with a 17.5 degree inclination from the vertical. As a result, the samples showed better reproducibility. To further eliminate variations with the mold, the mold cavity was cleaned and the mold was heated to 200°C and coated with graphite for each test. The mold was preheated to and held at 250 °C for 2 hours before casting. The castings were removed from the mold after the top of the sprues was completely solidified. The mold was cooled to 250°C before the next sample was cast (mold heats up with each casting). During the experiments, mold temperatures were monitored with a thermocouple, which was embedded in or on the surface of the mold.

3.2.2 Melting and Casting

For each experiment, about 8.5 kg of alloy was melted in a SiC crucible. The inner surface of the crucible was coated with a layer of refractory coating to avoid melt crass-contamination. Two furnaces were needed in each test, one for melting the metal and the other one for preheating the mold. The furnace used for melting was a PYRADIA electric resistance furnace with a power source of 6 kw. The advantages of this furnace are rapid melting of the alloy and effective temperature control.

Before casting, the liquid melt was filtered and degassed. Filtration was carried out at about 100°C higher than its liquidus temperature through a 13 mm thick ceramic foam Al_2O_3 filter (20ppi). The melt was filtered into another crucible, which was preheated at 750°C, and then

returned to the furnace. After the melt temperature reached the present pouring temperature, the melt was degassed by bubbling argon through the melt with a mechanical propeller at a rotation speed of 120 rpm for 20 min.

The pouring temperature was 120°C above the liquidus. The castings were removed from the mold after the tops of the sprues were alloyed to completely solidify. During the experiments, the melt temperature in the ladle was also monitored using a thermocouple (Figure 3.1). In each experiment, it took about fifty minutes to cast ten sets of samples. The melt surface was protected against hydrogen absorption by a tube bringing Ar Gas. Two samples for chemical analysis were taken at the beginning and the end of the each experiment. The casting set-up is schematically shown in Figure 3.2. For each alloy, three experiment runs were carried out; and a total of thirty castings were poured. Since the casting parameters usually become stable after the first three castings in each test, the four castings that were analyzed for hot tearing susceptibility of the alloys were generally chosen from the subsequent castings, which had the more reproduce casting parameters.

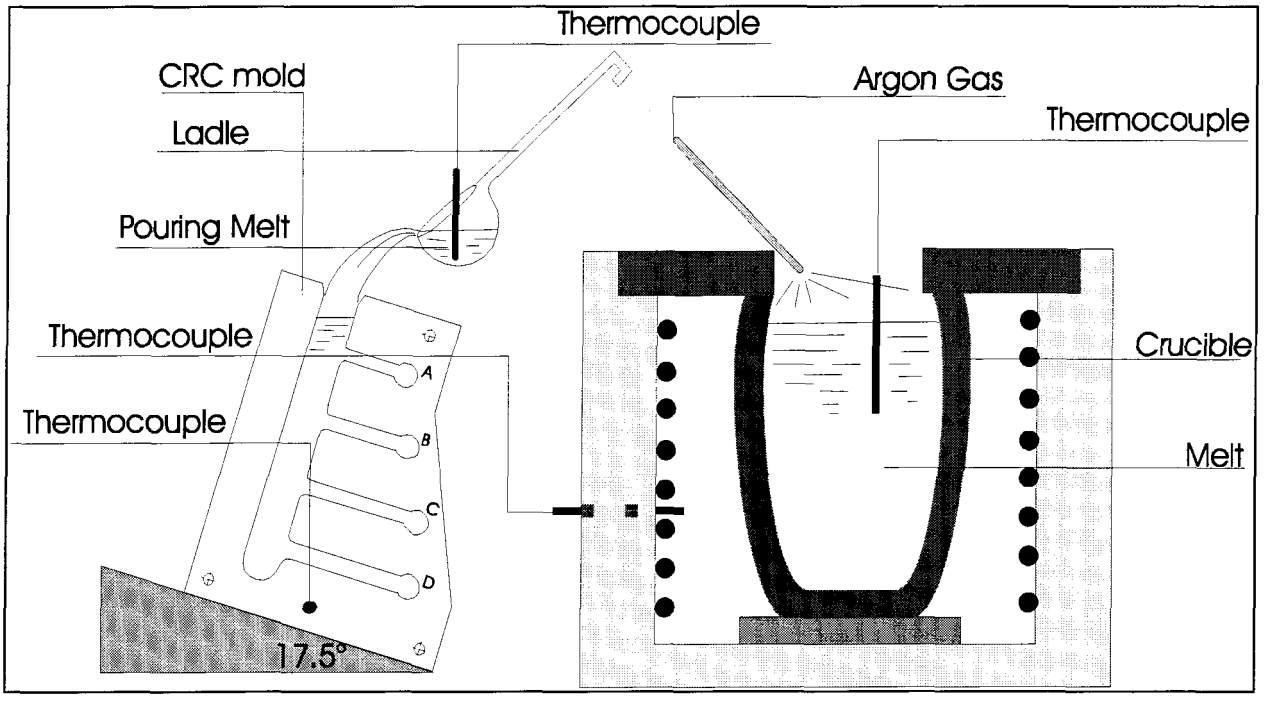

Figure 3.2. A schematic illustration of the CRC mold casting process.

3.2.3 Grain Refinement

Identical experimental conditions were used in the tests conducted with and without grain refinement. The grain refiner (master alloy) was added 10 min before casting. The melt was stirred in order to accelerate the dissolution and to disperse the titanium borides in the molten metal. This was done carefully so as not to extensively disturb the oxide layer on the melt surface. For each wrought aluminum alloy, two tests were carried out with each level of grain refinement. Ten castings were poured in each test.

3.2.4 Preparation of the Al-Si Binary Alloy

About 8.5 kg of purity commercial aluminum was melted in a SiC crucible. The required amount of pure silicon was added into the melt one hour before casting. The melt was degassed for twenty minutes using argon. The pouring temperature of the melt was chosen to be 120°C above the liquidus of the alloy. For each Al-Si binary alloy, one single experiment was conducted, in which ten castings were poured. Experiments with different alloys were carried out with the procedure shown in Table 3-5.

Table 3-5 Experimental Procedure of CRC Casting Method

Order	Procedure
1	Coat the mold with graphite;
2	Preheat mold to 250°C;
3	Set melt temperature at 120°C above the liquidus of the alloy;
4	Set up the mold at 17.5° tilt angle;
5	Filter the melt with Al_2O_3 filter (not for binary alloys);
6	Prepare Al-Si binary alloy;
7	Degas the melt;
8	Add grain refiners;
9	Keep the argon gas flow on the surface of the melt;
10	Take first sample for chemical analysis;
11	Cast ten samples;
12	Take second sample for chemical analysis;
13	Reject the first three and the last cast sample.
14	Discard the two samples with the highest and the lowest value of hot tear severity, and select the remaining four castings for analysis;
15	Record observations.

3.3 Hot Tearing Indices

Cracks on different bars were inspected visually with the naked eye. Five categories of hot tear severity are described below; and photos of hot tears of different severities are shown in Figure 3.3.

- Not Cracked: a casting that appears to be crack free;
- Hairline Crack: a hairline crack that extends over approximately half the circumference of the bar;
- Light Crack: a hairline crack that extends over the entire circumference of the bar;
- Severe Crack: a crack that extends over the entire circumference of the bar;
- Complete Crack: a complete or almost completely separation of the bar.

Two indices were used to quantify hot tear sensitivity of the alloys. The first one is called Hot Tearing Sensitivity (HTS) index. To obtain this index, first, each category of crack severity was assigned a numerical value (C) shown in Table 3-6. Then, bars of different lengths were each given a different numerical value as listed in Table 3-7. The numerical values of the bars were given based on the fact that, the longer bars were less resistant to hot tearing than the shorter ones.

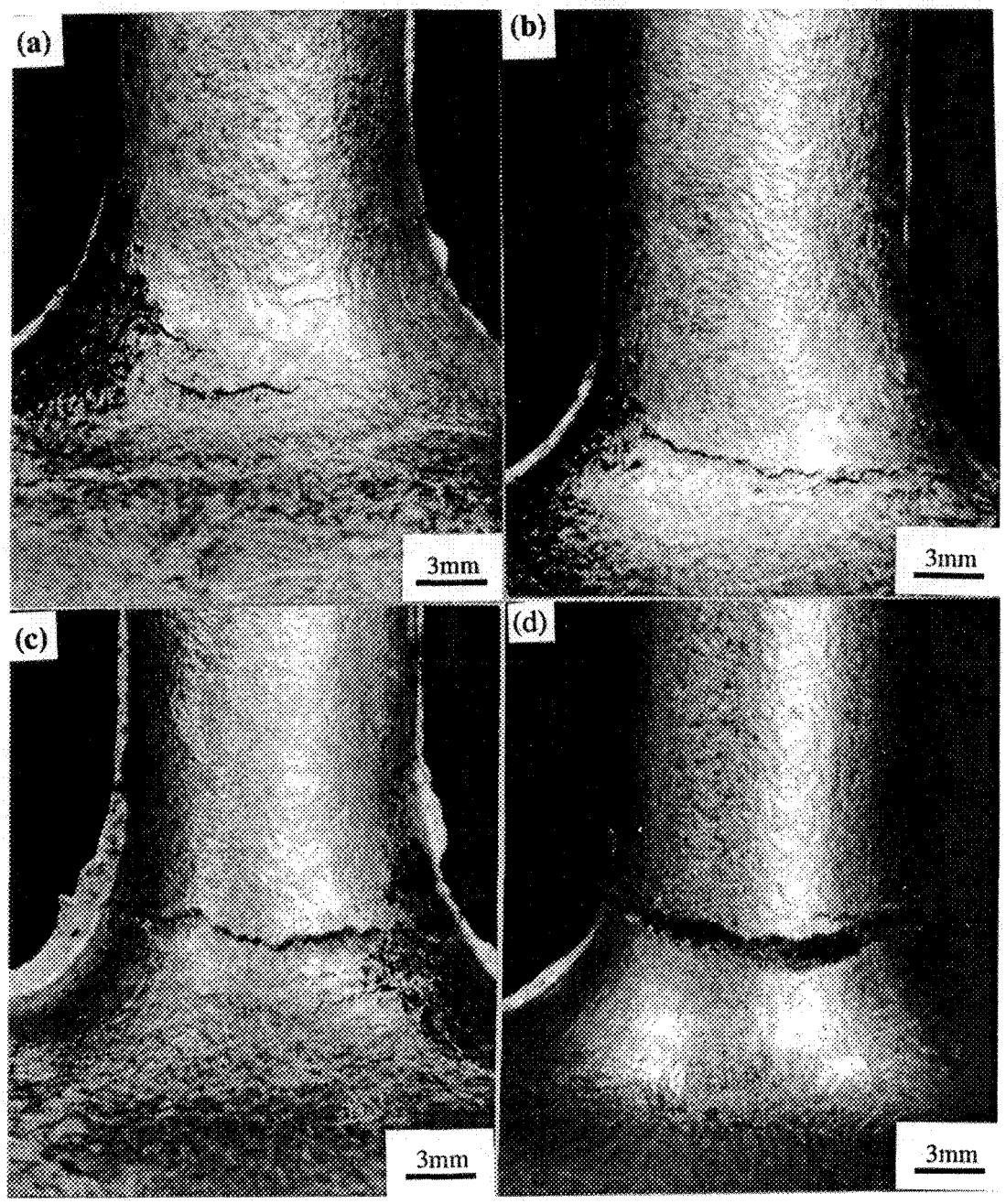

Figure 3.3. Photos of typical hot tearing with different levels of severity: (a) hairline crack, (b) light crack, (c) severe crack, and (d) complete crack.

Table 3-6 The Numerical Values C_i that Represent Crack Severity

Categories	Numerical Value (C_i)
Complete Crack	4
Severe Crack	3
Light Crack	2
Hairline Crack	1
No Crack	0

Table 3-7 The Numerical Values L_i that Represent Bars of Different Lengths

Bar Type (length, inch)	Numerical Value (L_i)
A (2.0)	4
B (3.5)	3
C (5.0)	2
D (6.5)	1

The value of HTS for a sample is given by

$$HTS = \sum_{i=A}^{D} (C_i \times L_i) \tag{3.1}$$

where C is the assigned numerical value for the severity of crack in the bars, L is the assigned numerical value corresponding to the length of the bar, and i represents the bars A, B, C, and D. Table 3-8 gives an example of the calculation of HTS for the AA6111 alloy. The HTS value for the alloy is the average value of the four castings that were selected from an experiment producing a total of ten castings.

Table 3-8 The Results of HTS Evaluation for the AA6111 Alloy

Test No.	$C_A \times L_A$	$C_B \times L_B$	$C_C \times L_C$	$C_D \times L_D$	HTS=$\sum (C_i \times L_i)$
1	1×4	3×3	4×2	4×1	25
2	1×4	3×3	4×2	4×1	25
3	1×4	3×3	4×2	4×1	25
4	1×4	3×3	4×2	4×1	25
Avg.	4.0	9.0	8.0	4.0	25.0

Using the HTS index described above, a second index, in the form of a footprint chart was developed to describe graphically the hot tearing susceptibility of the alloys. A foot print chart is shown in Fig 3.4, in which each axis represents one bar of the sample. The value in each axis is the multiplication of the average numerical value associated with the crack severity on one bar and the numerical value of that bar ($C_i \times L_i$). The area S represents the global hot tearing susceptibility of the alloy. From a footprint chart, it can easily be seen whether or not hot tearing has occurred on one particular bar and the severity of that tear.

The calculation of the S value for the foot-print chart is similar to the calculation of HTS value. The average S value of the shaded area can be calculated for each casting according to $C_i \times L_i$ values of four bars. The average S value of the casting (four castings for each test) was calculated and compared. The alloy with a greater S value has a higher hot tearing susceptibility.

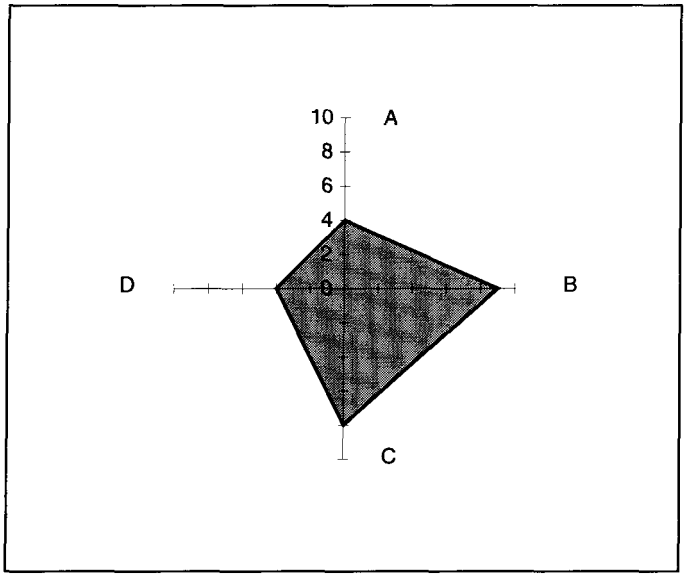

Figure 3.4. A Foot-Print Chart for the AA6111 alloy.

3.4 Preparation of Metallographic Specimens

3.4.1 Tearing Surface Specimen Preparation

Examples of Constrained Rod Castings of the four wrought aluminum alloys AA1050, AA3104, AA5182, and AA6111 are shown in Figure 3.5. It can be seen that the locations of cracks differ from alloy to alloy.

Since only hairline and light cracks occurred in AA1050 and AA5182 alloys, special measures were taken in preparing the specimens of these alloys. As a first step, segments of bars containing hot tears were removed from the castings, usually at the junctions of the bars and the sprue. Then,

the specimens were ground untill the tear surfaces were exposed (Figure 3.6). During the whole process, the hot tear surfaces were protected from any damage and contamination.

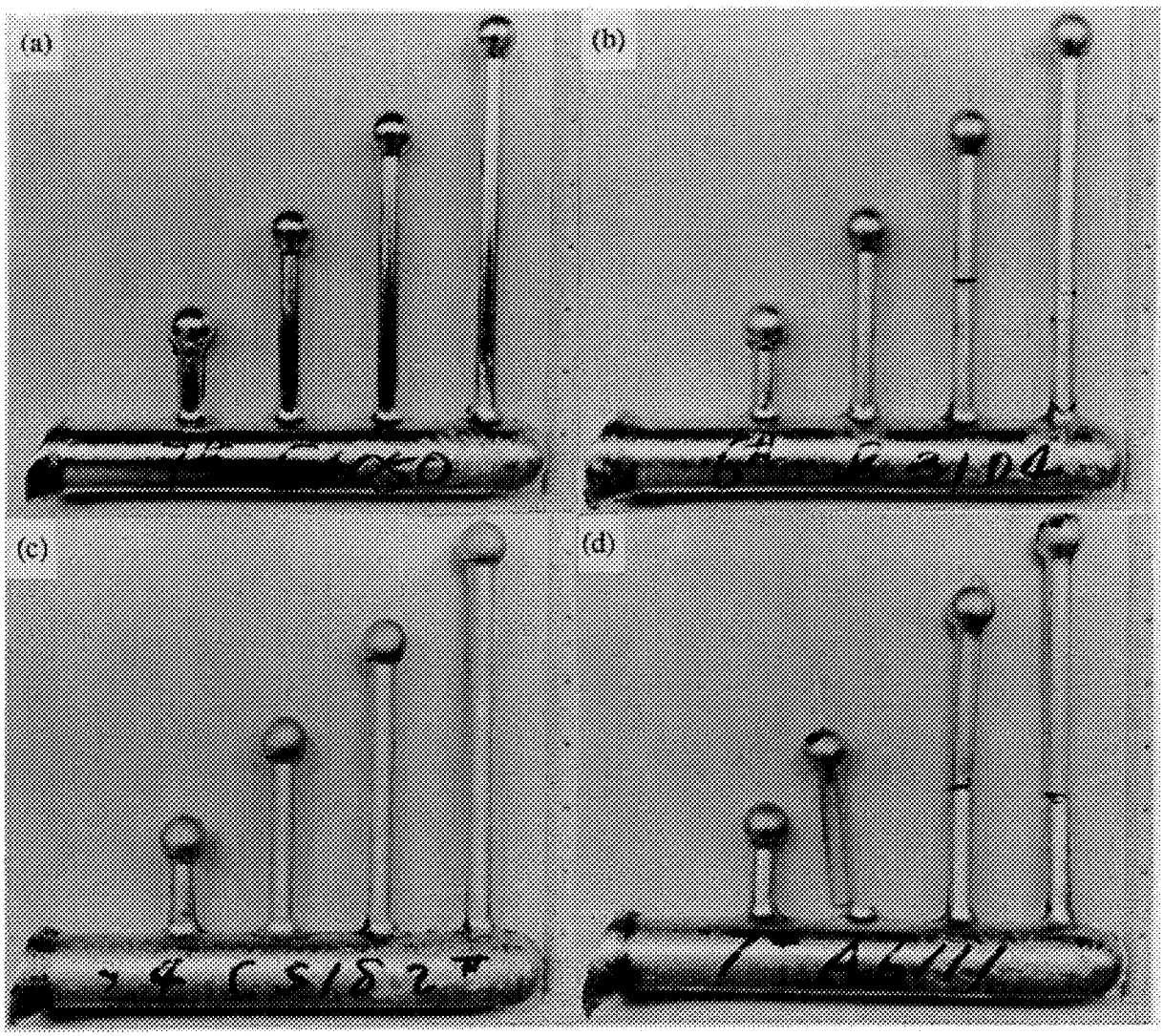

Figure 3.5. Photos of typical CRC castings of the four wrought aluminum alloys: (a) AA1050, (b) AA3104, (c) AA5182, and (d) AA6111.

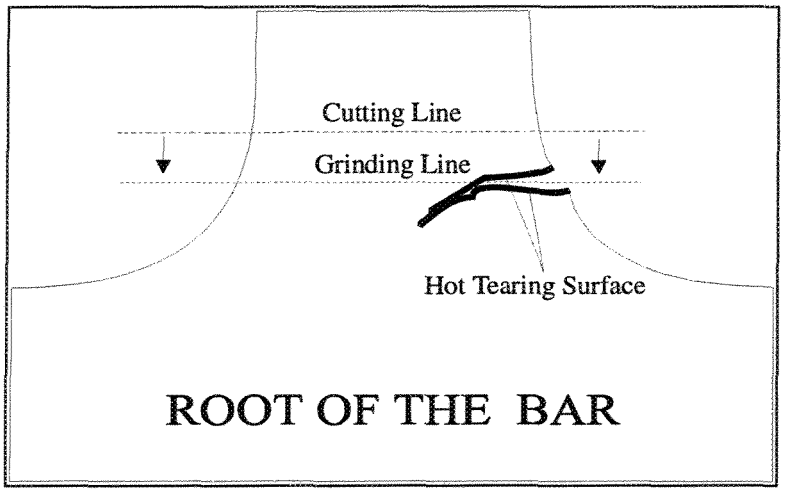

Figure 3.6. Schematic illustration of hot tear surface preparation.

Since the tear surfaces of AA3104 and AA6111 were completely separated during casting, the specimens of AA3104 and AA6111 alloys were more easily obtained by just cutting the castings at a location close to the completely torn surfaces.

3.4.2 Macrostructural Specimen Preparation

The macrostructures of the entire CRC mold cast were analyzed for each alloy. In order to obtain the longitudinal section of the whole cast sample, It was horizontally placed in a wooden box. A low-viscosity epoxy resin was poured around the part at room temperature. The resin took four to eight hours of cure time to harden. The mounted specimen was ground down until the maximum longitudinal section and smoothest surfaces were obtained. An etching solution of 15 ml HCl, 15

gram $CuSO_4$, and 90ml H_2O was used to reveal the grain structure of the cross-section. The macrostructure was observed with the naked eye and low magnification.

3.4.3 Microstructural Specimen Preparation

In order to study the constituents and structure of the alloys and for hot tearing characterization, the specimens were taken as close as possible to the hot tear location or to the initiation of hot tears. The castings were carefully observed and the locations of the metallogaphic samples were established in order to ensure the inclusion of all representative sections. The samples were cut in a way shown in Figure 3.7.

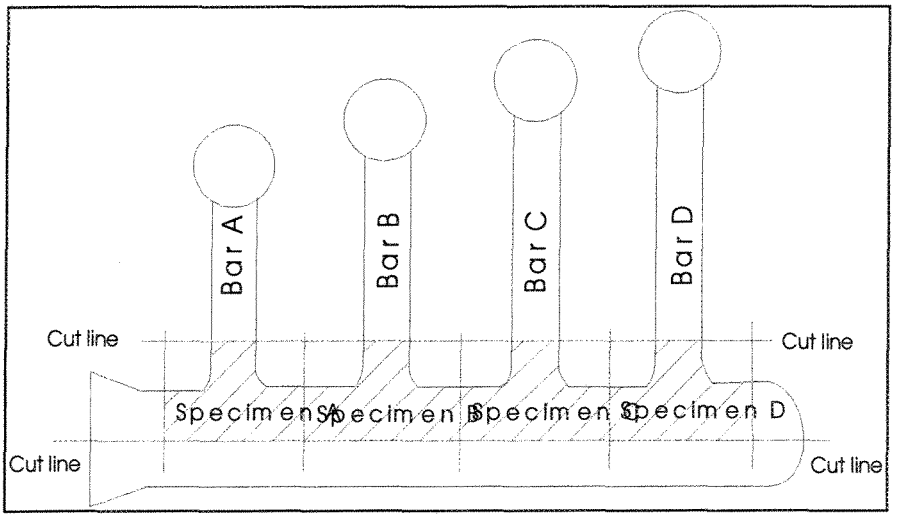

Figure 3.7. Section of the specimens for microstructural analysis.

The samples were mounted in thermoplastic resin and ground using 240, 320, 400 grit SiC papers. Polishing was performed using wetcloth with diamond-paste (6μm and 1μm). Final mechanical polishing was carried out by using two different polishing media alternately. Then, the specimens, etched with 0.5%HF or without etching were observed with an OLYMPUS PMG3 optical microscope.

In order to reveal the grain size of the alloys, electrolytic etching was carried out for the different alloys. The mounted specimens were polished mechanically, then an electrical contact was made through a small hole drilled through the back of the mount into the sample. A suitable electrolysis cell and a controllable power source were used. The sample arrangement and the schematic of the apparatus are shown in Figure 3.8. The voltage and the current of the system could be adjusted to around 40V and 1.5A, respectively. The electrolytes used were 0.5% Barker solution for all the alloys.

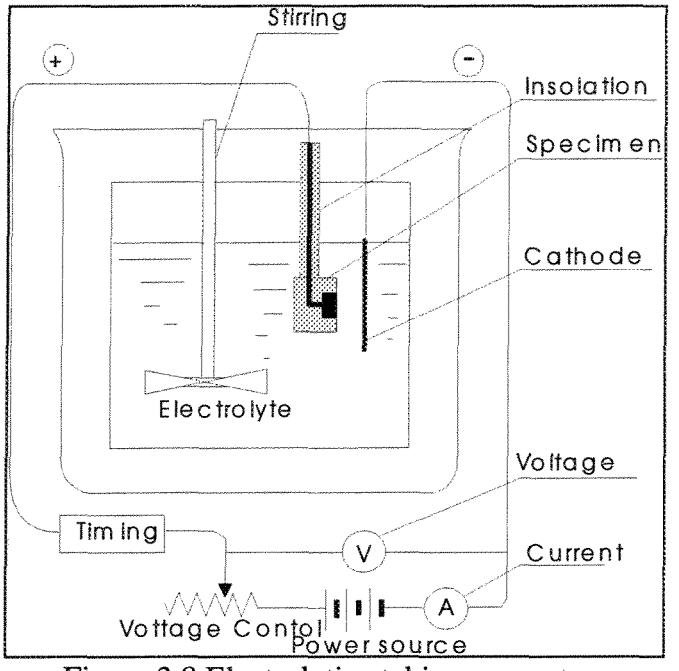

Figure 3.8 Electrolytic etching apperatus.

3.5 Analytical Methods

3.5.1 Grain Size Measurement

The linear intercept method was used to measure the grain size. The test grid, consisting of a number of parallel, straight test lines with a spacing greater than the apparent mean grain diameter, was randomly superimposed over the live microscope image. This procedure was repeated on five fields, each randomly selected, until five hundred grain intercept lengths (chords) were measured. Then, the average intercept length, τ, was determined from the N measured values of l_i in accordance with the following equation:

$$\tau = \frac{\sum_{i=1}^{N} l_i}{N} \tag{3.2}$$

where each l_i value is in true length unit (μm or mm) obtained by dividing the apparent length on the image by the magnification used, M.

3.5.2 Scanning Electron Microscopy (SEM) and Energy-Dispersive X-Ray (EDX) Analyses

An HITACHI S-2700 scanning electron microscope was used to study the hot tear and microstructure characteristics of the alloys. Two types of analyses were conducted: tear surface fractography, and phase analysis from polished samples. Before start-up, an acceleration voltage of 20 kV was set, and the filament current was adjusted to about 100 μA. The working distance used was usually ranging from 10 to 20 mm.

Polished samples were also examined to identify and to analyze the morphology and distribution of second phases around the tear surface and in the matrix. The samples were usually etched before they were put into the SEM; and if necessary, the sample surface was coated with a thin layer of gold to improve the contrast of the image.

The SEM-based energy-dispersive x-ray (EDX) analysis unit used in the investigation was from Link Analytical which can give a semi-quantitative determination of the chemical composition of

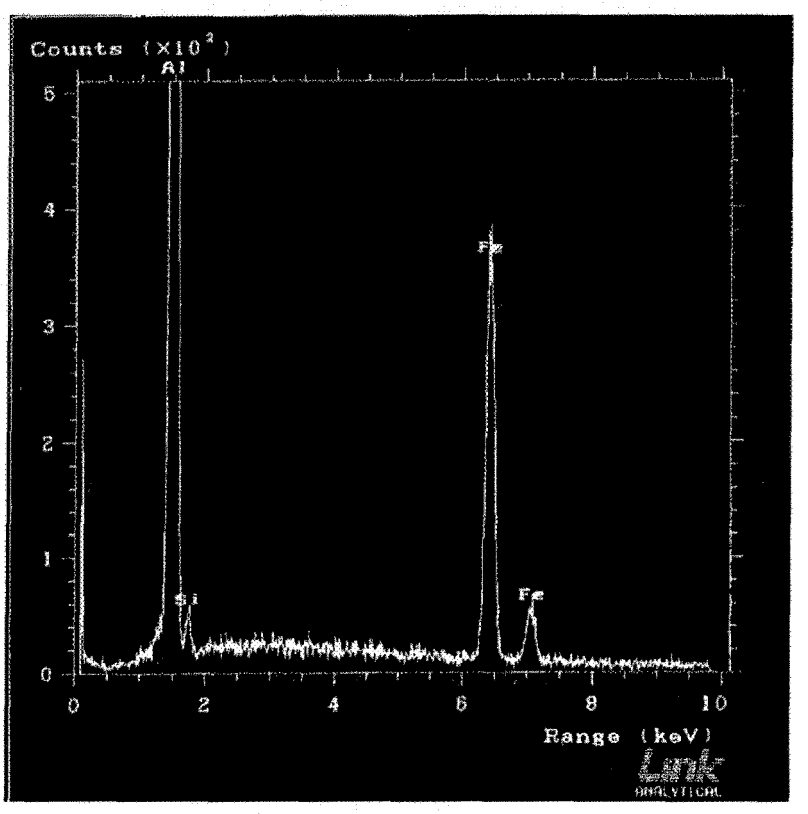

Figure 3.9. EDS spectrum of a second phase in the AA1050 alloy.

the second phases. Depending on the size of the object to analyze, an areas analysis or a point analysis was applied. Figure 3.9 shows a typical EDX spectrum obtained from a second phase particle in an AA1050 alloy.

3.5.3 Matrix Dissolution and X-Ray Diffraction (XRD)

Specimens for matrix dissolution were selected from the areas where hot tears occurred. Each specimen, about 0.5~3.0 g, contained both sides of the tear surface. The specimen was first put into hot phenol solution which dissolved the aluminum matrix and extracted the intermetallic constituents that would become insoluble residues. Benzyl alcohol was used to stabilize the aluminum phenol solution. The intermetallic particles were separated from the solution with a series of ultrasound treatments; and the final separation was achieved by using a centrifuge. The intermetallic particles could then be filtered out onto a silver filter. The identification of those particles was carried out by using XRD.

The XRD measurement of the extracted particles was carried with a D-5000 Siemens diffractometer. Firstly, a certain amount of alcohol wetted intermetallic particles was placed and dried on a hot silicon pan. Then, together they were put into a sample holder together. The X-ray diffraction was started at 10° angle and terminated at a 60° relative to the surface of the sample, and the step size of diffraction was 0.04°. It took about 9.6 seconds to finish the diffraction of each step. To record the diffraction pattern of the whole sample, three hours and twenty minutes were needed.

The XRD analysis was performed by using a Diffrac-plus software. An intermetallic compound was identified by comparing its diffraction pattern with the standard patterns for different

intermetallic phases stored in the computer. The amount of the intermetallic compound was also estimated according to the heights of the peaks of its diffraction pattern. The automatically recorded diffraction pattern of the intermetallic compounds of an AA1050 alloy is shown in figure 3.10.

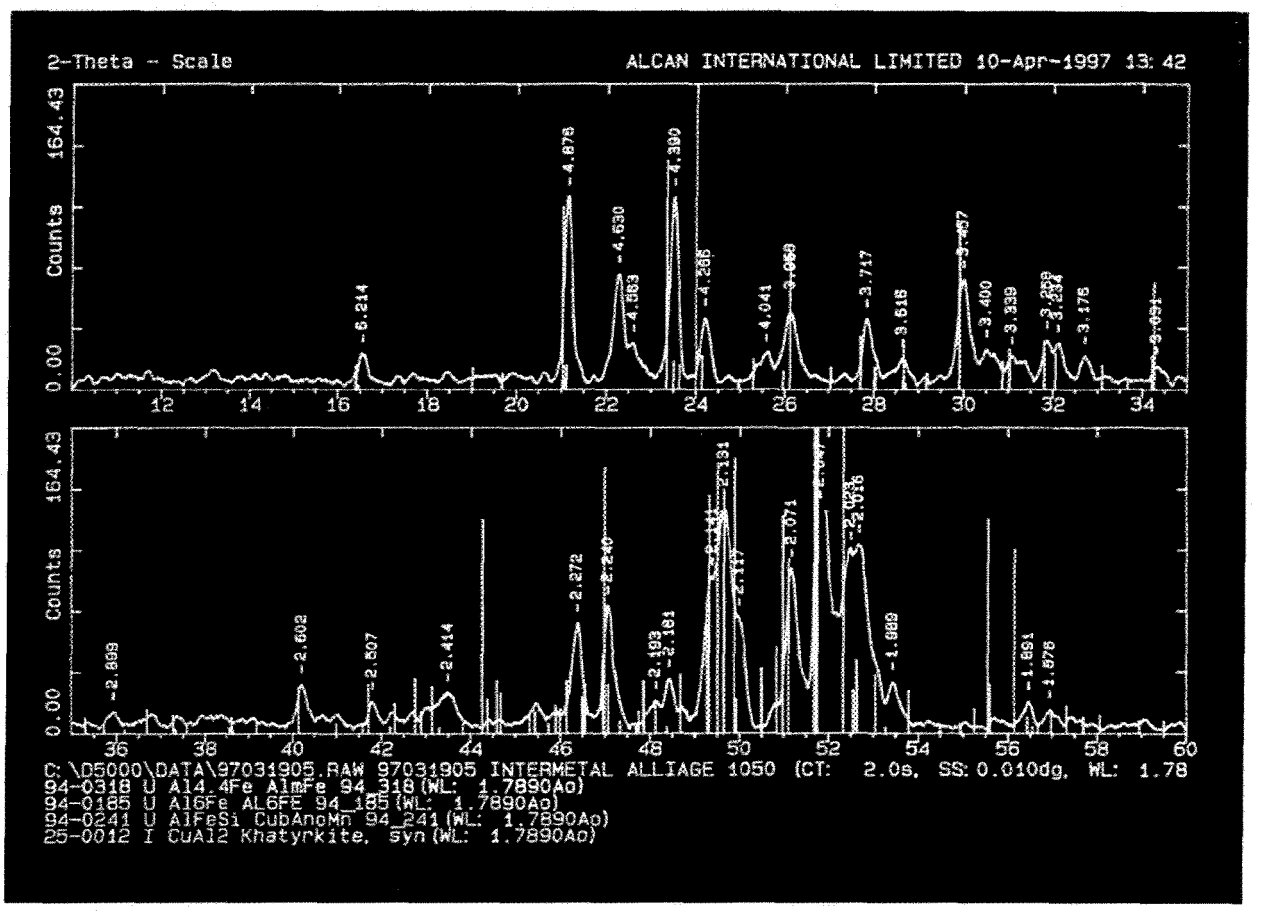

Figure 3.10. X-ray diffraction pattern of intermetallic compounds in AA1050 alloy.

CHAPTER IV RESULTS AND DISCUSSION

4.1. Hot Tearing Tendencies of Wrought Aluminum Alloys

4.1.1 Quantitative Indices for Hot Tearing Tendency

An investigation of hot tearing in alloys from four different series AA1050, AA3104, AA5182, and AA6111 was carried out using the Constrained Rod Casting method. Three experiments run were conducted on each alloy. Ten samples were cast in each experiment. Since the mold temperature reached a steady-state value only after the third casting, the first three castings in each test were not included in the analysis.

The calculation of Hot Tearing Sensitivity (HTS) value and the Foot Print Chart for the each test were given in Appendix I. The average HTS values for different wrought aluminum alloys are given in Table 4-1 and shown in Figure 4.1. The results show that the alloys have a wide range of hot tearing tendencies. The AA1050 alloy displayed the greatest resistance to hot tearing while the AA6111 alloy exhibited the lowest. The laboratory test results demonstrated the ability of the CRC mold for comparing the hot tearing susceptibility of various commercial wrought aluminum alloys. The results obtained have been found to be reproducible and have displayed moderate experimental scatter as seen in Table 4.1.

From Table 4-1 and Figure 4.1, the order of hot tearing tendency for the four aluminum alloys can be ranked as follow,

$$AA1050 < AA5182 < AA3104 < AA6111$$

Table 4-1. Average HTS Values for Different Wrought Al Alloys

Alloy	No Castings	$HTS_{Avg.}$*	$HTS_{S.D.}$**
AA1050	30	4.33	1.37
AA3104	30	15.25	2.38
AA5182	30	8.08	1.50
AA6111	30	23.33	1.78

*$HTS_{Avg.}$: average of HTS values. **$HTS_{S.D.}$: standard deviation of HTS values.

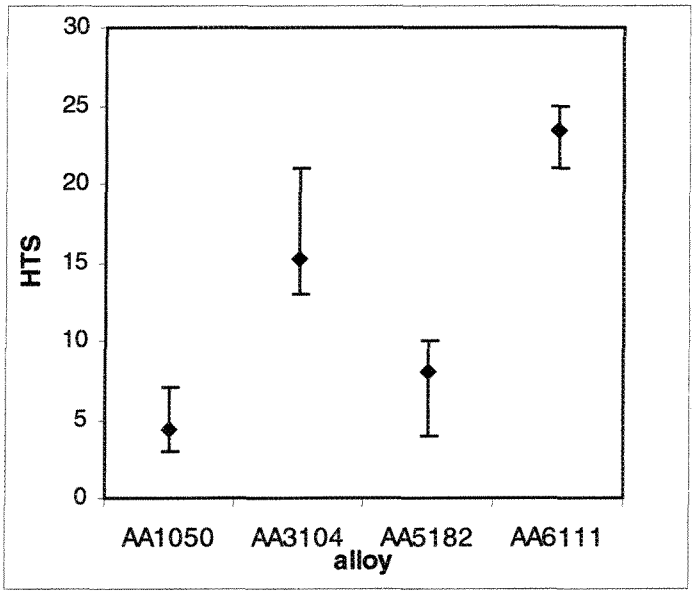

Figure 4.1. Hot Tearing Sensitivity (HTS) values of wrought aluminum alloys.

The ranking shows that the AA1050 alloy had higher hot tearing resistance than the others, and that the AA6111 alloy is more susceptible to hot tearing. The relative hot tearing ratings assigned to these commercial alloys are in good agreement with DC casting experience. The CRC casting method can provide a fairly rapid and convenient method for surveying an extensive range of testing conditions (casting temperature and mold temperature, etc.). Alloys exhibiting a wide range of hot tearing susceptibility can be assessed.

4.1.2 Characterization of Hot Tearing in Wrought Aluminum Alloys

It has been shown that AA1050, AA3104, AA5182, and AA6111 alloys have different hot tearing susceptibilities. It is also known that many metallurgical and mechanical factors determine hot tearing susceptibility of alloys.

4.1.2.1 Hot Tearing Surface Analysis

The objective in carrying out an analysis of the hot-tearing surface was to analyze and determine the hot tear features and to relate the fractography of the tear surface to the probable causes and mechanisms of hot tearing. Hot tear surfaces may reveal the history of events preceding the failure. Knowledge of the fracture surface characteristics of the alloys can help in determining their solidification characteristics.

Usually, a hot tear should ideally consist of a free dendritic surface which points out the fact that the separation occurred before the solidification was completed in and particular before the dendrites completely merged. A free dendritic surface can also indicate a microshrinkage cavity. When there is a fracture however the features are considerably different. A fracture indicates that a surface is created in a material which was initially continuous and connected. A fracture may be brittle or ductile. Ductile fracture occurs mainly by shear and exhibits characteristic features called dimples indicating that some plastic deformation occurred prior to the fracture. Brittle fractures do not exhibit dimples and one of the most common mechanisms is cleavage. Little or no plastic deformation occurs prior to a brittle fracture.

The fracture surface analysis was carried out on completely and partially broken bars of the alloys AA6111, AA3104, AA5182, and AA1050. It can be seen that the fracture surfaces are remarkably different for these four wrought aluminum alloys. The macroscopic photos of the hot tear surfaces of these alloys are shown in Figure 4.2.

AA1050 Alloy

A partial hot tear surface of the AA1050 alloy is shown in Figure 4.2(a). The small hot tear surface of this alloy looks like the radial zone of a tensile fracture surface. The differences, however, can be seen via SEM analysis (Figure 4.3) which shows: (a) a rather coarse free dendritic surface; and (b) a surface partially covered with a eutectic phase which exhibits both a fine dendrite structure and fine secondary particles.

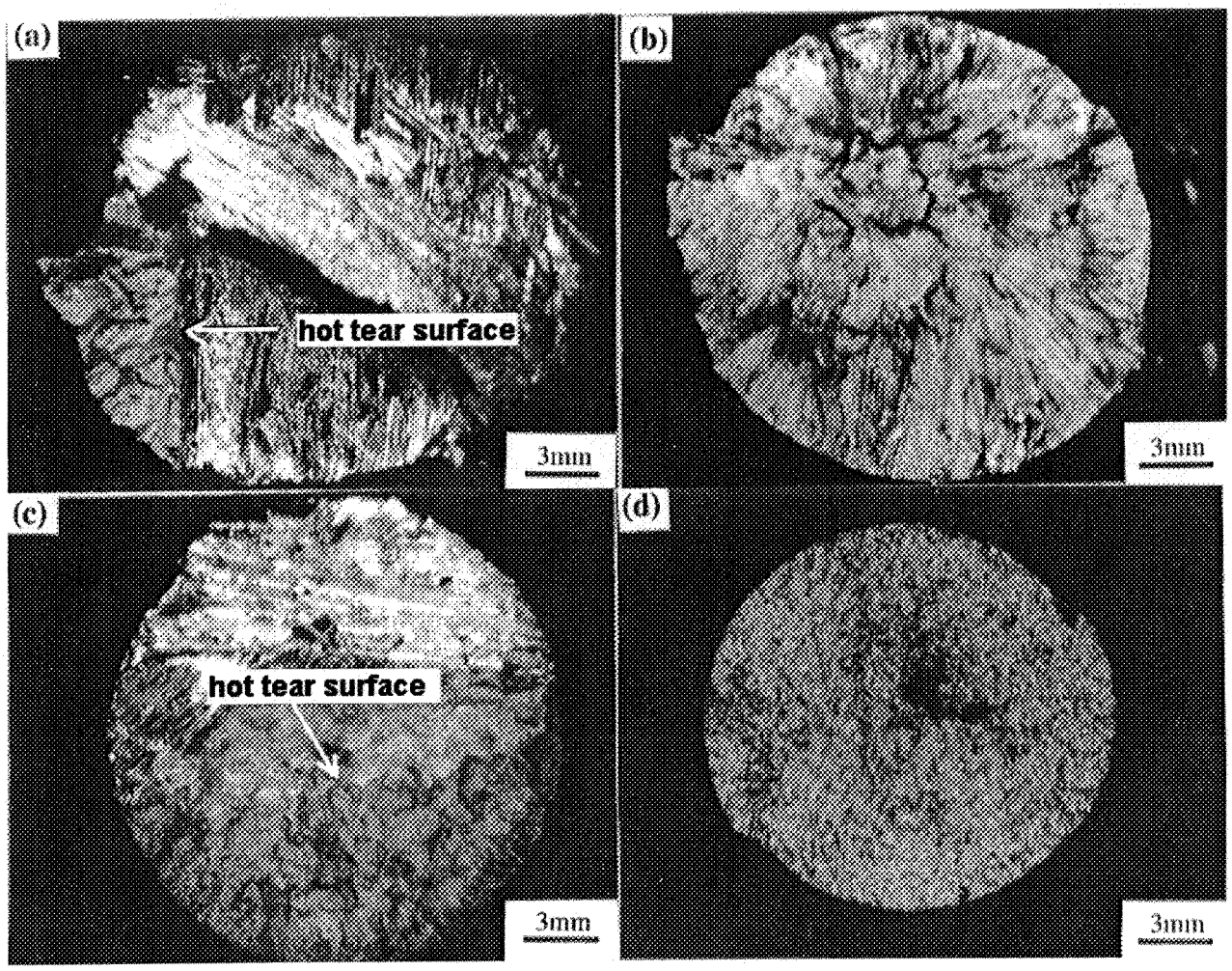

Figure 4.2. The macroscopic photos of the hot tear surface of (a) AA1050, (b) AA5182, (c) AA3104, and (d) AA6111 alloys.

These features indicate that the hot tear started as an interdendritic separation within the mushy zone. The eutectic liquid appears to have flown into the interdendritic channel and solidified rapidly into a fine two-phase structure partially filling the tear. If the amount of eutectic is sufficient and the flow of the eutectic liquid into the tear is not blocked, partial complete healing of the tear can conceivably occur. It is important to note that everything that can facilitate the

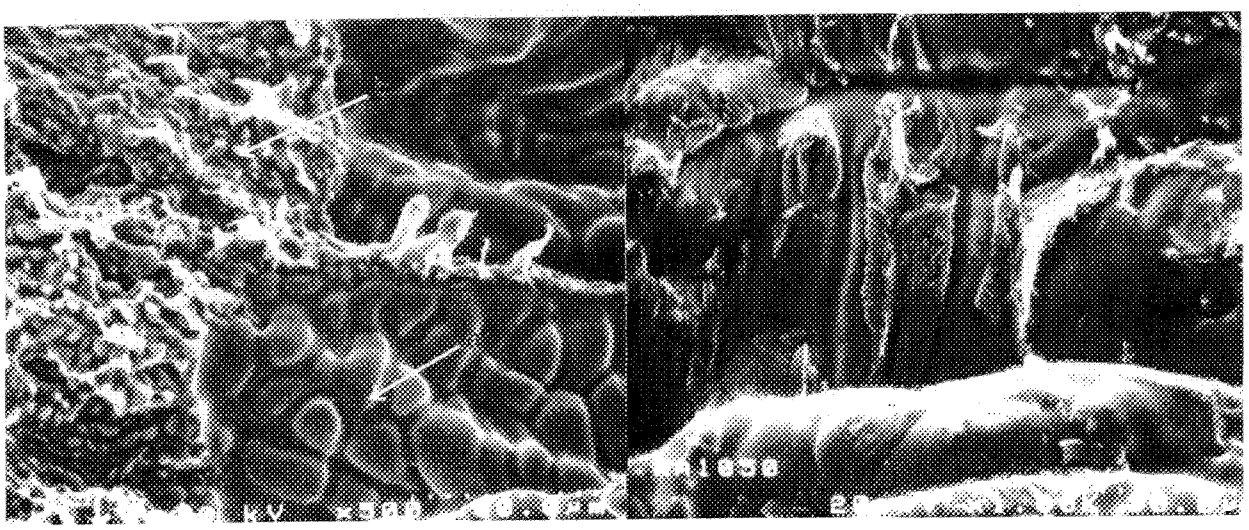

Figure 4.3. A SEM photo showing that the hot tearing surface was partially covered by liquid in the AA1050 alloy, (a: free dendritic surface, b: solute segregation and partial healing).

interdendritic healing such as grain refining or the increase in the wettability of the interdendritic liquid would decrease hot tearing in the AA1050 alloy at a given stress level.

AA5182 Alloy

This alloy was found to show low tendency to hot tearing. The hot tearing surface was covered with a thin layer of eutectic which solidified yielding agglomerates of second phases. It can be seen in the same image in Fig. 4.4 that both the dendrites and the second phases on the AA5182 are fine. Some free dendritic surface was found in this alloy for the tear region. It can be concluded that, as for the AA1050 alloy the hot tear was an interdendritic separation with solute segregation providing the eutectic liquid covering the surface.

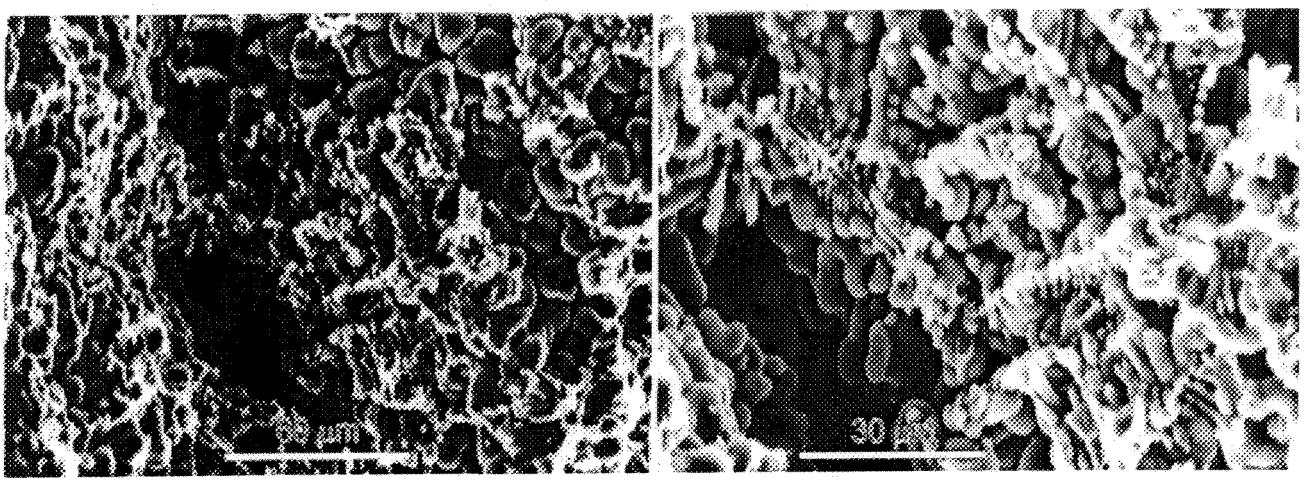

Figure 4.4. SEM photos of a hot tearing surface of the AA5182 alloy at various magnifications.

AA3104 Alloy

The surface from the AA3104 alloy was from a completely broken bar. It is similar to the radial zone of a tensile fracture surface, and the surface was rougher than that of the AA1050 alloy. A small shrinkage at the center of the bar can be observed, and the outer area of the surface is much darker than the central part.

SEM analysis shows that the hot tear surface exhibits different features in its outer portion and central portion. Figure 4.5(a) shows the central part of the tear surface of the AA3104 alloy. The interesting feature is that some dimples, which are characteristics of a ductile fracture, are evident.

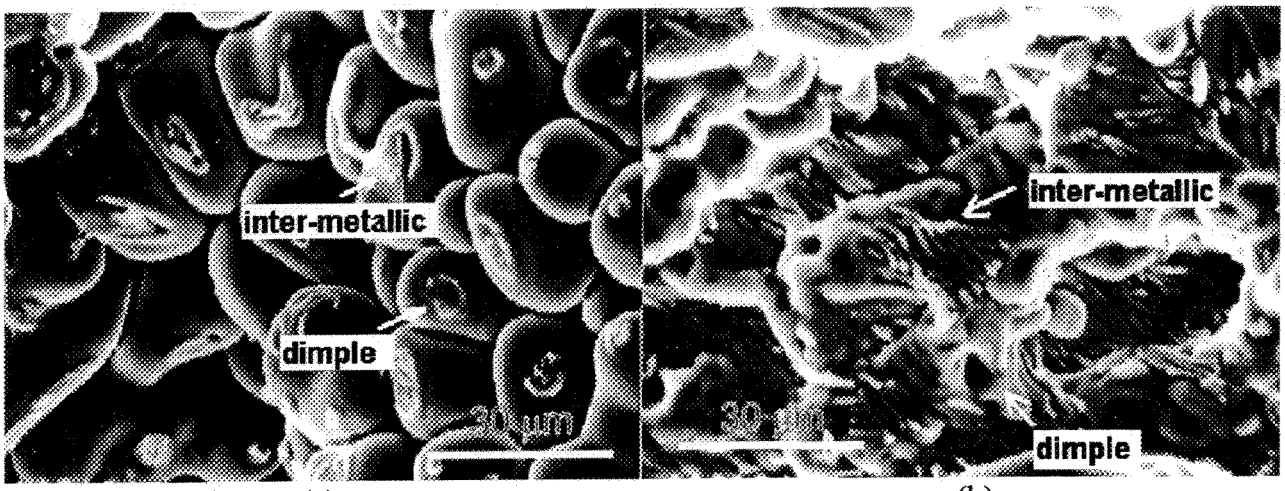

(a) (b)

Figure 4.5. SEM photos of the hot tearing surface of the AA3104 alloy: (a) the central portion of the hot tear surface, (b) the outer portion of hot tear surface.

The individual, small dimples on the tear surface of the AA3104 alloy can be the evidence of contacts established between solidified dendrites prior to hot tearing. This indicates the points where separation happened after the dendrites formed an interconnected network. The dimples on the dendrites imply that hot tearing occurred due to over-strain of the interconnected network at points of contact. It is important to note that in the AA3104 alloy the strength of the coherent dendritic network probably an important role in hot tearing tendency.

The outer part of the tear surface is shown in Figure 4.5(b), in which another important feature can be seen. It shows that the free dendrites of the tear surface are partially covered by a eutectic phase. A high concentration of second phases can be observed on the surface. The dimples can also be observed. It is conceivable that the outer region solidified earlier and segregated solute,

indication of a hot tear in the late film stage. The dendrites and the second phases seem to be coarser than in the AA5182 alloy.

The most interesting feature of the AA3104 alloy is that unlike the AA1050 and the AA5182 alloys, its hot tear is characterized by a ductile fracture of a partially interconnected dendrite network. Physical measurement techniques, such as Acoustic Emission, should be used in order to determine whether hot tearing occurs above the solidus or if it extends below the solidus.

AA6111 alloy

In the AA6111 alloy, the tear surface is concave-convex and consists of facets to the contours of the dendrites formed during solidification. The whole tear surface is relatively flat and has the same gray level (Figure 4.2 (d)).

The free dendrites can be observed on the tear surface of the AA6111 alloy, which are shown in Figure 4.6(a). The tear surface here exhibits no distortion, dimples, or second phases. Free dendrites combined with second phases are found in some areas as shown in Figure 4.6(b). This points out to an interdendritic separation with a eutectic liquid film present but probably not covering the whole surface. Coherency, and the formation of an interconnected solid network is not evident.

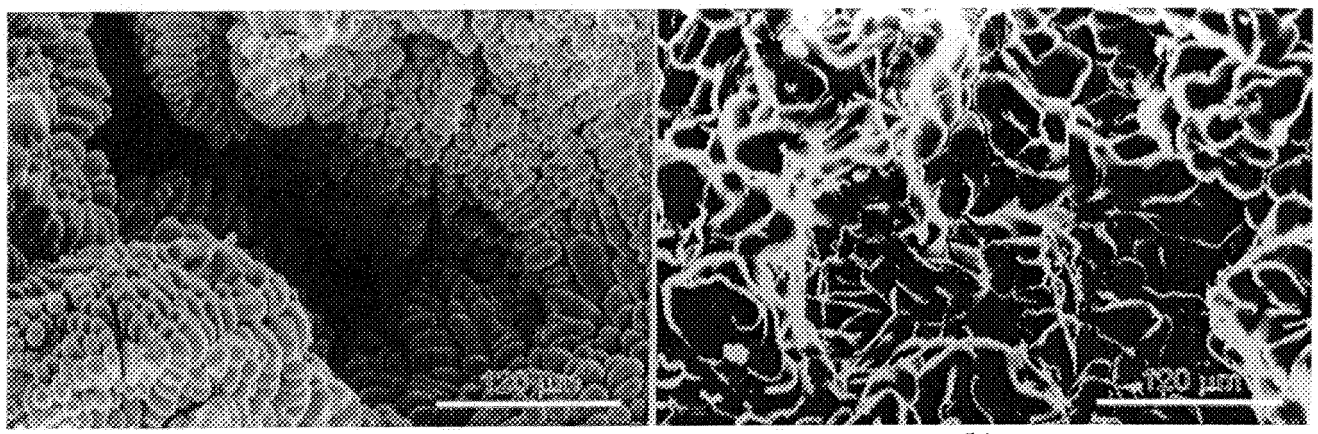

(a) (b)

Figure 4.6. SEM photos of Hot tearing surface of AA6111 alloy: (a) free dendrite surface without second phases, (b) dendrite surface with second phases.

The AA6111 alloy seems to have hot tears that may be described as the result of an interdendritic separation. The presence of microshrinkage, however, cannot be excluded. The alloy does not seem to have an interdendritic liquid that can fill the interdendritic cavity and yield healing. The amount of the eutectic phase present during the separation, and its wettability are important factors to further study. Acoustic emission can again be used to determine at what stage (early film or late film) the hot tear occurs.

4.1.2.2 Macro and Microstructural Investigation

In order to relate the formation of hot tearing to the cast structure, the macrostructures of the CRC castings were investigated. The macrostructure of the four alloys are shown in Figure 4.7.

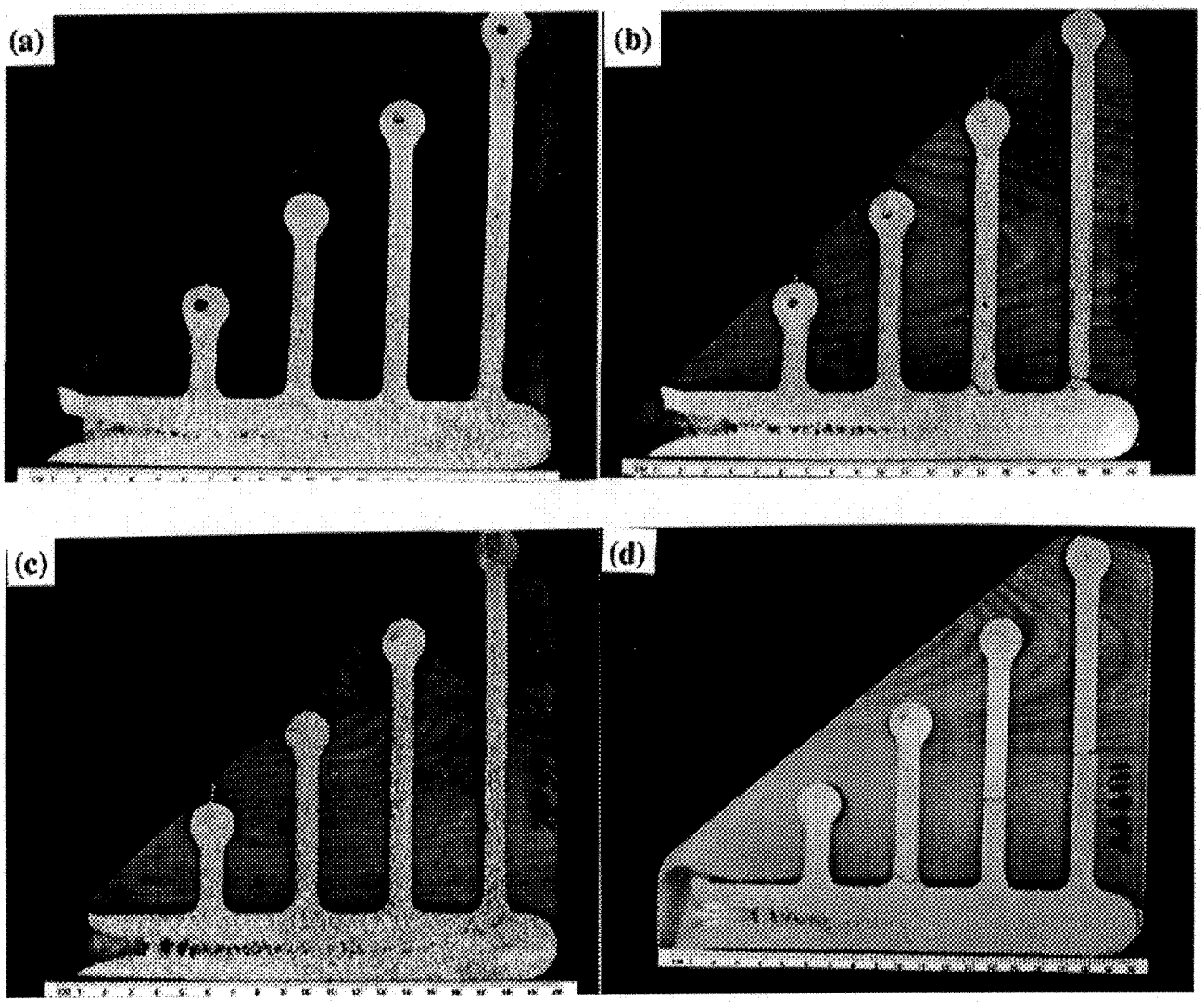

Figure 4.7. The macrostructures of the wrought aluminum alloys (a) AA1050, (b) AA3104, (c) AA5182, and (d) AA6111 (etched with 0.125%$CuSO_4$+0.125%HCl).

In the AA1050 alloy, the major part of the structure exhibits columnar grains, except for equiaxed-grains in a small inner section of the bar and a very thin shell of fine equiaxed grain layers. This is typical of a short freezing-range alloy such as AA1050 (the freezing range of AA1050 alloy is about 10-20°C [81]). In the AA5182 and AA3104 alloys, columnar grains are

found in the outer section of the bars and equiaxed grains in the central section. These alloys exhibit grain structures that are typical of medium freezing-range alloys (the freezing range of AA5182 and AA3104 is around 60-70°C [81]). AA6111 alloy has fine equiaxed grains (the freezing range of AA6111 is about 140-150°C by experimental measurement), which is typical of a high alloy, long-freezing range alloy.

The grain structures of the castings of the four wrought aluminum alloys with hot tears are shown in Figure 4.8. It can be seen that the AA1050 and the AA3104 alloys have coarse columnar grains; the AA6111 alloy has fine equiaxed grains; the AA5182 alloy has medium sized grains, both equiaxed and columnar.

It is also observed that only intergranular cracks occurred in the AA6111 alloy; and in other alloys, both transgranular and intergranular tears can be seen in Fig 4.8. The direction of hot crack is always perpendicular to the surface of the castings.

An examination was also carried out of polished and etched (0.5%HF) samples. It can be observed that the microstructure of the AA1050 alloy in the hot tear region is different from the other alloys (Figure 4.9). The edge of the hot tear surface as well as the region leading to it, is decoration with agglomerates of eutectic phases. It is a good evidence of the healing phenomenon of AA1050 alloy.

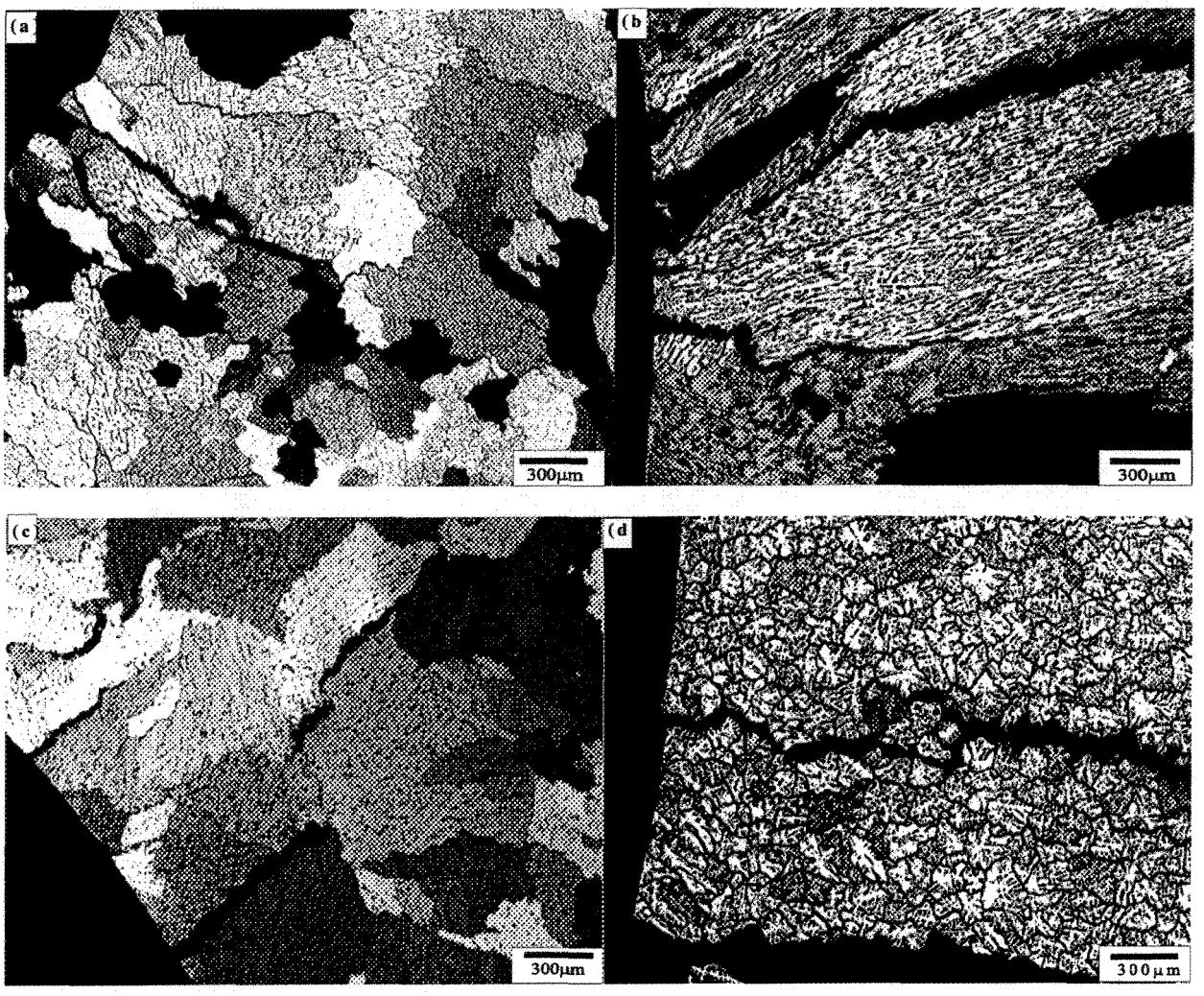

Figure 4.8. Photomicrographs of the alloys: (a) AA6111, (b) AA3104, (c) AA5182, and (d) AA6111 (anodized and with polarized light).

This is a phenomenon where a hot tear separation is filled back by the remaining liquid still present in the late stages of solidification. This liquid, being rich in solute elements, presents itself as regions with high amounts of second phases after solidification.

In the areas of high stress concentration (such as the junctions of the bars to the gating) healing of hot tears is evident. The healing phenomenon of the AA1050 alloy was also confirmed by hot tearing surface analysis (explained in the 4.1.2.1 section), in which a large amount of fine eutectic phase was observed to be covering a part of the hot tearing surface (Figure 4.9(a)). The analysis of the partial hot tear surfaces of AA3104 and AA5182 alloys also revealed eutectic phases as also explained 4.1.2.1 section. However, microstructural examination shows that the healing phenomenon is not as evident as it is in the AA1050 alloy. The results of the optical microscopy and SEM analyses are summarized in Table 4-2.

Table 4-2 Hot Tearing Characteristics of Wrought Aluminum Alloys

Alloy	Hot Tear Characteristics
1050	Small hot tears on long bars. Hot tear is seen as a separation between the columnar dendrites. A free dendritic surface is evident. The interdendritic region is filled and partially healed with the eutectic liquid.
5182	Small hot tears near the surface in the longer bars. An interdendritic separation and the presence of interdendritic liquid are evident.
3014	A higher tendency to hot tearing is seen than in the previous alloys. The operative mechanism seems to be uniquely different. A ductile fracture of an inter-connected coherent solid network leads to hot tears. The ductile fracture occurs only at points of contact where dendrite tips have met and formed a coherent network in the inner section of completely cracked bar. An interdendritic separation and the presence of interdendritic liquid are observed at the outer section of completely cracked bars, as well as indications ductile of fracture.
6111	This alloy shows complete tears and a high tendency to hot tearing. The hot tear surface exhibits a free dendritic surface. The mechanism seems to be an interdendritic separation. The second phases indicate the presence of the eutectic liquid on the tear surface. There are also regions where very little interdendritic liquid is present.

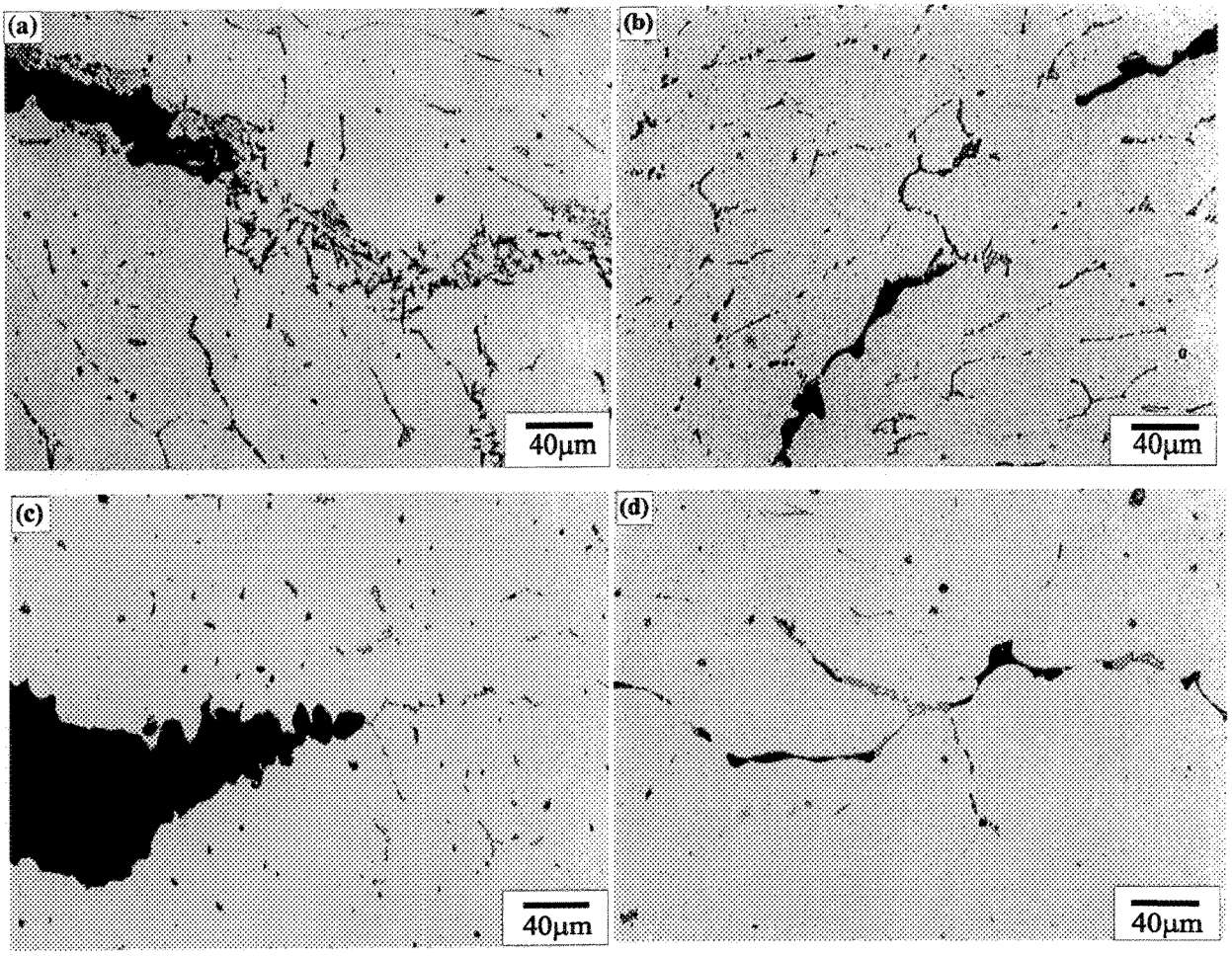

Figure 4.9. Photomicrographs of the alloys: (a) AA1050, (b) AA3104, (c) AA5182, and (d) AA6111 (0.5% HF etched).

4.1.2.3 Second Phase Analysis

Second phases may play an important role in hot tearing.

(a) Low melting point second phases may decrease the solidus temperature of the alloy thereby increasing the liquid film stage where hot tearing is likely to occur.

(b) Brittle higher melting point second phases may contribute to the fracture of the interconnected coherent solid network during the critical temperature range.

(c) The presence of second phases may also shed light on the properties of the interdendritic liquid that was present in the hot tear region, (i.e., wettability) [46].

Both the AA6111 and AA3104 alloys have moderate Si contents (0.7%-1.1% and 0.6% respectively) and AA6111 also have a moderate Cu content (0.5%-0.9%). According to a general theory, both Si and Cu contribute to a wider freezing range in aluminum [79]. In alloys with high concentrations of Si and Cu, the first precipitated particles during freezing may coalesce to larger aggregates as they are held in a liquid during a prolonged period of time, as systems with long freezing ranges are prone to heavy micro and macrosegregation. Due to enhanced interdendritic flow in such alloy systems, the particles may be unevenly distributed over the cross section of the casting.

The hot tearing is frequently associated with the microsegregation of certain elements, and this had been studied in steel in which P and S are suspected to reduce hot tearing resistance. Since both elements may promote the formation of low melting second phases with the base metal and extend the life of the liquid film stage.

The second phases in the cast CRC samples (of the different wrought alloys) were studied with SEM and EDS analysis on both polished and fracture surfaces, especially at the areas close to hot tears. The SEM Backscattered Electron Image (BEI) photos of second phases in the four alloys in areas close to hot tears are shown in Figure 4.10.

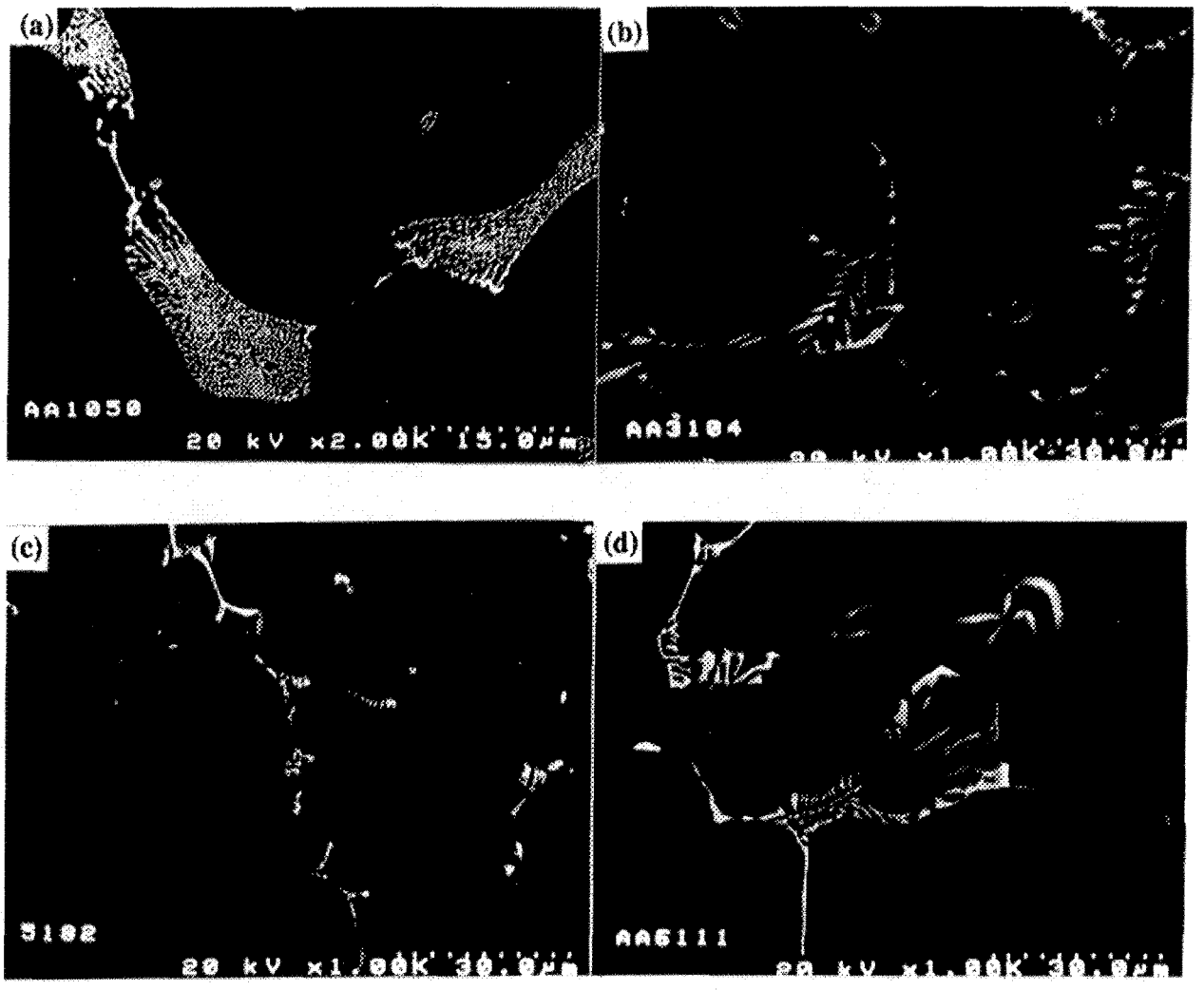

Figure 4.10. SEM (BEI) photos of second phases in different alloys: (a) AA1050, (b) AA3104, (c) AA5182, and (d) AA6111 (etched 0.5% HF and gold coated).

AA1050 Alloy

According to the morphology and EDS analysis, most of the phases in the AA1050 alloy are eutectic stable and metastable. The results suggest that the healed zone of the AA1050 alloy consists of three eutectic phases: Al_3Fe, Al_6Fe and α-AlSiFe. On the other hand, matrix dissolution and XRD analysis indicate Al_mFe, Al_6Fe and AlFeSi as the major compounds, and also show minor and trace amounts of Al_3Fe and Al_xFe. A complex α-Al(Fe, X)Si phase was also detected. However, this phase did not seem to play an important role in hot tearing as seen by SEM of the tear surface and by optical microscopy. They seem to be the end results of the healing phenomenon by the interdendritic liquid. The presence of the metastable phases (e.g. Al_mFe) also indicates that the interdendritic liquid froze rapidly as it was drawn into the interdendritic regions.

AA5182 Alloy

In the AA5182 alloy, the eutectic phases, Mg_2Si and Al_8Mg_5 were detected by SEM based and EDS analysis. Mg_2Si is known to be a brittle phase. However, the AA5182 alloy exhibited low hot tearing tendency. Again these intermetallics do not seem to have played a major role in hot tearing. They are present as constituents from the interdendritic liquid in the tear region.

AA3104 Alloy

By means of SEM based EDS analysis, the second phase $Al_6(FeMn)$, $Al_{15}(FeMn)_3Si_2$ and Mg_2Si are probably the major compounds in the AA3104 alloy. A unique second phase was discovered on the free dendrite surfaces. According to the morphology, this leaf-shaped second phase may be a brittle particle (Figure 4.11).

It is not evident if this second phase contributed to hot tearing in any way. Since the SEM analysis of the hot tear surface indicated a ductile fracture at dendrite tips, the effect, if any, may be due to the presence of a low melting points compound that decreases the solidus temperature, thereby increasing the extent of the liquid film stage.

AA6111 Alloy

Al_8Fe_2Si and Al_5FeSi phases were identified in the AA6111 alloy. On the hot tear surface of the AA6111 alloy, a leaf-shaped phase was found in appearance similar to the one found in AA3104 alloy (Figure 4.12). Identification of these leaf-shaped phases in the two alloys was carried out by EDS analysis. Since the EDS identification was carried out on the hot tearing surfaces (not flat and polished), it is hard to say whether or not it shows real elemental compositions or an influence from the composition of surround matrix

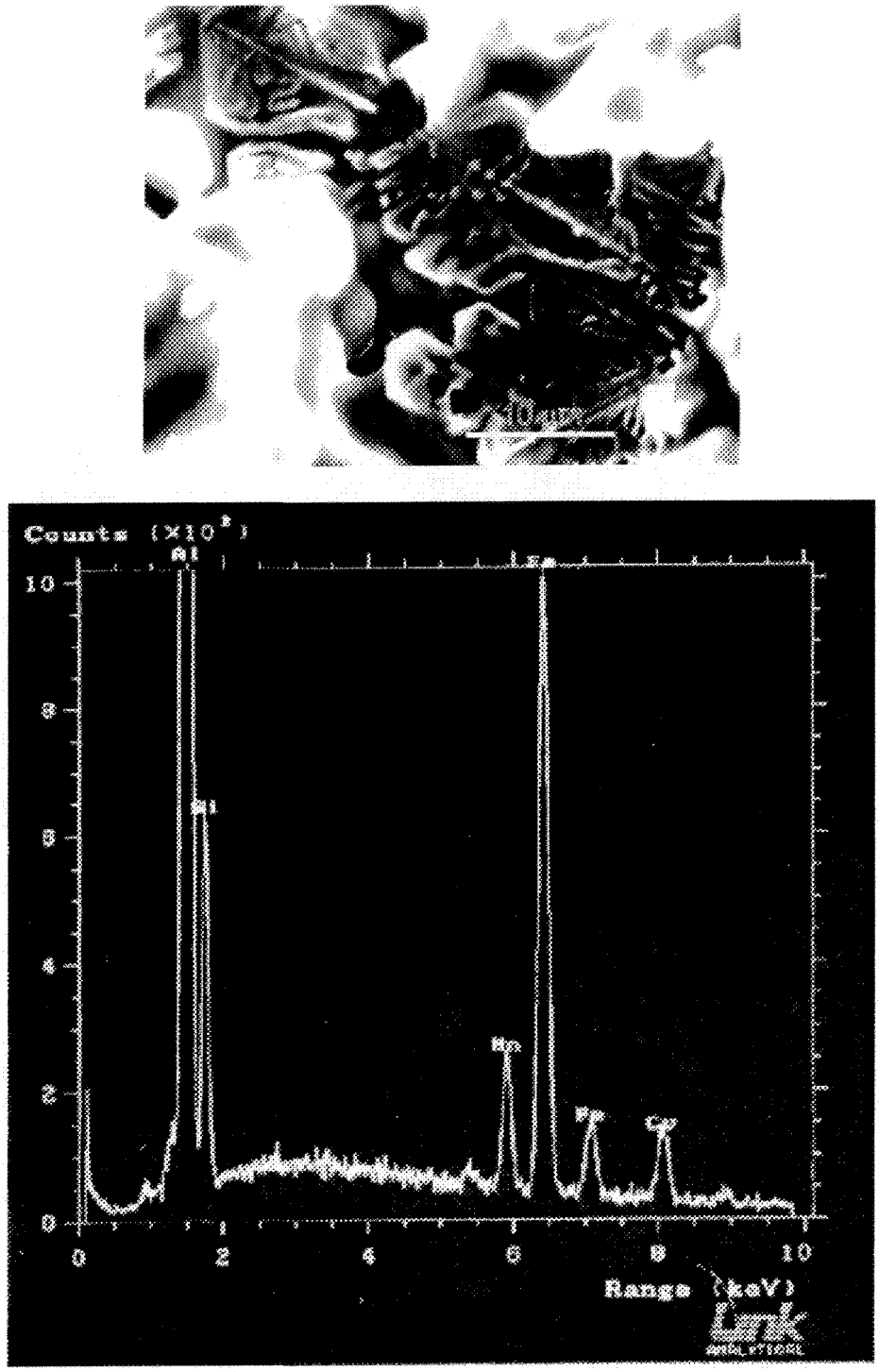

Figure 4.11. An SEM photo of a leaf-shaped second phase in the AA3104 alloy and its EDS analysis.

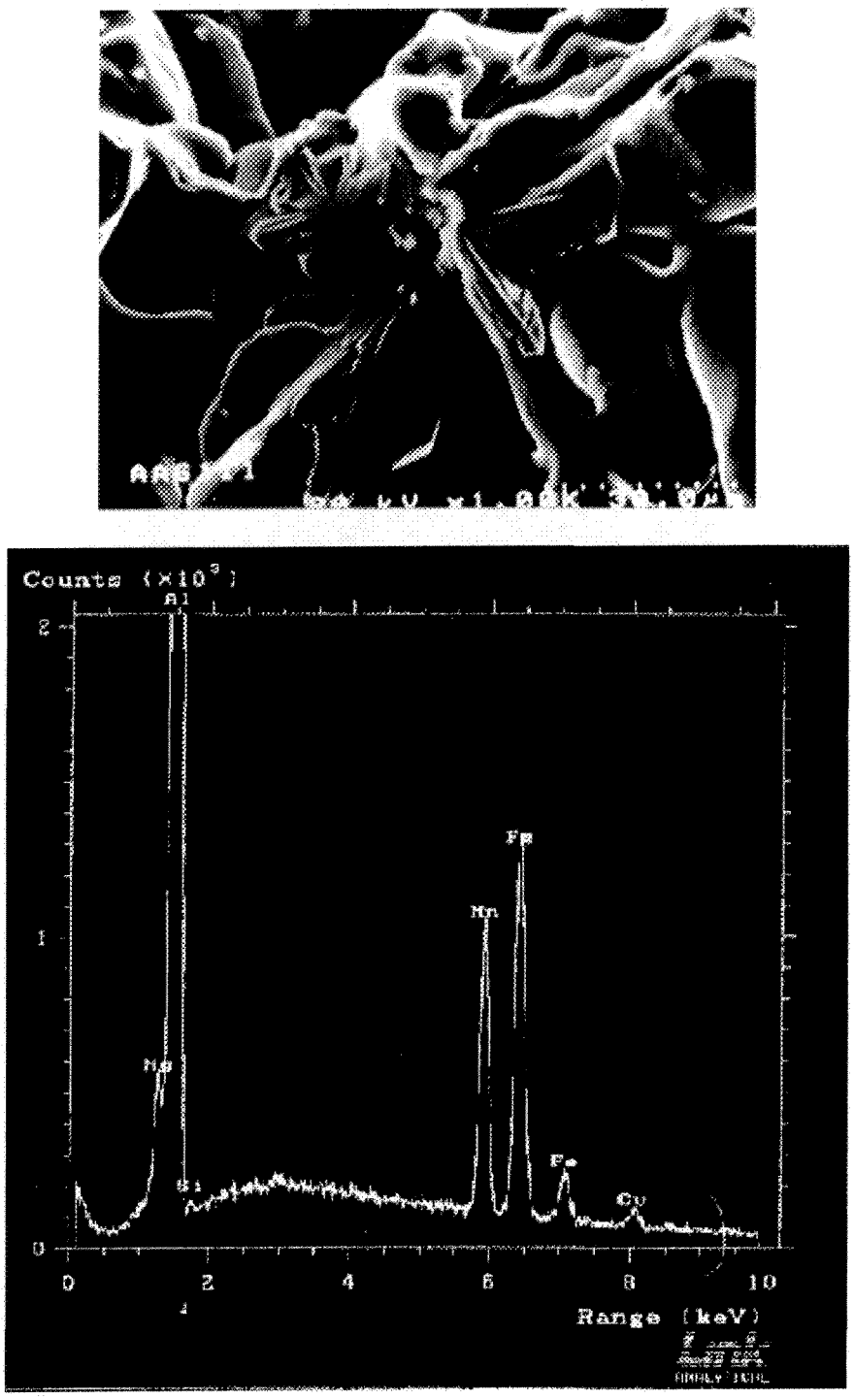

Figure 4.12. An SEM photo of the leaf-shaped second phase in the AA6111 alloy and the EDS analysis result.

The presence of Cu in this phase again leads to the fact that the Cu containing alloys may have extended freezing range and an extended liquid film stage contributing to high hot-tearing tendency. The EDS results of the leaf-shaped phases in the AA3104 and AA6111 alloys are shown in Figures 4.11 and 4.12, respectively.

4.1.2.4 Solidification Characteristics and Qualitative Assessment of Stress Distribution in the CRC Mold

Over the years, numerous studies on the hot tearing mechanisms and test methods to measure hot tearing susceptibility have been conducted in different alloys. A consistent agreement was found in the literature that the solidification interval ($\Delta T=T_L-T_S$) is a critical factor that affects hot tearing tendency. A wide freezing range will make the last region to solidify subject to contraction stresses over a greater temperature interval. Therefore an alloy that has a wide solidification interval is considered to be more prone to hot tearing [3,4,36]. A wide freezing range alloy is also prone to microporosity which may contribute to a decrease in the cross-sectional area and strength.

The four wrought alloys used are known to exhibit different degrees of hot tearing sensitivity. The AA1050 alloy has the most narrow freezing range (around 10-20°C) [81], and it exhibited good resistance to hot tearing. The AA6111 alloy has a wide freezing range (around 140-150°C), and it showed a strong susceptibility to hot tearing. The other two alloys, AA3104 and AA5182,

have very similar medium freezing ranges (around 60-70°C) [81]. However, the hot tearing behavior of these two alloys are quite different. The AA3104 alloy is more vulnerable to hot tearing than AA5182 alloy. It can be concluded that freezing range is not the sole parameter that can describe the hot tearing behavior in an alloy.

This investigation of hot tearing in the four alloys shows that the tear surfaces are always perpendicular to the surface of the sample, and, so to the tensile stress direction in the casting. All tears, hairline, light, and severe, occurred at the junctions of the bars and the sprue of the castings for the AA1050, AA5182, and AA3104 alloys. Most complete cracks happened in the middle section of the bars in the AA6111 alloy. It is very likely that there is a close connection between the solidification characteristics, the contraction stresses and hot tearing susceptibilities. Especially, the analysis of the strength and ductility of the alloys in semi-solid stage is important.

The AA1050 alloy has a narrow freezing range and low thermal conductivity. When it is cast in the CRC mold, the temperature differences across the various sections of the castings may become significant with respect to the solidification range [80]. The alloy produces a solidified skin with a narrow demarcation zone between the solid and the liquid (Figure 4.13(a)). The solid shell with its columnar structure soon covers the surface of the casting. At this time, the center of the casting is still liquid. Freezing continues by inward growth of the skin. At the junctions of the bars and sprue, the shell zone is weaker than it is in other areas because of multi-stresses that arise. The corresponding strains which cause the formation of these stress include the strain produced by the volume contraction associated with the liquid/to/solid phase change in metals,

and the strain reinforced by thermal contraction caused by the temperature difference between the inner and outer sections. If the strength of the metal shell cannot accommodate these strains, surface tears may occur at the junctions.

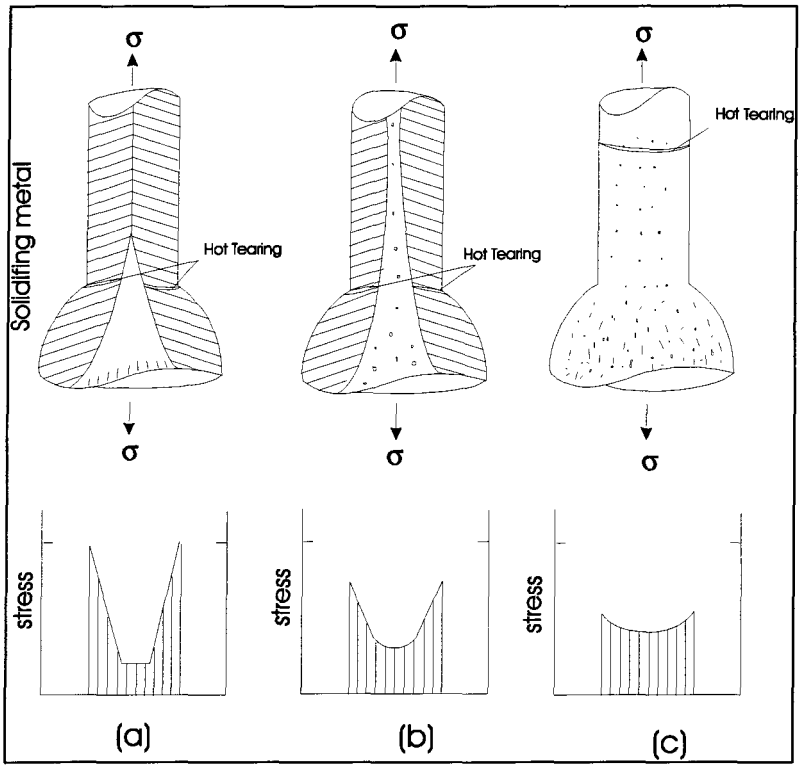

Figure 4.13. A schematic illustration of solidification characteristics and stress distribution on the bars, (a) AA1050, (b) AA3104 and AA5182, (c) AA6111.

From the analysis, it can be understood that the contraction stress is probably highly concentrated in the shell zone of the junction area. Even thought the AA1050 has good strength and ductility

at the critical temperature, hot tears can still occur because the stress is imposed on the shell zone of the bar.

The AA6111 alloy has a much wider freezing range and bed fluidity than the other alloys. Under a given temperature gradient there is a greatly extended mushy zone (Figure 4.13 (c)). This is a region of free dendrites at various stages of development. Due to its wide freezing range microshrinkage cavities may form leading to a reduction of the cross-sectional area. When the contraction of the bars reaches a critical value, a complete tear may occur across the weakened section of the bars, where the contraction stress is higher than the strength of the mushy metal.

The freezing ranges of AA3104 and AA5182 are wider than for the AA1050 alloy and more narrow than for the AA6111 alloy. The solidification characteristics of these two alloys should both have characteristics that are possessed by the AA1050 and the AA6111 alloys. A solid shell with columnar structure covers the surface of the casting by inward growth of the skin. Free dendrites form in the central sections. Figure 4.13 (b) gives a schematic illustration of the assessed solidification characteristics and stress distribution in these alloys.

The difference between the AA3104 and the AA5182 alloy can be deduced from the hot tear surface analysis. One of the main contributors to the difference seems to lie in the growth characteristics of primary dendrites. While AA3104 alloy forms an interconnected network where the dendrite tips join, preventing mass feeding, this is unlikely to occur in the AA5182.

4.2 Effect of Grain Refinement on Hot-Tearing Tendency

Since grain refinement is widely used in DC casting of aluminum alloys, it is important to investigate its effect on hot tearing. The CRC mold casting method was used in this investigation. The Al-5wt%Ti-1wt%B grain refiner (master alloy) was used in the experiments. The AA1050 was tested with four different Ti levels ranging from 0.001wt%Ti to 0.01wt% Ti. The other alloys, AA3104, AA5182, and AA6111, were tested with a single Ti level (0.01wt%Ti). The values of HTS and Foot Print Charts of the four wrought aluminum alloys are given in Appendix II. The results of the HTS of the AA1050 alloy with different Ti additions are summarized in Table 4-3 and shown in Figure 4.14.

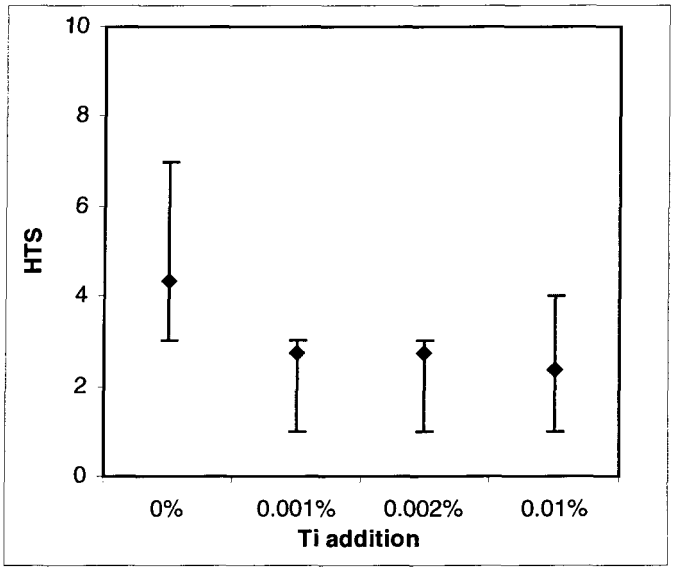

Figure 4.14. The HTS values of the AA1050 alloy with different Ti additions.

Table 4-3 HTS Results of the AA1050 Alloy With and Without Grain Refining

Alloy (Actual Ti Percentage)	Nb. of Casting	Approximate Grain Size (μm)	$HTS_{Avg.}$*	$HTS_{S.D.}$**
AA1050 (0.012%Ti)	30	368	4.33	1.37
AA1050 (0.013%Ti)	20	215	2.75	0.66
AA1050 (0.014%Ti)	20	147	2.75	0.66
AA1050 (0.022%Ti)	20	75	2.38	1.22

* $HTS_{Avg.}$: average of HTS values. **$HTS_{S.D.}$: standard deviation of HTS values.

It can be observed that Ti addition into the AA1050 alloy results in a refined equiaxed structure and reduced hot tearing tendency. This agrees with previous studies which concluded that additions of grain refiner can reduce hot tearing tendency in this alloy. This is likely due to the fact that in the equiaxed (grain-refined) structure mass feeding is facilitated and healing of the tears occurs easily. The columnar structure may also have less stress accommodation than it is in an equiaxed structure. It can also be observed that the mold can distinguish between nongrain-refined AA1050 and AA1050 with a grain refining level of 0.01%Ti. It is not, however, sensitive to very small variations in grain refining. Microstructural analysis of the alloy has also showed an increasingly refined equiaxed structure with increasing levels of Ti additions. The structures of the AA1050 alloy with different levels of Ti are shown in Figure 4.15.

Table 4-4 Hot-Tearing Susceptibilities of Wrought Aluminum Alloys with 0.01%Ti

Alloy(Actual Ti Percentage)	Nb of Test	$HTS_{Avg.}$	$HTS_{S.D.}$
AA1050 (0.022%Ti)	30	2.38	1.22
AA3014 (0.025%Ti)	20	10.25	8.29
AA5182 (0.024%Ti)	20	0	0
AA6111 (0.108%Ti)	20	22.5	1.5

$HTS_{Avg.}$: average of HTS values. **$HTS_{S.D.}$: standard deviation of HTS values.

The results of the four wrought aluminum alloys grain refined with 0.01% Ti are summarized in Table 4-4 and Figure 4.16. Comparative results of the alloys with and without grain refinement are shown in Table 4-5 and Figure 4.17. It is important to note that the HTS ranking of the hot tearing tendency of the alloys changes slightly with grain refining –Thus,

HTS(AA5182 (g.r.))<HTS(AA1050 (g.r.))<HTS(AA3104 (g.r.))<HTS(AA6111 (g.r.))

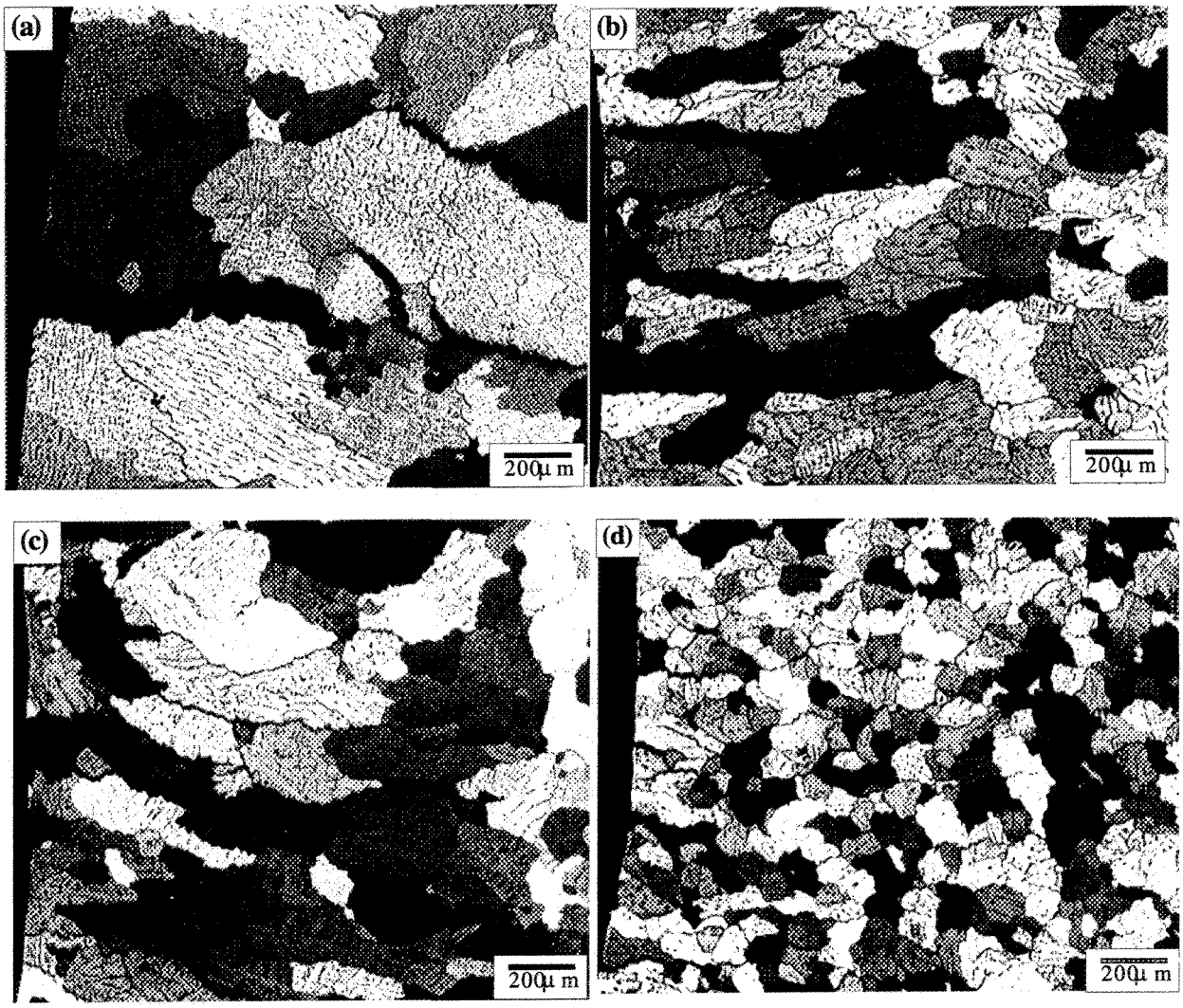

Figure 4.15. Photomicrographs showing the effect of grain refinement in AA1050: (a) not grain refined, (b) with 0.0035%Ti, (c) with 0.0045%Ti, and (d) with 0.0125% Ti (Anodized and with polarized light).

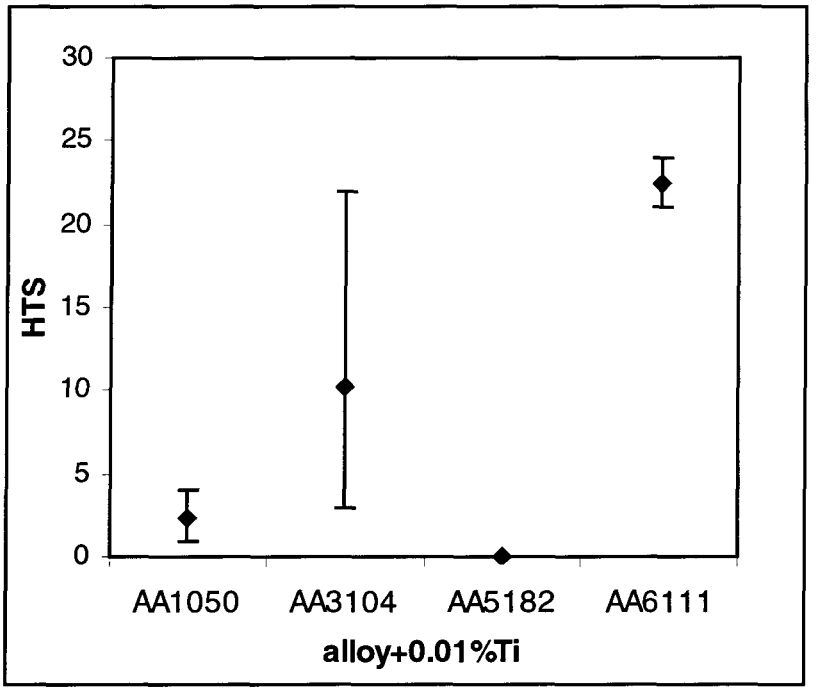

Figure 4.16. The HTS values of different alloys with grain refinement.

Table 4-5 Results of HTS for the Alloys with and without Grain Refinement

Alloy	Nb. of Test	Approximate Grain Size (μm)	$HTS_{Avg.}$	$HTS_{S.D.}$
AA1050	30	368	4.33	1.37
AA1050+0.01%Ti	30	75	2.38	1.22
AA3104	30	560	15.25	2.38
AA3014+0.01%Ti	20	89	10.25	8.29
AA5182	30	376	8.08	1.58
AA5182+0.01%Ti	20	67	0	0
AA6111	30	124	23.33	1.78
AA6111+0.01%Ti	20	89	22.5	1.5

From the figures, it can be found that the standard deviation of the HTS values of grain refined AA3104 alloy is very large. This is possibly due to the experimental errors, associated with variation of the casting parameters, especially the cooling rate.

In comparing the HTS values of the wrought aluminum alloys with and without grain refinement, it can be seen that the hot tearing susceptibilities of AA1050, AA5182, and AA3104 alloys can be reduced extensively with grain refinement. On the other hand, grain refinement showed little effect on the AA6111 alloy. The grain structures of AA3104, AA5182, and AA6111 alloys in the unrefined condition are compared to the grain refined condition (0.01% Ti) in Figures 4.18 through 4.20.

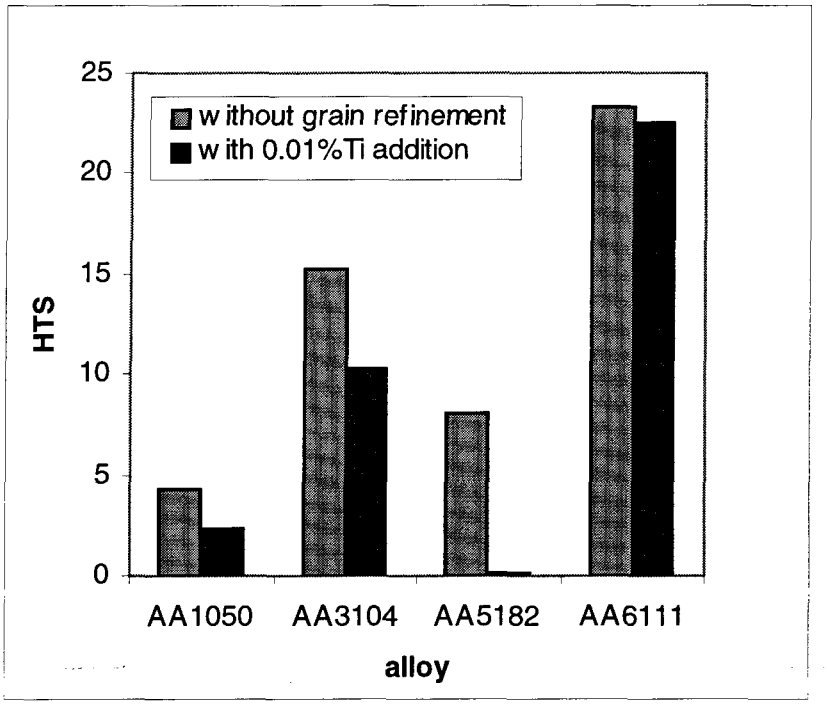

Figure 4.17. The HTS values of the alloys with and without grain refinement.

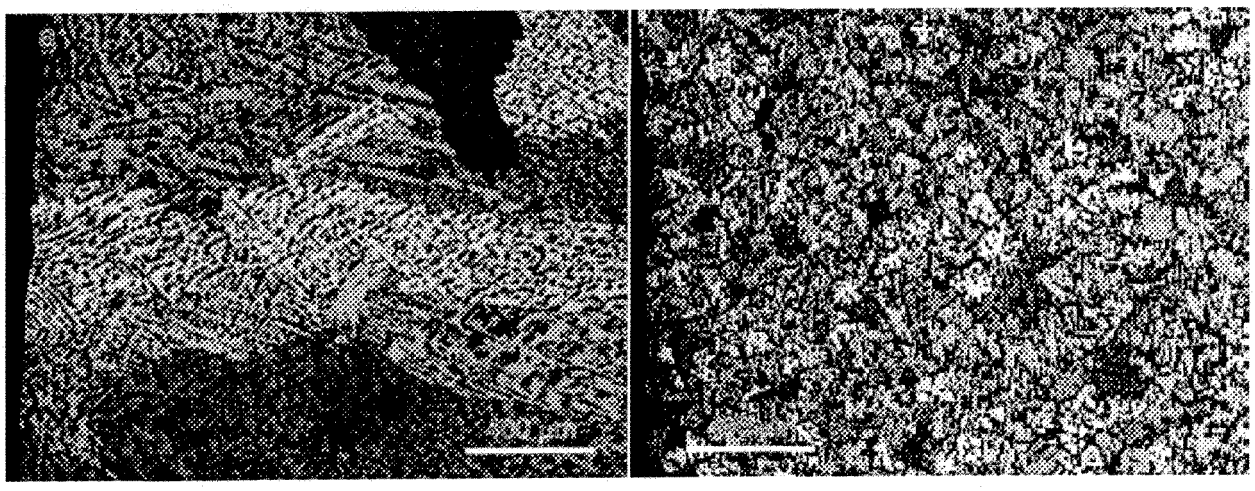

Figure 4.18. Photomicrographs showing the effect of grain refinement in AA3104 alloy: (a) not grain refined, (b) with 0.01%Ti addition (anodized, polarized light).

It is known that hot tearing may occur at the Coherency Temperature where the dendrites begin to interlock. In the solidification of a nongrain-refined alloy, the growing tips of the coarse dendrites or large columnar grains meet at an early stage of solidification. In addition, the mobility of the coarse grains is limited and restrained within the solidifying network. This reduces the duration of the mass feeding stage. Therefore, it is easy for hot tearing to take place. In the solidification of grain-refined alloys, however, the solidification conditions are altered. Small equiaxed dendrites nucleate and grow at a lower undercooling corresponding to a lower growth rate and greater tip radius. The dendrites are surrounded with a more saturated liquid. The dendrites will impinge at a later stage of solidification corresponding to a delayed Coherency Point. Therefore, the tearing tendency is reduced by lower coherency temperature in the grain-refined alloys.

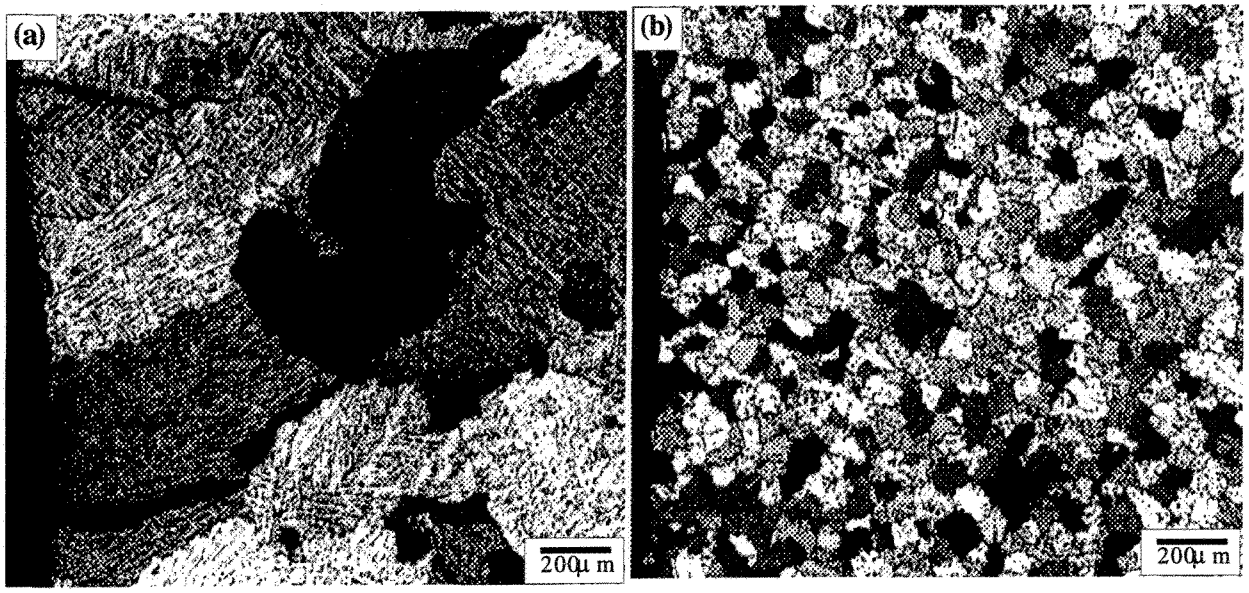

Figure 4.19. Photomicrographs showing the effect of grain refinement in the AA5182 alloy: (a) not grain refined, (b) with 0.01% Ti addition (anodized and with polarized light).

The AA6111 alloy is highly alloyed. Lower melting point phases, intermetallic compounds, and second phases, etc. concentrate at the grain boundaries during solidification. Since heavy micro and macrosegregation during solidification occur in the alloy, low melting point compounds can depress the solidus to a much lower temperature than that at equilibrium conditions. The characteristics of liquid long film life and poor wettability of the liquid film for AA6111 alloy cannot be improved much by the aid of grain refinement. This, probably, is the main reason that hot tearing susceptibility was not extensively reduced by grain refinement in the AA6111 alloy. Also, this alloy already exhibited a rather fine grain size in the nongrain-refined state (125 μm) and any additional TiB_2 grain refinement had a negligible effect.

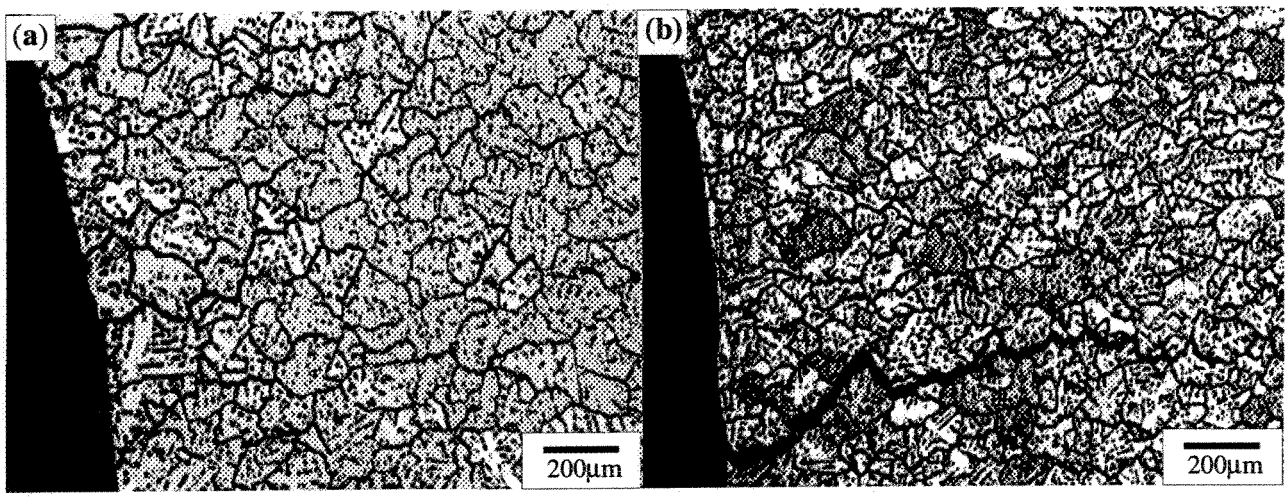

Figure 4.20. Photomicrographs showing the effect of grain refinement in the AA6111 alloy (a) not grain refined, (b) with 0.01%Ti addition (Anodized and with polarized light).

4.3 Hot-Tearing Tendency in Binary Al-Si Alloys

An important factor for an in-depth understanding of hot tearing during casting is the mechanism by which changes in solute level influence hot tearing susceptibility. Experiments have been conducted in this study with Al-Si binary alloys that contain different Si contents. The experimental results show that with slight changes in silicon content in pure aluminum, the hot tearing susceptibility is dramatically changed.

4.3.1 Experimental Results

In order to study the effect of alloy composition on hot tearing, a binary alloy system was studied. Pure aluminum with different levels of silicon additions, from 0.5wt% to 3.0wt% Si, was tested using the CRC mold. The experimental results show that pure aluminum with low levels of Si additions exhibits high hot tearing susceptibility. With the increase in Si content, hot tearing resistance is increased. The HTS values of those Al-Si alloys are given in Table 4-6 and shown in Figure 4.21. The Al-0.5wt%Si alloy exhibit the highest HTS average value; and the Al-3wt%Si alloy shows the lowest hot tearing tendency. Al-1.0wt%Si, and Al-1.5wt%Si alloys also show high relatively hot tearing susceptibilities. With increase in the silicon content, the hot tearing susceptibilities are reduced, such that Al-2wt%Si, and Al-3wt%Si alloys show relatively low hot tearing susceptibilities.

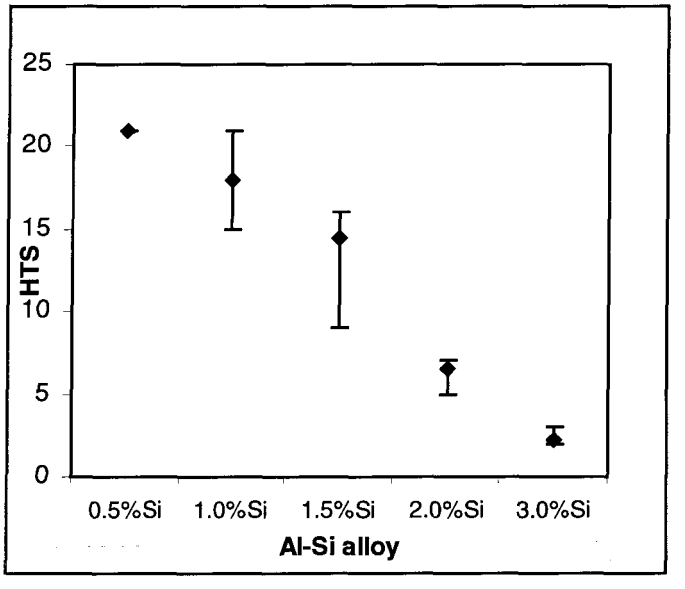

Figure 4.21. Hot tearing susceptibility of Al-Si alloys.

Table 4-6 The HTS Values of Pure Aluminum with Different Si Contents

Alloy	Nb. Of Test	$HTS_{Avg.}$*	$HTS_{S.D.}$**
Al+0.5%Si	10	21.00	0
Al+1.0%Si	10	18.00	2.45
Al+1.5%Si	10	14.25	3.5
Al+2.0%Si	10	6.50	1.0
Al+3.0%Si	10	2.25	0.5

* $HTS_{Avg.}$: average of HTS values. ** $HTS_{S.D.}$: standard deviation of HTS values.

4.3.2 Discussion

Microstructures of the binary Al-Si alloys were studied in order to find relationships between the structures of the alloys and formation of hot tearing. Metallographic examination of the Al-0.5wt%Si alloy showed the presence of large rod-shaped silicon phases and a very small amount of eutectic phases at the grain boundaries (Figure 4.22(a)). With an increase in silicon content from 1.0wt% to 1.5wt%, The amount of eutectic phases are increased. It shows that the primary solid dendrites are almost completely surrounded by eutectic phases at 1.5wt% Si (Figures 4.22(c)). By increasing Si content to 2wt%-3wt%, the amount of eutectic increases (Figures 4.22(d) and (e)). It can also be observed that the grain size decreases with increasing Si content. This may be the major contributing factor to the decrease in hot tearing tendency with increasing silicon levels.

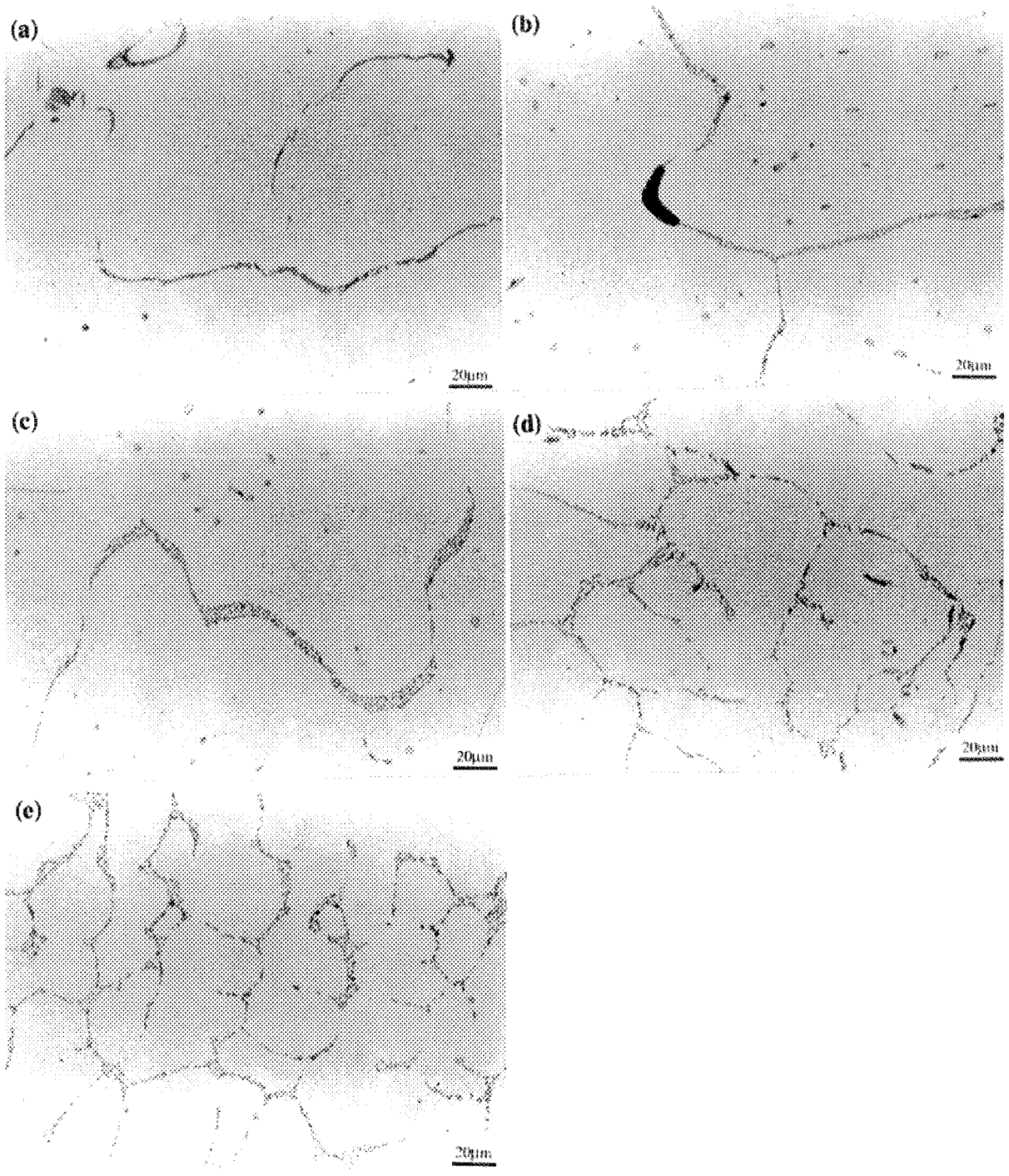

Figure 4.22. The microstructure of Al-Si binary alloys with (a) 0.5wt% Si, (b) 1.0wt% Si, (c) 1.5wt% Si, (d) 2.0wt%Si, and (e) 3.0wt% Si.

It has been noted that the hot tearing tendency of Al-Si alloys peaks at 0.5wt%Si content, which is just below the theoretical maximum solid solubility (1.65%Si) shown on the phase diagram (Figure 4.23). It is known that castings solidify under non equilibrium conditions. However, especially in the CRC mold, casting conditions are characterized by a fast cooling rate and non-uniform temperature. High macro and microsegregation will depress the solidus and eutectic liquid temperature to lower values. The experimental results of hot tearing susceptibility of the Al-Si alloys are shown in relation to the equilibrium Al-Si binary system and hypothetical non-equilibrium binary system (dotted line) plotted in Figure 4.23. The small amount of eutectic found in the 0.5wt%Si alloys can confirm this assumption.

In a non-equilibrium hypoeutectic binary system, if an alloy has a limited or intermediate Si content, a moderate amount of liquid exists over a large temperature interval and the metal will have a substantial freezing range corresponding to a longer time at the critical temperature stage, which results in higher hot tearing susceptibility. This is the case for the alloys with 0.5wt%Si, 1.0wt%Si, and 1.5wtwt%Si. Conversely, if the Si content is increased, the alloys will have a smaller freezing range corresponding to a shorter time at the critical temperature stage so that the hot tearing susceptibility will be reduced. This is the case for the alloys with 2wt% - 3wt% Si.

It has been observed that eutectic appears in the Al-Si alloy with 0.5wt% Si content under non-equilibrium freezing conditions. The eutectic amount is augmented with increasing Si contents, and a reduction in the severity of tearing is accompanied with the increase in the amount of eutectic. The experimental results agree with basic hot tearing theory. When the amount of eutectic is

more than a critical value, sufficient to surround the primary dendrites, accommodation and healing phenomena of liquid eutectic will be significant, and the resistance to hot tearing is enhanced.

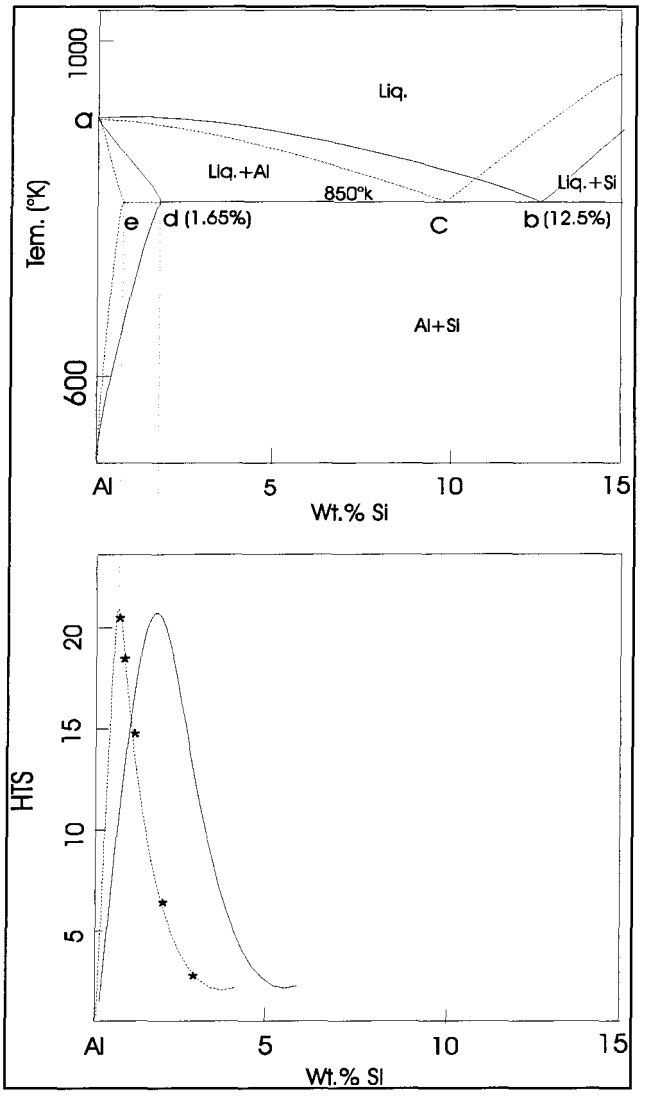

Figure 4.23. HTS values superimposed on Al-Si binary system.

Alloys with fine and equiaxed grain structures have better hot tearing resistance than those with coarse and columnar structures. This was also confirmed with the Al-Si alloys. The transformation of coarse columnar structure to fine equiaxed one has been observed to accompany the reduction of hot tearing tendency.

Hence, the three factors that contribute to the increase in hot-tearing resistance as the Si content increases from 0.5wwt% to 2.0wt% Si in Al-Si binary systems are:

(a) decrease in the grain size,

(b) decrease in the freezing range, and

(c) increase in the amount of eutectic.

CHAPTER V CONCLUSIONS AND RECOMMENDATIONS FOR FUTURE WORK

5.1 Conclusions

From the results of the present investigation, the following conclusions were drawn:

1. The Constrained Rod Casting (CRC) method was successfully used to evaluate the hot tearing susceptibility of four wrought aluminum alloys (AA1050, AA3104, AA5182, AA6111). Two quantitative indices, the Hot Tearing Sensitivity Index (HTS) and the Footprint Chart, were developed and used very effectively to quantify the hot tearing susceptibility of the alloys. It was found that the hot tearing susceptibility of the alloys can be ranked as

   HTS (AA1050) < HTS (AA5182) < HTS (AA3104) < HTS (AA6111).

   This ranking agrees with observations from typical industrial DC-casting experience.

2. Grain refinement can reduce hot tearing tendency in AA1050, AA5182, and AA3104 alloys. However, the effect of grain refinement was not significant in AA6111 alloy, despite the fact that the grain-refined structure is finer and equiaxed. The ranking of the alloys with respect to hot tearing susceptibility in the grain refined condition is

   AA5182<AA1050<AA3104<AA6111.

3. The microstructural investigation showed a direct relationship between the degree of grain refinement and the hot tearing tendency for the AA1050, AA5182, and AA3104 alloys. The AA6111 alloy showed little dependence on grain refinement, mainly because the alloy already exhibits a fine grained structure without the addition of the grain refiner.

4. The microstructural investigation of the CRC-cast AA1050 alloy showed clear evidence of tear healing occurring during solidification. The tears were sometimes completely or partially healed due to the intrusion of the solute rich liquid into the interdendritic regions. It was observed that the low hot tear tendency of the AA1050 alloy is probably due to the ability of the alloy to have tear healing phenomena occurring during solidification. Grain refining dramatically reduced hot tearing in this alloy.

5. The AA5182 alloy exhibited little tendency to hot tearing and the microstructural investigation showed that the tear surface had a high concentration of eutectic phase. Tear healing is not evident so the hot tearing resistance seems to be more related to the nature, amount and distribution of the eutectic. Grain refining was not effective in eliminating hot tearing in this alloy.

6. The AA3104 alloy showed uniquely different hot-tearing characteristics. Hot tear was not as an interdendritic separation, but the ductile fracture of joined dendrite tips. Grain refining reduced the hot tearing tendency in this alloy. Inverse segregation is evident in the surface.

Cu containing phases were observed on the tear surface. Grain refining decreased hot tearing severity.

7. The AA6111 alloy exhibited hot tears that can be described as interdendritic separation. The possible existence of microshrinkage cavities in the hot tear region is also noted. The hot tear surface is covered only in certain regions by a eutectic phase. Hot tearing in this alloy seems to be related to the wide freezing range, microshrinkage, and the nature and amount of the eutectic phase. Complex Cu containing phases were seen on the tear surface. This alloy exhibited a very fine structure even in the non grain-refined condition, but has still a high hot tearing susceptibility. Further grain refining treatments yielded only a little more refinement. However, this did not produce a significant improvement in the hot tearing resistance.

8. The CRC test is also suitable for assessing the hot tearing tendency in Al-Si binary alloys. The hot tearing susceptibility of the binary alloys is in agreement with foundry practice and with some previous investigations. The HTS values of Al-Si binary alloys are in following order,

0.5wt%Si>1.0wt%Si>1.5wt%Si>2.0wtt%Si>3.0wt%Si

10. Hot-tearing susceptibility in Al-Si binary alloys in the 0wt% – 2.0% Si range showed a direct relationship with freezing range, grain size and an inverse relationship with the amount of eutectic.

5.2 Recommendations for Future Work

This study was to a large extent exploratory in nature. A number of suggestions for potential future work is given below.

1. To correlate the hot tearing behavior of the alloys and the stress in the test pieces cast in the CRC mold, Simulation of the metal flow, solidification and stress formation needs to be carried out. A potential software to be used for this purpose is PROCAST software (available from UES Inc., Dayton, Ohio) which has all the required modules.

2. For all four alloys studied, the hot tear event should be investigated in-situ via the acoustic emission technique to determine the time of occurrence of hot tearing with respect to the solidification for both the non grain-refined and non grain-refined conditions. In addition, the dendrite coherency point should be determined using a rheological apparatus. Furthermore, the wettability of the interdendritic liquid should be determined for each alloy. The information so obtained will yield a fundamental basis for understanding the mechanisms of hot-tearing in various alloys.

3. The CRC mold should be optimized or converted into a more sensitive and practical mold by including more stress-raisers and notches to obtain a better response to differences in grain-refining levels. Grain refining studies should be conducted around the commercially accepted Ti levels.

4. For the AA6111 alloy the relationship between hot-tearing and shrinkage microporosity should also be investigated. Additions of trace elements such as Sr, which can alter microporosity distribution in aluminium alloys, should be investigated as a possible means to reduce hot tearing tendency in the AA6111 alloy.

APPENDIX I CRC RESULTS FOR WROUGHT ALUMINUM ALLOYS

Experiment No. 1

- Alloy: AA1050
- Grain Refiner: No
- Melt Temperature: 777 °C
- Mold Temperature: 250 °C

Table I-1 HTS Results of AA1050 Alloy in Test No. 1

Trial No.	$L_i \times C_i$				HTS	S
	Bar A	Bar B	Bar C	Bar D		
1	4×0	3×0	2×1	1×1	3	1
2	4×0	3×0	2×1	1×2	4	2
3	4×0	3×0	2×1	1×1	3	1
4	4×0	3×0	2×1	1×1	3	1
Average					3.3	1.3
Standard Deviation					0.5	0.5

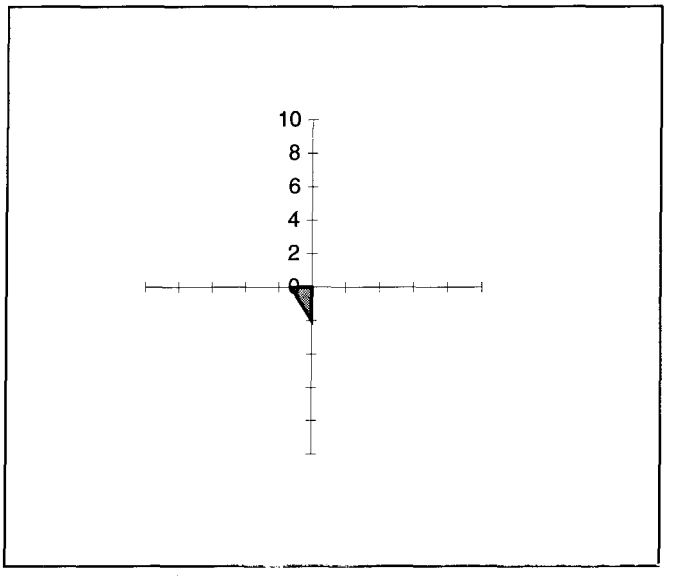

Figure I-1. Foot Print Chart of AA1050 alloy in test No. 1.

Experiment No. 2

- Alloy: AA1050
- Grain Refinement: No
- Melt Temperature: 777 °C
- Mold Temperature: 250 °C

Table I-2 HTS Results of AA1050 Alloy in Test No. 2

Trial No.	$L_i \times C_i$				HTS	S
	Bar A	Bar B	Bar C	Bar D		
1	4×0	3×0	2×2	1×2	6	4
2	4×0	3×0	2×1	1×2	4	2
3	4×0	3×0	2×1	1×3	5	3
4	4×0	3×0	2×1	1×2	4	2
Average					4.8	2.8
Standard Deviation					1	1

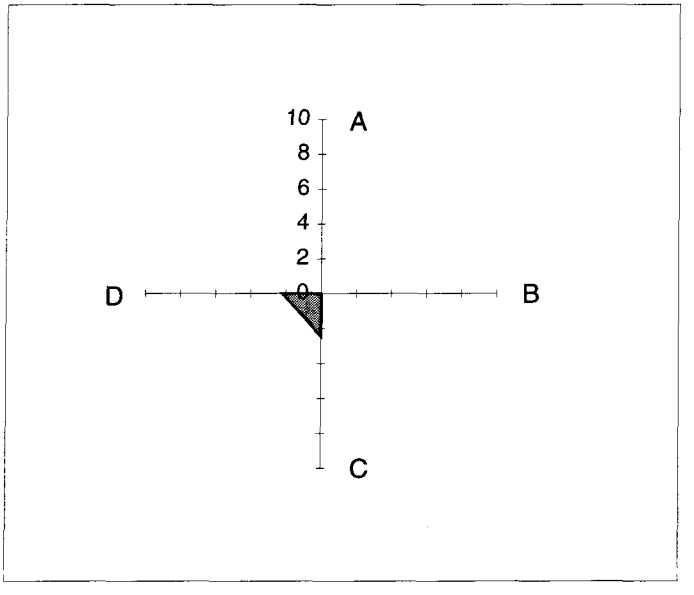

Figure I-2. Foot Print Chart of AA1050 alloy in test No. 2.

Experiment No. 3

- Alloy: AA1050
- Grain Refinement: No
- Melt Temperature: 777 °C
- Mold Temperature: 250 °C

Table I-3. HTS Results of AA1050 Alloy in Test No. 3

Trial No.	$L_i \times C_i$				HTS	S
	Bar A	Bar B	Bar C	Bar D		
1	4×0	3×0	2×2	1×2	6	4
2	4×0	3×0	2×1	1×1	3	1
3	4×0	3×0	2×3	1×1	7	3
4	4×0	3×0	2×1	1×2	4	2
Average					5	2.6
Standard Deviation					1.8	1.3

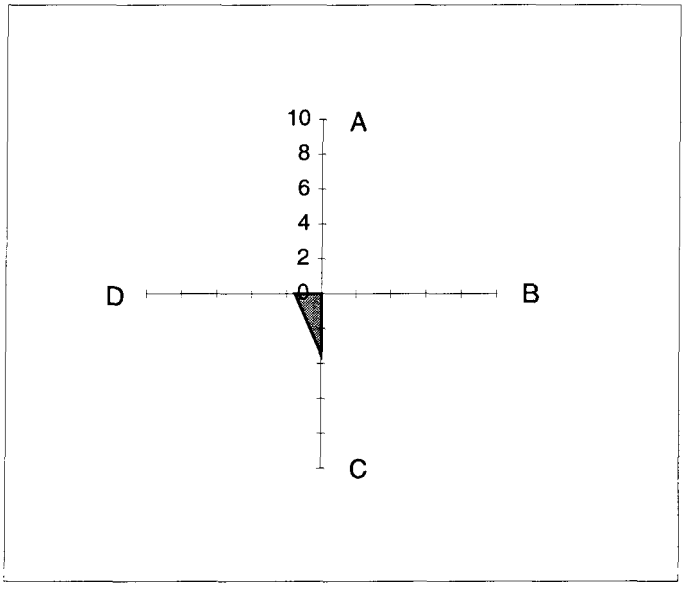

Figure I-3. Foot Print Chart of AA1050 alloy in test No. 3.

Experiment No. 4

- Alloy: AA3104
- Grain Refinement: No
- Melt Temperature: 772 °C
- Mold Temperature: 250 °C

Table I-4. HTS Results of AA3104 Alloy in Test No. 4

Trial No.	$L_i \times C_i$				HTS	S
	Bar A	Bar B	Bar C	Bar D		
1	4×0	3×1	2×3	1×4	13	21
2	4×0	3×1	2×3	1×4	13	21
3	4×0	3×1	2×3	1×4	13	21
4	4×0	3×1	2×3	1×4	13	21
Average					13	21
Standard Deviation					0	0

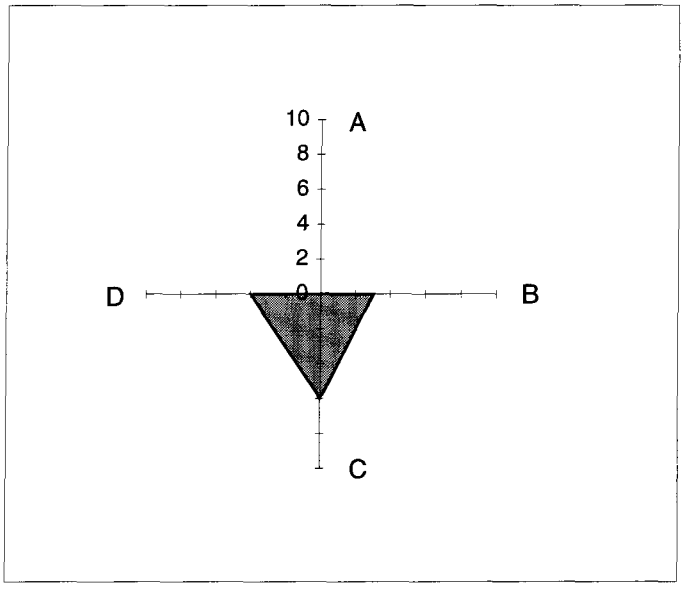

Figure I-4. Foot Print Chart of AA3104 alloy in Test No. 4.

Experiment No. 5

- Alloy: AA3104
- Grain Refinement: No
- Melt Temperature: 772°C
- Mold Temperature: 250°C

Table I-5 HTS Results of AA3104 Alloy in Test No. 5

Trial No.	$L_i \times C_i$				HTS	S
	Bar A	Bar B	Bar C	Bar D		
1	4×0	3×2	2×3	1×4	16	30
2	4×0	3×3	2×4	1×4	21	52
3	4×0	3×2	2×4	1×4	18	40
4	4×0	3×1	2×3	1×4	13	21
Average					17	35
Standard Deviation					3	13

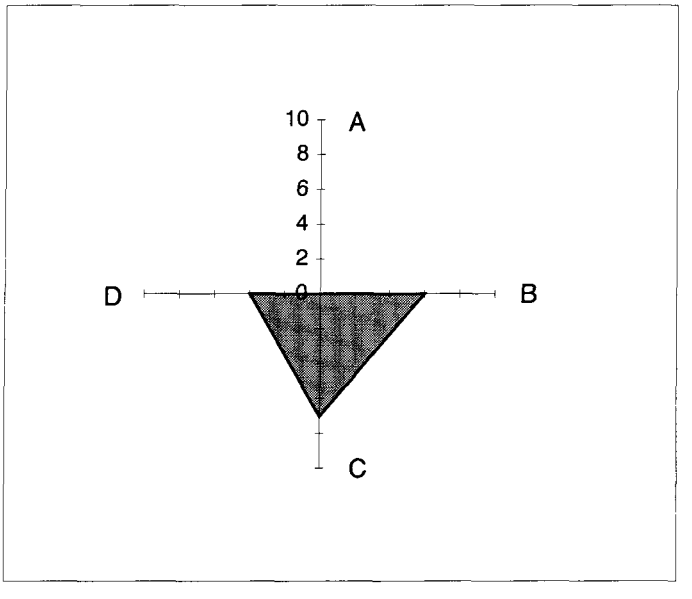

Figure I-5. Foot Print Chart of AA3104 alloy in Test No. 5.

Experiment No. 6

- Alloy: AA3104
- Grain Refinement: No
- Melt Temperature: 772°C
- Mold Temperature: 250°C

Table I-6 HTS Results of AA3104 Alloy in Test No. 6

Trial No.	$L_i \times C_i$				HTS	S
	Bar A	Bar B	Bar C	Bar D		
1	4×0	3×2	2×3	1×4	16	30
2	4×0	3×2	2×3	1×4	16	30
3	4×0	3×2	2×3	1×4	16	30
4	4×0	3×2	2×3	1×3	15	27
Average					16	29
Standard Deviation					0.5	1.5

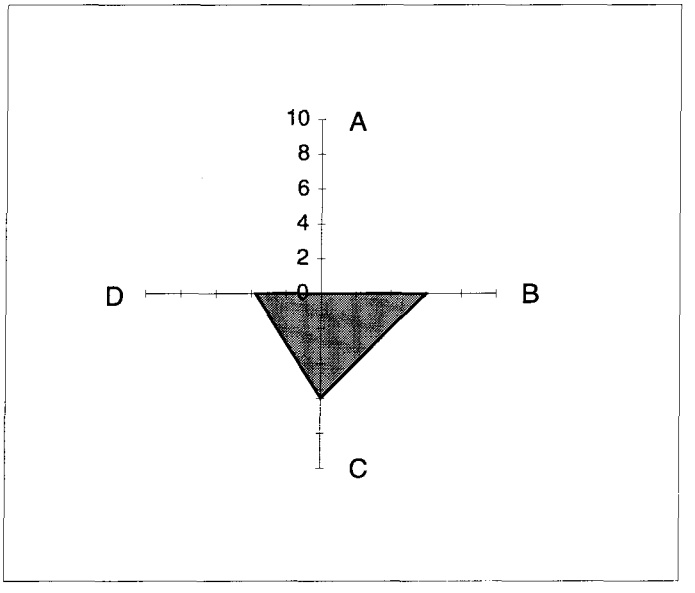

Figure I-6. Foot Print Chart of 3104 alloy in test No. 6.

Experiment No. 7

- Alloy: AA5182
- Grain Refinement: No
- Melt Temperature: 758°C
- Mold Temperature: 250°C

Table I-7 HTS Results of AA5182 Alloy in Test No. 7

Trial No.	$L_i \times C_i$				HTS	S
	Bar A	Bar B	Bar C	Bar D		
1	4×0	3×1	2×1	1×2	7	5
2	4×0	3×1	2×2	1×2	9	10
3	4×0	3×1	2×2	1×2	9	10
4	4×0	3×1	2×1	1×3	8	6
Average					8	8
Standard Deviation					1	2.6

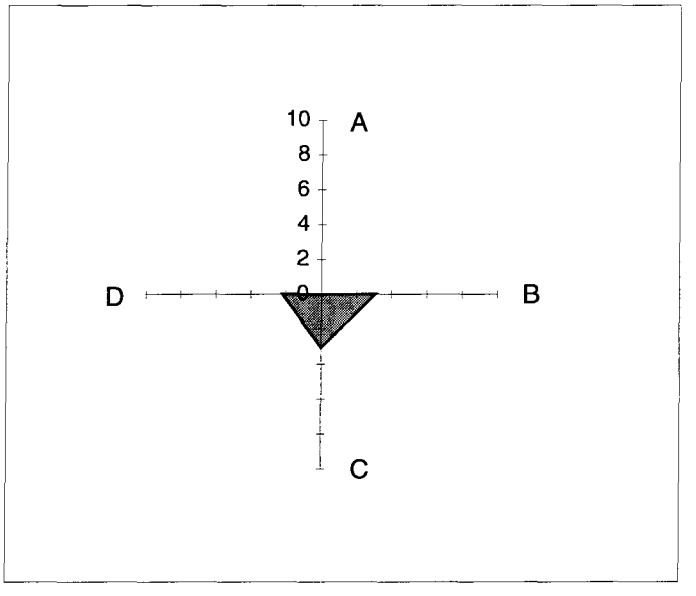

Figure I-7. Foot Print Chart of AA5182 alloy in Test No. 7.

Experiment No. 8

- Alloy: AA5182
- Grain Refinement: No
- Melt Temperature: 758°C
- Mold Temperature: 250°C

Table I-8. HTS Results of AA5182 Alloy in Test No. 8

Trial No.	$L_i \times C_i$				HTS	S
	Bar A	Bar B	Bar C	Bar D		
1	4×0	3×0	2×1	1×2	4	2
2	4×0	3×1	2×2	1×3	10	12
3	4×0	3×1	2×2	1×2	9	10
4	4×0	3×1	2×2	1×2	9	10
Average					8	8
Standard Deviation					2.7	4.4

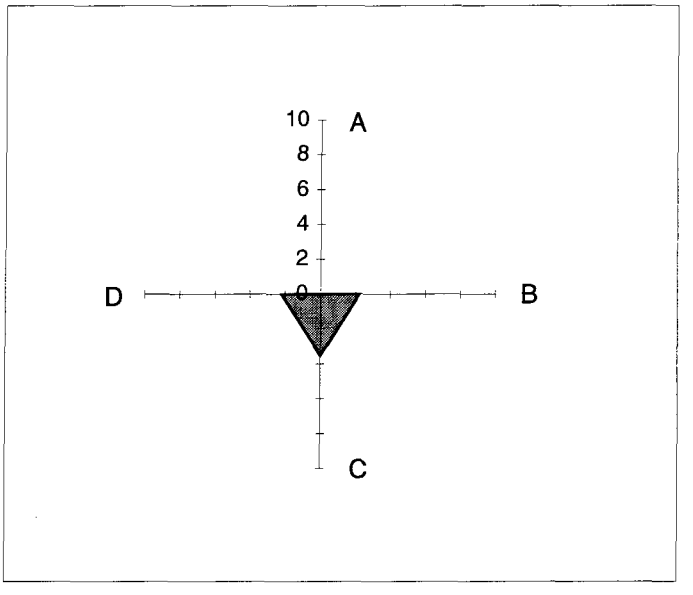

Figure I-8. Foot Print Chart of AA5182 alloy in test No. 8.

Experiment No. 9

- Alloy: AA5182
- Grain Refinement: No
- Melt Temperature: 758°C
- Mold Temperature: 250°C

Table 9. HTS Results of AA5182 Alloy in Test No. 9

Trial No.	$L_i \times C_i$				HTS	S
	Bar A	Bar B	Bar C	Bar D		
1	4×0	3×1	2×2	1×1	8	8
2	4×0	3×1	2×2	1×1	8	8
3	4×0	3×1	2×2	1×1	8	8
4	4×0	3×1	2×2	1×1	8	8
Average					8	8
Standard Deviation					0	0

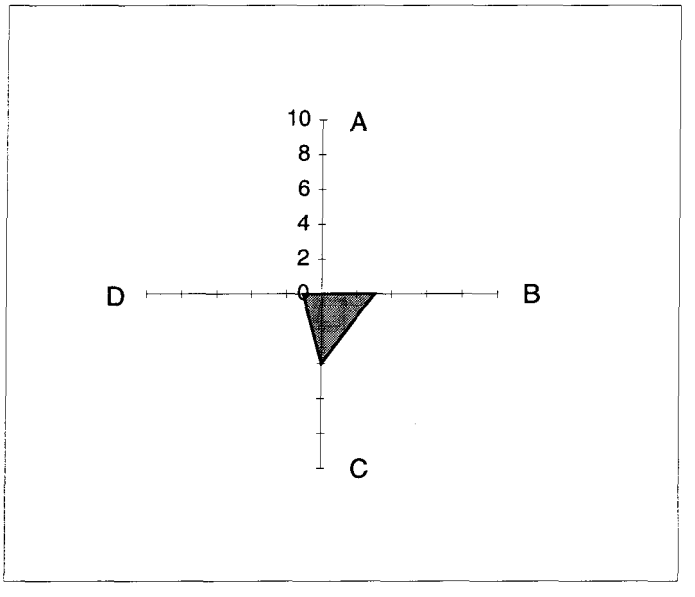

Figure I-9. Foot Print Chart of AA5182 alloy in test No. 9.

Experiment No. 10

- Alloy: AA6111
- Grain Refinement: No
- Melt Temperature: 770°C
- Mold Temperature: 250°C

Table I-10 HTS Results of AA6111 Alloy in Test No. 10

Trial No.	$L_i \times C_i$				HTS	S
	Bar A	Bar B	Bar C	Bar D		
1	4×0	3×4	2×4	1×4	24	64
2	4×0	3×4	2×4	1×4	24	64
3	4×0	3×4	2×4	1×4	24	64
4	4×0	3×4	2×4	1×4	24	64
Average					24	64
Standard Deviation					0	0

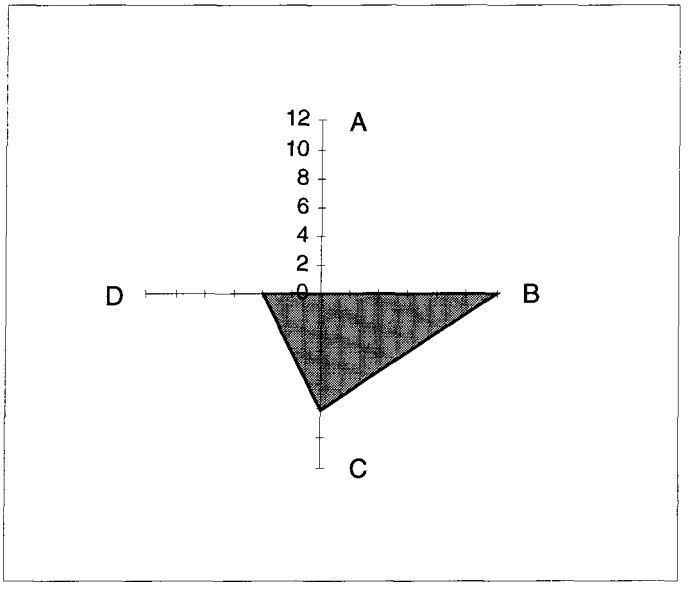

Figure I-10. Foot Print Chart of AA6111 alloy in test No. 10.

Experiment No. 11

- Alloy: AA6111
- Grain Refinement: No
- Melt Temperature: 770°C
- Mold Temperature: 250°C

Table I-11 HTS Results of AA6111 Alloy in Test No. 11

Trial No.	$L_i \times C_i$				HTS	S
	Bar A	Bar B	Bar C	Bar D		
1	4×0	3×3	2×4	1×4	21	52
2	4×0	3×3	2×4	1×4	21	52
3	4×0	3×3	2×4	1×4	21	52
4	4×0	3×3	2×4	1×4	21	52
Average					21	52
Standard Deviation					0	0

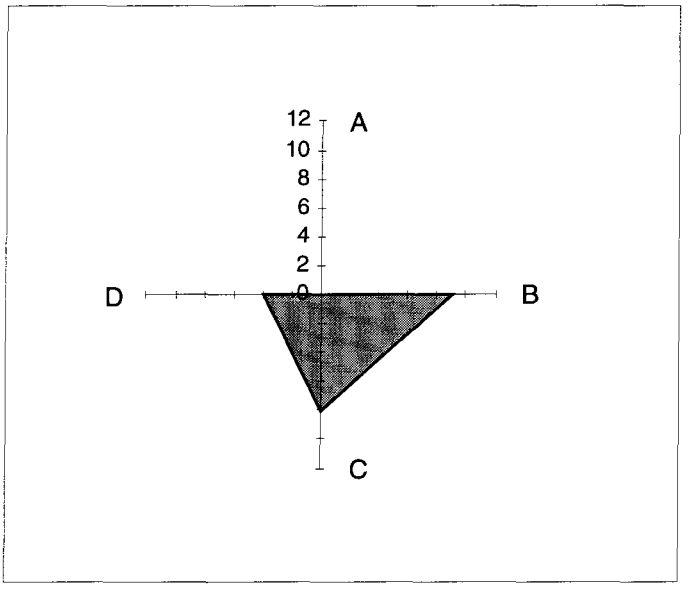

Figure I-11. Foot Print Chart of AA6111 alloy in test No. 11.

Experiment No. 12

- Alloy: AA6111
- Grain Refinement: No
- Melt Temperature: 770°C
- Mold Temperature: 250°C

Table I-12 HTS Results of AA6111 Alloy in Test No. 12

Trial No.	$L_i \times C_i$				HTS	S
	Bar A	Bar B	Bar C	Bar D		
1	4×1	3×3	2×4	1×4	25	52
2	4×1	3×3	2×4	1×4	25	52
3	4×1	3×3	2×4	1×4	25	52
4	4×1	3×3	2×4	1×4	25	52
Average					25	52
Standard Deviation					0	0

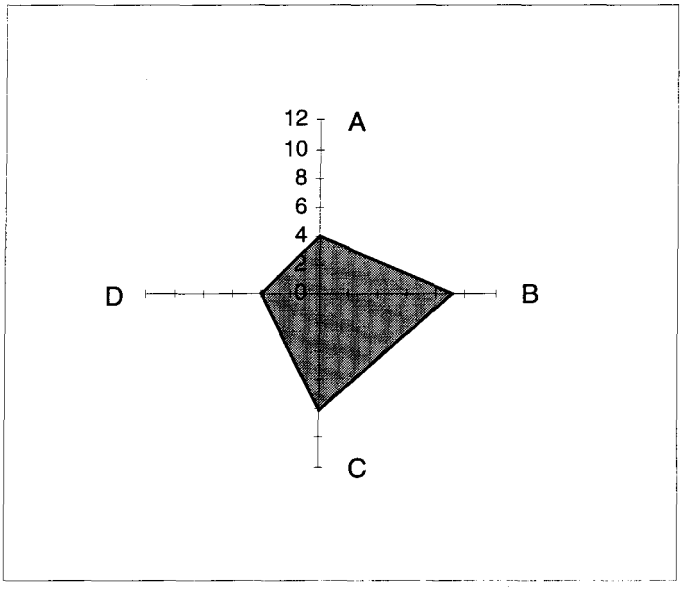

Figure I-12. Foot Print Chart of AA6111 alloy in test No. 12.

APPENDIX II CRC TEST RESULTS OF GRAIN-REFINED ALLOYS

Experiment No. 13

- Alloy: AA1050
- Grain Refinement: 0.001% Ti+0.0002% B
- Melt Temperature: 777 °C
- Mold Temperature: 250 °C

Table II-1 HTS Results of AA1050 Alloy with 0.001%Ti Addition in Test No. 13

Trial No.	$L_i \times C_i$				HTS	S
	Bar A	Bar B	Bar C	Bar D		
1	4×0	3×0	2×1	1×1	3	1
2	4×0	3×0	2×0	1×1	1	0
3	4×0	3×0	2×1	1×1	3	1
4	4×0	3×0	2×1	1×1	3	1
Average					2.5	0.8
Standard Deviation					1	0.5

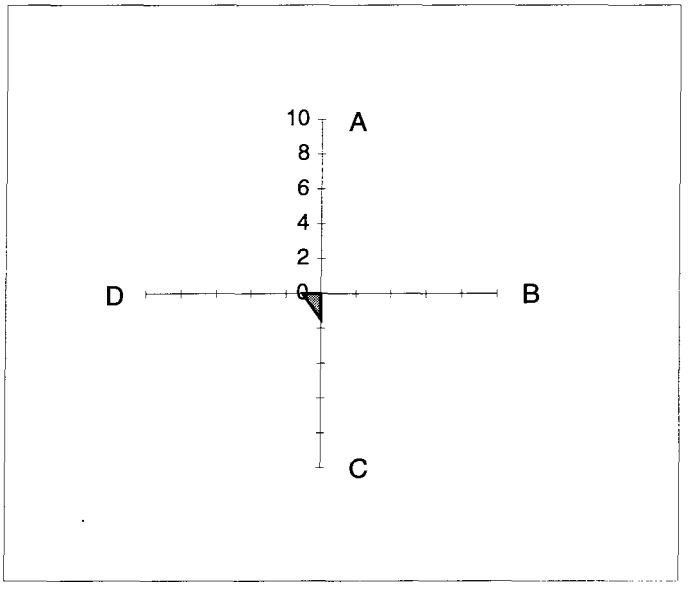

Figure II-1. Foot Print Chart of AA1050 alloy with 0.001%Ti addition in test No. 13.

Experiment No. 14

- Alloy: AA1050
- Grain Refinement: 0.001% Ti+0.0002% B
- Melt Temperature: 777 °C
- Mold Temperature: 250 °C

Table II-2 HTS Results of AA1050 Alloy with 0.001%Ti Addition of Test No. 14

Trial No.	$L_i \times C_i$				HTS	S
	Bar A	Bar B	Bar C	Bar D		
1	4×0	3×0	2×1	1×2	4	2
2	4×0	3×0	2×1	1×2	4	2
3	4×0	3×0	2×1	1×2	4	2
4	4×0	3×0	2×1	1×2	4	2
Average					4	2
Standard Deviation					0	0

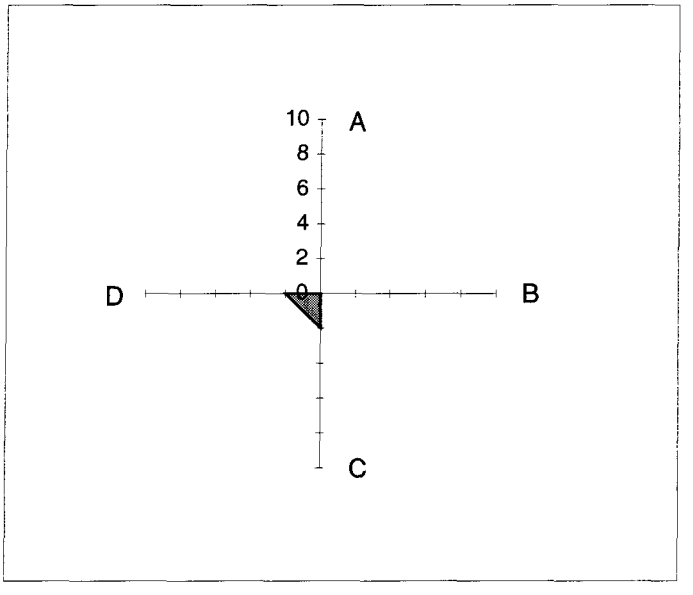

Figure II-2. Foot Print Chart of AA1050 alloy with 0.001%Ti addition in test No. 14.

Experiment No. 15

- Alloy: AA1050
- Grain Refinement: 0.002% Ti+0.0004% B
- Melt Temperature: 777 °C
- Mold Temperature: 250 °C

Table II-3 HTS Results of AA1050 Alloy with 0.002%Ti Addition in Test No. 15

Trial No.	$L_i \times C_i$				HTS	S
	Bar A	Bar B	Bar C	Bar D		
1	4×0	3×0	2×1	1×1	3	1
2	4×0	3×0	2×1	1×1	3	1
3	4×0	3×0	2×1	1×1	3	1
4	4×0	3×0	2×1	1×1	3	1
Average					3	1
Standard Deviation					0	0

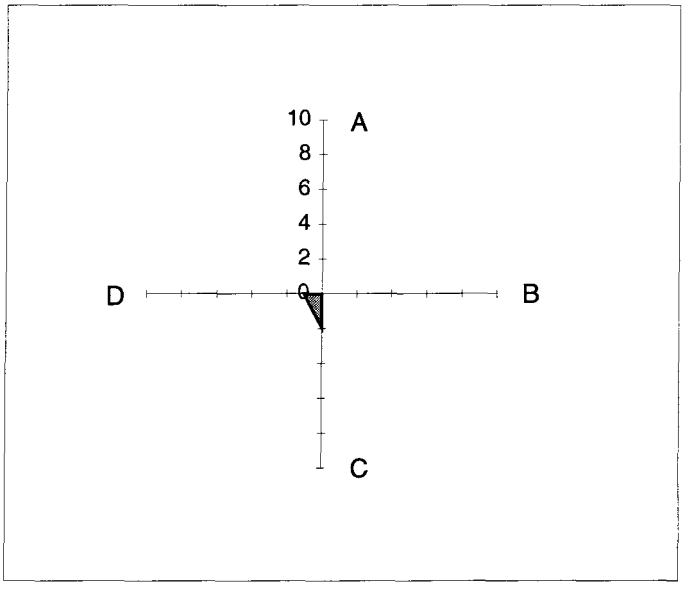

Figure II-3. Foot Print Chart of AA1050 alloy with 0.002%Ti addition in test No. 15.

Experiment No. 16

- Alloy: AA1050
- Grain Refinement: 0.002% Ti+0.0004% B
- Melt Temperature: 777 °C
- Mold Temperature: 250 °C

Table II-4 HTS Results of AA1050 Alloy with 0.002%Ti Addition in Test No. 16

Trial No.	$L_i \times C_i$				HTS	S
	Bar A	Bar B	Bar C	Bar D		
1	4×0	3×0	2×0	1×1	1	0
2	4×0	3×0	2×1	1×1	3	1
3	4×0	3×0	2×1	1×1	3	1
4	4×0	3×0	2×1	1×1	3	1
Average					2.5	0.8
Standard Deviation					1	0.5

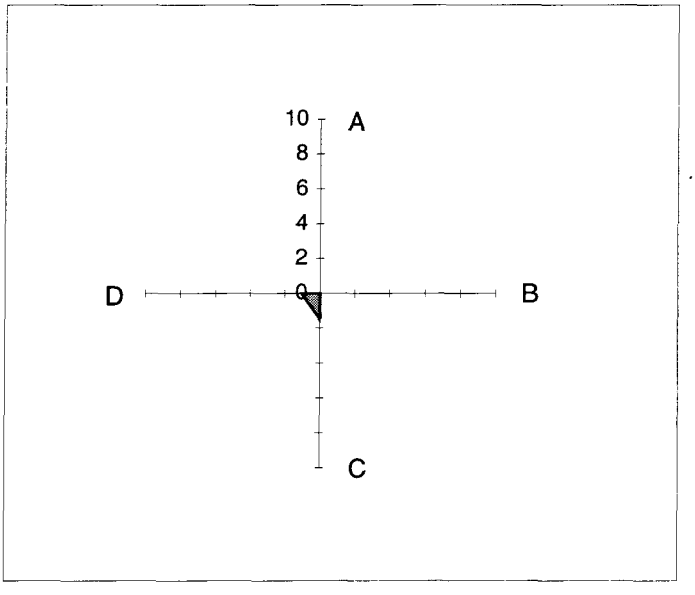

Figure II-4. Foot Print Chart of AA1050 alloy with 0.002%Ti addition in test No. 16.

Experiment No. 17

- Alloy: AA1050
- Grain Refinement: 0.01% Ti+0.002% B
- Melt Temperature: 777 °C
- Mold Temperature: 250 °C

Table II-5 HTS Results of AA1050 Alloy with 0.01%Ti Addition in Test No. 17

Trial No.	$L_i \times C_i$				HTS	S
	Bar A	Bar B	Bar C	Bar D		
1	4×0	3×0	2×1	1×2	4	2
2	4×0	3×0	2×1	1×2	4	2
3	4×0	3×0	2×0	1×1	1	1
4	4×0	3×0	2×0	1×2	2	0
Average					2.8	0.9
Standard Deviation					1.5	1.2

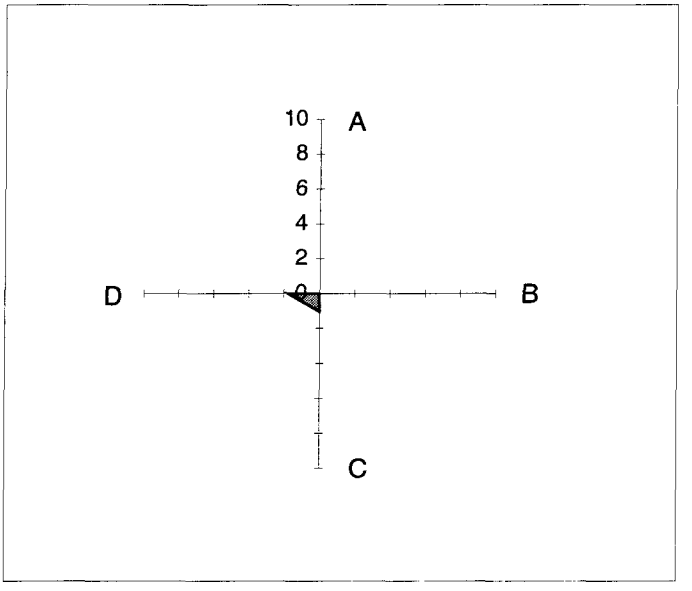

Figure II-5. Foot Print Chart of AA1050 alloy with 0.01%Ti addition in test No. 17.

Experiment No. 18

- Alloy: AA1050
- Grain Refinement: 0.01% Ti+0.002% B
- Melt Temperature: 777 °C
- Mold Temperature: 250 °C

Table II-6 HTS Results of AA1050 Alloy with 0.01%Ti Addition in Test No. 18

Trial No.	$L_i \times C_i$				HTS	S
	Bar A	Bar B	Bar C	Bar D		
1	4×0	3×0	2×0	1×1	1	0
2	4×0	3×0	2×0	1×1	1	0
3	4×0	3×0	2×1	1×1	3	1
4	4×0	3×0	2×0	1×1	1	0
Average					1.5	0.3
Standard Deviation					1	0.5

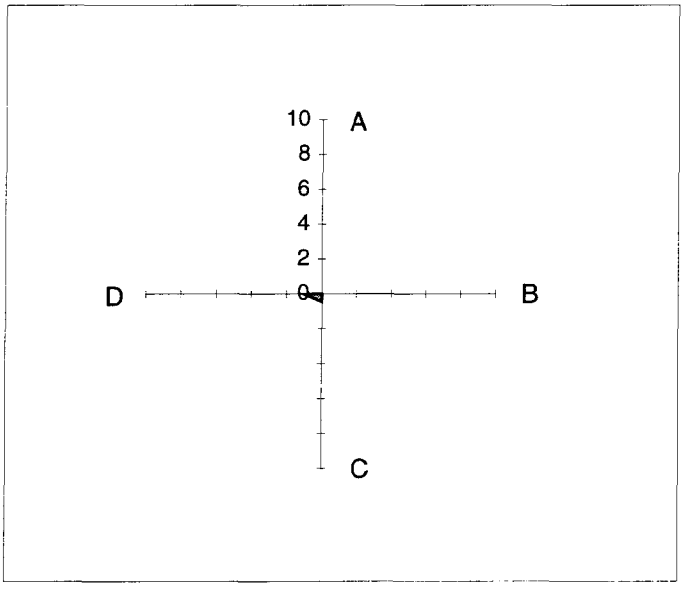

Figure II-6. Foot Print Chart of AA1050 alloy with 0.01%Ti addition in test No. 18.

Experiment No. 19

- Alloy: AA3104
- Grain Refinement: 0.01% Ti+0.002% B
- Melt Temperature: 772 °C
- Mold Temperature: 250 °C

Table II-7 HTS Results of AA3104 Alloy with 0.01%Ti Addition in Test No. 19

Trial No.	$L_i \times C_i$				HTS	S
	Bar A	Bar B	Bar C	Bar D		
1	4×0	3×0	2×2	1×4	8	8
2	4×0	3×4	2×3	1×4	22	48
3	4×0	3×4	2×1	1×4	18	16
4	4×0	3×4	2×2	1×4	20	32
Average					6.2	17.7
Standard Deviation					3	5

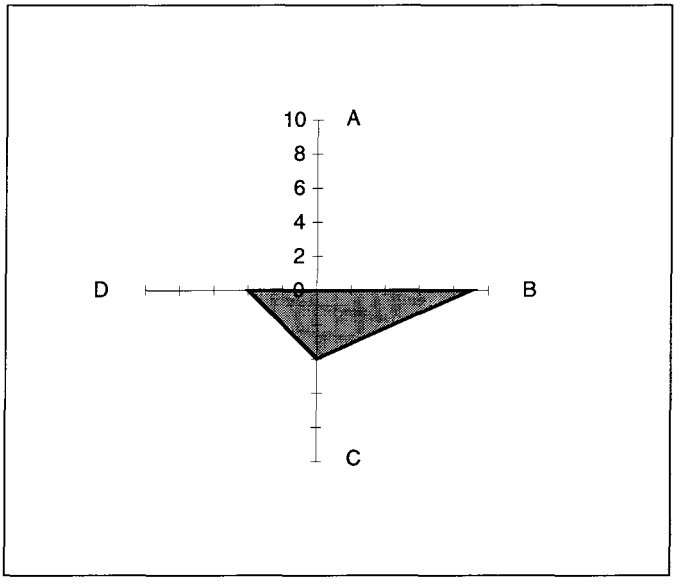

Figure II-7. Foot Print Chart of AA3104 alloy with 0.01%Ti addition in test No. 19.

Experiment No. 20

- Alloy: AA3104
- Grain Refinement: 0.01% Ti+0.002% B
- Melt Temperature: 772 °C
- Mold Temperature: 250 °C

Table II-8 HTS Results of AA3104 Alloy with 0.01%Ti Addition in Test No. 20

Trial No.	$L_i \times C_i$				HTS	S
	Bar A	Bar B	Bar C	Bar D		
1	4×0	3×0	2×0	1×3	3	0
2	4×0	3×0	2×0	1×3	3	0
3	4×0	3×0	2×0	1×4	4	0
4	4×0	3×0	2×4	1×4	4	16
Average					5.5	3.5
Standard Deviation					4.4	8

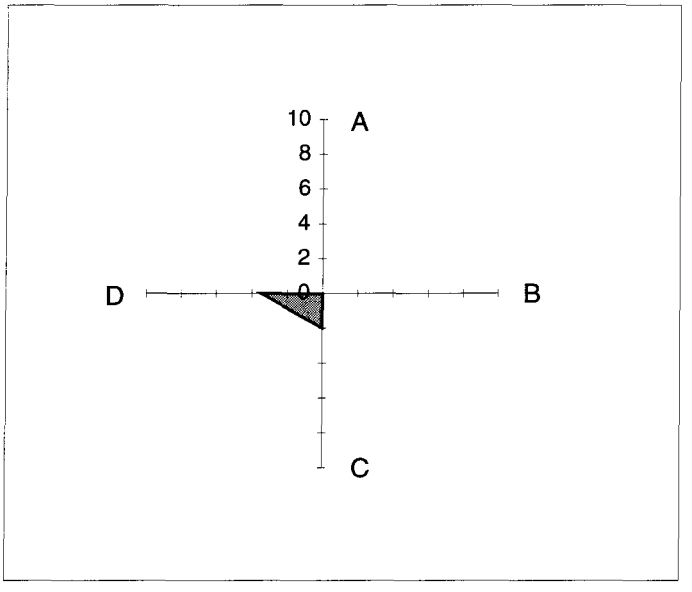

Figure II-8. Foot Print Chart of AA3104 alloy with 0.01%Ti addition in test No. 20.

Experiment No. 21

- Alloy: AA5182
- Grain Refinement: 0.01% Ti+0.002% B
- Melt Temperature: 770 °C
- Mold Temperature: 250 °C

Table II-9 HTS Results of AA5182 Alloy with 0.01%Ti Addition in Test No. 21

Trial No.	$L_i \times C_i$				HTS	S
	Bar A	Bar B	Bar C	Bar D		
1	4×0	3×0	2×0	1×0	0	0
2	4×0	3×0	2×0	1×0	0	0
3	4×0	3×0	2×0	1×0	0	0
4	4×0	3×0	2×0	1×0	0	0
Average					0	0
Standard Deviation					0	0

Experiment No. 22

- Alloy: AA5182
- Grain Refinement: 0.01% Ti+0.002% B
- Melt Temperature: 758 °C
- Mold Temperature: 250 °C

Table II-10 HTS Results of AA5182 Alloy with 0.01%Ti Addition in Test No. 22

Trial No.	$L_i \times C_i$				HTS	S
	Bar A	Bar B	Bar C	Bar D		
1	4×0	3×0	2×0	1×0	0	0
2	4×0	3×0	2×0	1×0	0	0
3	4×0	3×0	2×0	1×0	0	0
4#	4×0	3×0	2×0	1×0	0	0
Average					0	0
Standard Deviation					0	0

Experiment No. 23

- Alloy: AA6111
- Grain Refinement: 0.01% Ti+0.002% B
- Melt Temperature: 770 °C
- Mold Temperature: 250 °C

Table II-11 HTS Results of AA6111 Alloy with 0.01%Ti Addition in Test No. 23

Trial No.	$L_i \times C_i$				HTS	S
	Bar A	Bar B	Bar C	Bar D		
1	4×0	3×3	2×4	1×4	21	52
2	4×0	3×4	2×4	1×4	24	64
3	4×0	3×4	2×4	1×4	24	64
4	4×0	3×3	2×4	1×4	21	52
Average					22.5	58
Standard Deviation					1.7	6.8

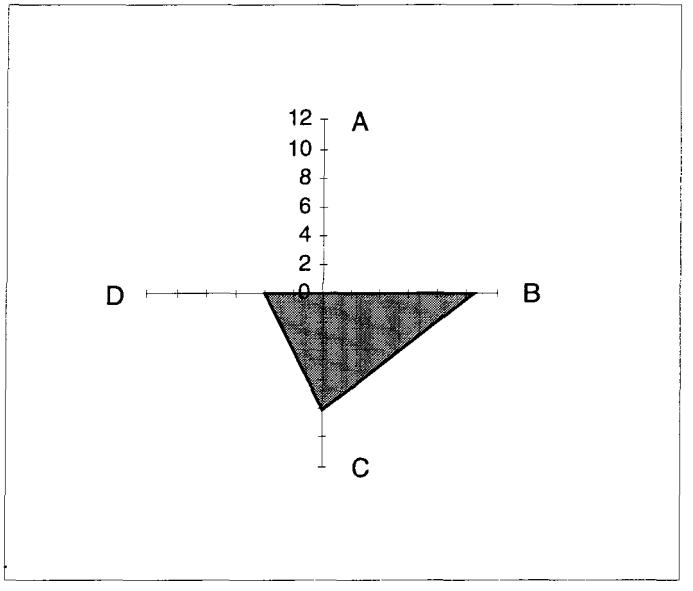

Figure II-9. Foot Print Chart of AA6111 alloy with 0.01%Ti addition in test No. 23.

Experiment No. 24

- Alloy: AA6111
- Grain Refinement: 0.01% Ti+0.002% B
- Melt Temperature: 770 °C
- Mold Temperature: 250 °C

Table II-12 HTS Results of AA6111 Alloy with 0.01%Ti Addition in Test No. 24

Trial No.	$L_i \times C_i$				HTS	S
	Bar A	Bar B	Bar C	Bar D		
1	4×0	3×3	2×4	1×4	21	52
2	4×0	3×3	2×4	1×4	21	52
3	4×0	3×4	2×4	1×4	24	64
4	4×0	3×4	2×4	1×4	24	64
Average					22.5	58
Standard Deviation					1.7	6.9

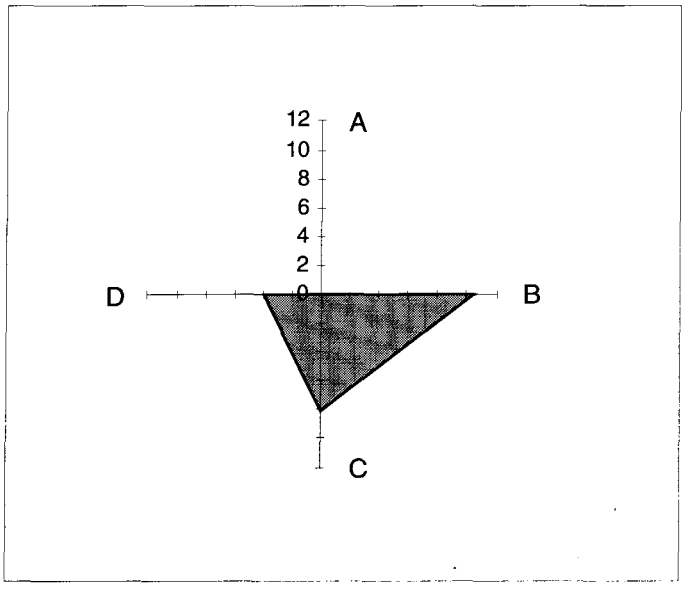

Figure II-10. Foot Print Chart of AA6111 alloy with 0.01%Ti addition in test No. 24.

APPENDIX III CRC TEST RESULTS OF AL-SI BINARY ALLOYS

Experiment No. 25

- Alloy: pure Al + 0.5wt% Si
- Melt Temperature: 779 °C
- Mold Temperature: 250 °C

Table III-1 HTS Results of Al-0.5wt%Si Binary Alloy in Test No. 25

Trial No.	$L_i \times C_i$				HTS	S
	Bar A	Bar B	Bar C	Bar D		
1	4×0	3×3	2×4	1×4	21	52
2	4×0	3×3	2×4	1×4	21	52
3	4×0	3×3	2×4	1×4	21	52
4	4×0	3×3	2×4	1×4	21	52
Average					21	52
Standard Deviation					0	0

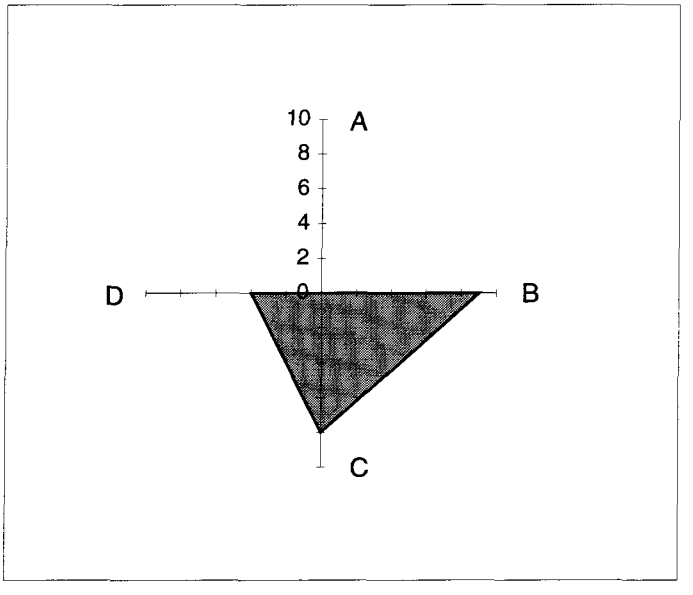

Figure III-1. Foot Print Chart of Al-0.5wt%Si binary alloy in test No. 25.

Experiment No. 26

- Alloy: pure Al + 1wt% Si
- Melt Temperature: 775 °C
- Mold Temperature: 250 °C

Table III-2 HTS Results of Al-1wt%Si Binary Alloy in Test No. 26

Trial No.	$L_i \times C_i$				HTS	S
	Bar A	Bar B	Bar C	Bar D		
1	4×0	3×2	2×4	1×4	18	40
2	4×0	3×1	2×4	1×4	15	28
3	4×0	3×2	2×4	1×4	18	40
4	4×0	3×3	2×4	1×4	21	52
Average					18	40
Standard Deviation					2.5	9.8

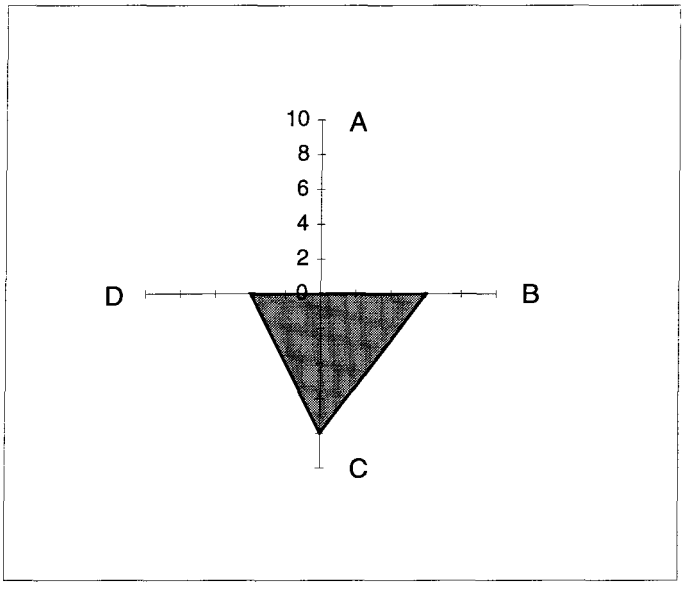

Figure III-2. Foot Print Chart of Al-1wt%Si binary alloy in test No. 26.

Experiment No. 27

- Alloy: pure Al + 1.5wt% Si
- Melt Temperature: 773 °C
- Mold Temperature: 250 °C

Table III-3 HTS Results of Al-1.5wt%Si Binary Alloy in Test No. 27

Trail/	$L_i \times C_i$				HTS	S
	Bar A	Bar B	Bar C	Bar D		
1	4×0	3×2	2×3	1×4	16	30
2	4×0	3×2	2×3	1×4	16	30
3	4×0	3×2	2×3	1×4	16	30
4	4×0	3×0	2×3	1×4	9	9
Average					14.3	24.8
Standard Deviation					3.5	10.5

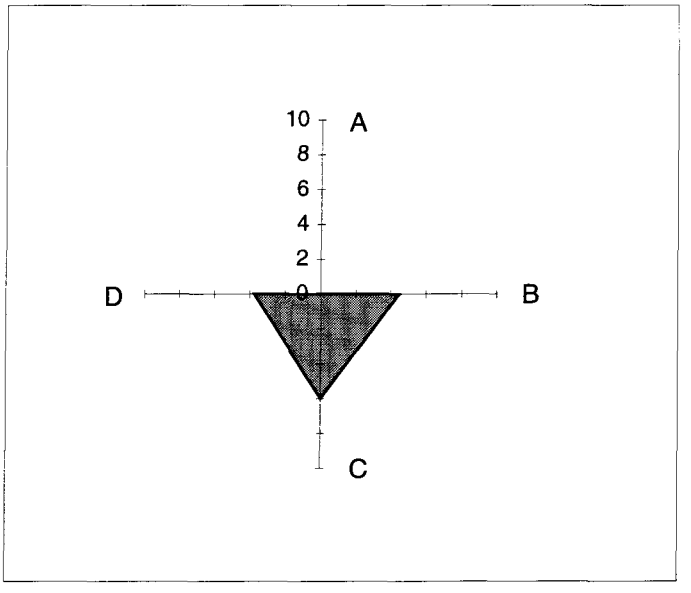

Figure III-3. Foot Print Chart of Al-1.5wt%Si binary alloy in test No. 27.

Experiment No. 28

- Alloy: pure Al + 2wt% Si
- Melt Temperature: 770 °C
- Mold Temperature: 250 °C

Table III-4 HTS Results of Al-2wt%Si Binary Alloy in Test No. 28

Trial No.	$L_i \times C_i$				HTS	S
	Bar A	Bar B	Bar C	Bar D		
1	4×0	3×0	2×2	1×3	7	6
2	4×0	3×0	2×1	1×3	5	3
3	4×0	3×0	2×2	1×3	7	6
4	4×0	3×0	2×2	1×3	7	6
Average					6.5	5.3
Standard Deviation					1	1.5

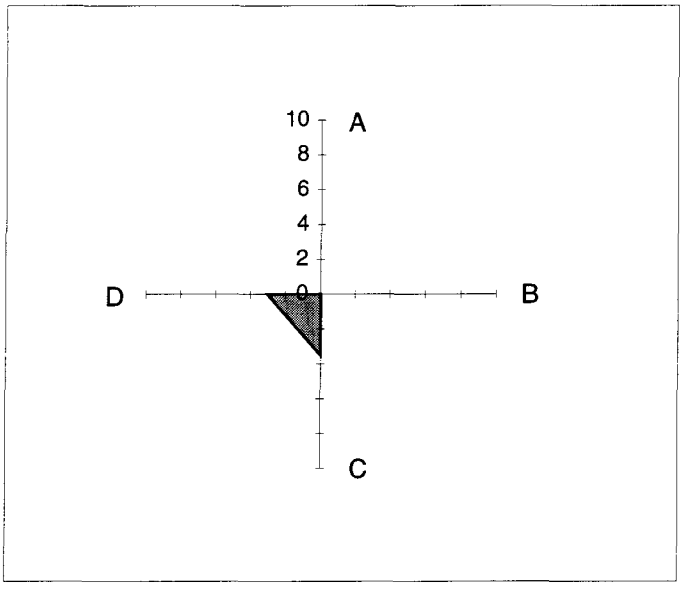

Figure III-4. Foot Print Chart of Al-2wt%Si binary alloy in test No. 28.

Experiment No. 29

- Alloy: pure Al + 3wt% Si
- Melt Temperature: 764 °C
- Mold Temperature: 250 °C

Table III-5 HTS Results of Al-3wt%Si Binary Alloy in Test No. 29

Trial No.	$L_i \times C_i$				HTS	S
	Bar A	Bar B	Bar C	Bar D		
1	4×0	3×0	2×1	1×1	3	1
2	4×0	3×0	2×1	1×0	2	0
3	4×0	3×0	2×1	1×0	2	0
4	4×0	3×0	2×1	1×0	2	0
Average					2.3	0.3
Standard Deviation					0.5	0.5

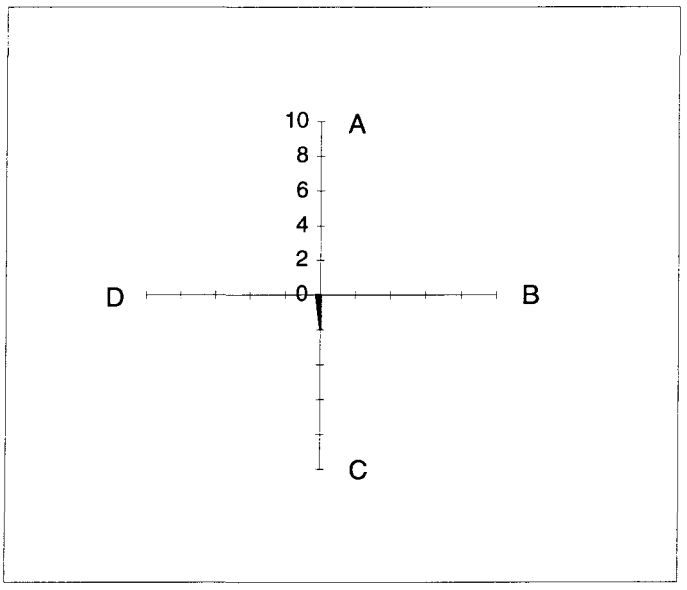

Figure III-5. Foot Print Chart of Al-3wt%Si binary alloy in test No. 29.

REFERENCES

1. S. Gowri and M. Bouchard, "Hot Cracking in Aluminium Alloys—Part 1. Literature Survey", Research Report, Université du Québec à Chicoutimi, December, 1994.
2. S. Gowri and M. Bouchard, "Hot Cracking in Aluminium Alloys—Part 2. Experimental Results", Research Report, Université du Québec à Chicoutimi, January, 1995.
3. A.R.E. Singer and P.H. Jennings, "Hot-Shortness of The Aluminium-1043 Silicon Alloys of Commercial Purity", J. Inst. Metals, vol. 72, 1946, pp.197-211.
4. R.A. Rosenberg, M.C. Flemings, and H.F. Taylor, "Nonferrous Binary Alloys Hot-Tearing", Trans. AFS., vol.68, 1960, pp.518-528.
5. E.J. Gamber, "Hot Cracking Test for Light Metal Casting Alloys", Trans. AFS., vol. 67, 1959, p. 237.
6. H.F. Hall, "The strength and Ductility of Cast Steel During Cooling from the Liquid State in Sand Molds, Part I", J. Iron Steel Inst., Special Report, vol. 15, 1946, p. 65.
7. W.I. Pumphrey and P.H. Jennings, "A Consideration of the Nature of Brittleness at Temperatures above the Solidus in Castings and Welds in Aluminum Alloys," J. Inst. Metals, vol. 75, 1948, p. 235.
8. M. Ohtaki, Nikko, U. Honma, Yokohama, and S. Oya, "In Situ Determination of Casting Defects in Solidifying Al-7%Si Alloy Casting by the Acoustic Emission Mehtod", Aluminum, vol. 64, no. 5, 1988, p. 521.
9. T.W. Clyne and G.J. Davies, "A Quantitive Solidification Test for Casting and An Evaluation of Cracking in Aluminium-Magnesium Alloys", The British Foundryman, vol. 68, no. 9, 1975, p. 238.
10. G. Upadhya, S. Cheng, and U. Chandra, "A Mathematical Model for Predication of Hot Tears in Castings", Light Metals, AIME, 1995, pp. 1101-1106.
11. L. Katgerman, "A Mathematical Model for Hot Cracking of Aluminum Alloys During DC Casting", Light Metals, AIME, 1981, p. 845.

12. J. Langlais, "Hot Tearing Mechanisms, Theory and Literature Survey", Work from Ph.D. thesis, McGill University, unpublished, 1997.
13. F. Körber and G. Schitzkowski, "Determination of the Contraction of Cast Steel", Stahl und Eisen, vol. 15, 1928, p.128.
14. C.W. Briggs, "Hot Tear Formation", Metallurgy of Steel Castings, 1946, p. 317.
15. J.M. Middleton, "Hot-tearing of Steel", J. Iron and Steel Inst., vol. 42, 1949, p. 407.
16. U.K Bhattacharya, C.M. Adams, and H.F. Taylor, "Hot Tear Formation in Steel Casting," Trans. AFS, vol. 60, 1952, p. 675.
17. J. Verö, "Hot-Tearing of Aluminum Alloys", Metals Industry, vol. 48, 1936, p. 431.
18. H.F. Bishop, C.G. Ackerlind, and W.S. Pellini, "Metallurgy and Mechanics of Hot Tearing", Trans. AFS, vol. 60, 1952, p. 818.
19. U.K. Bhattacharya, C.M. Adams, and H.F. Taylor, "Stress Required to Hot Tear Plain Carbon Cast Steel", Trans. AFS, vol. 62, 1954, p. 557.
20. W.S. Pellini, "Strain Theory of Hot-tearing", Foundry, vol. 80, 1952, p. 124.
21. W.R. Apblett and W.S. Pellini, "Factors Which Influence Weld Hot Cracking" Welding Research, vol.19, 1954, p. 83.
22. J.C. Borland, "Generalized Theory of Super-Solidus Cracking in Welds and Casting", British Welding Journal, vol. 7, no. 8, 1960, pp. 508-512.
23. R.A. Flinn, Fundamentals of Metal Casting, Addison-Wesley, 1963, pp. 103-111.
24. A.R.E. Singer and S.A. Cottrell, "Properties of the Al-Si Alloys at Temperatures in the Region of the Solidus", J. Inst. Metals, vol. 73, 1947, p. 33.
25. V.N. Saveiko, "Theory of Hot Tearing", Russian Casting Production, vol. 11, October, 1961, p. 453.
26. I. Novikov and O.E. Grushko, "Hot Cracking Susceptibility of Al-Cu-Li and Al-Cu-Li-Mn Alloys", Mater. Sci. Tech., vol. 11, no. 9, 1995, p. 926.
27. M. Kubota and S. Kitaoka, "Solidification Behavior and Hot Tearing Tendency of Aluminum Casting Alloys", Trans. AFS, vol. 81, 1973, p. 424.
28. C.S. Smith, "Grains, Phases, and Interfaces: An Interpretation of Microstructure", Trans. AIME, vol. 185, 1949, p. 762.

29. A.A. Gokhale, "Solidification Cracking, A Review", Trans. Indian Inst. Met., vol. 39, no.2, 1986, pp. 153-163.

30. J.H. Rogerson and J.C. Borland, "Effect of the Shapes of Intergranular Liquid on the Hot Cracking of Welds and Castings",. Trans. AIME, vol. 227, 1963, p.2.

31. K. Wilken and H. Kleislner, "The Classification and Evaluation of Hot Crack Test for Weldments", Welding in the World, vol. 28, no. 7/8, 1990, pp. 37-48.

32. E.A. Lange and R.W. Heine, "A Test for Hot Tearing Tendency", Trans. AFS, vol. 65, 1957, pp. 247-258.

33. C.G. Lees, "The Hot-Tearing Tendencies of Aluminum Casting Alloys", J. Inst. Metals, vol. 72, 1946, p.343.

34. S.A. Metz and M.C. Flemings, "A Fundamental Study of Hot Tearing", Trans. AFS, vol. 78, 1970, p. 453.

35. J. Zhao and G. Chen, "Study of Influence of the Solidification Characteristics of Al-Si Casting Alloys on the Hot Tearing", J. Dalian Inst. Tech., vol. 24, no. 4. 1985, pp. 31-36.

36. W.I. Pumphrey and J.V. Lyons, "Cracking During the Casting and Welding of the More Common Binary Aluminum Alloys", J. Inst. Metals, vol. 74, 1948, p. 439.

37. T.W. Clyne, M. Wolf, and W. Kurz, "The Effect of Melt Composition on Solidification Cracking of Steel, with Particular Reference to Continuous Casting". Met. Trans., vol. 13B, 1982, p. 259.

38. H. Nishimura, Nippon Kinzoku Gakkai-Si, vol. 1, 1937, p. 8.

39. E.F. Chirkov, "Relationships of Change in Hot Shortness of Aluminum Alloys in the Al-Cu-Mg System", Russ. Metall., vol. 3, 1983, p. 157.

40. T.A. Engh, Principles of Metal Refining, Oxford University Press, London, 1992.

41. F. Matsuda, K. Nakata, and Y. Shimokusu, "Effect of Additional Element on Weld Solidification Crack Susceptibility of Al-Zn-Mg", J. Japanese Welding Research Inst., vol. 12, no. 1, 1983, p. 81.

42. D. Warrington and D.G. McCartney, "Hot-Cracking in Aluminum Alloys 7050 and 7010, A Comparative Study", Cast Metals, vol. 3, no. 3, 1991, p. 202.

43. H.F. Bishop, C.G. Ackerlind, and W.S. Pellini, "Investigation of Metallurgical and Mechanical Effects in Development of Hot Tearing", Trans. AFS, vol. 65, 1957, p. 247.

44. J.M. Middleton and H.T. Protheroe, "The Hot Tearing of Steel", J. Iron Steel Inst., vol. 168, 1951, p.384.

45. J. Van Eghem and A. de Sy, Mod. Cast., vol. 48, 1965, p. 100.

46. T.W. Clyne and G.J. Davies, "The Influence of Composition on Solidification Cracking Susceptibility in Binary Alloy Systems", The British Foundryman, vol. 74, 1981, pp. 65-73.

47. Q.Z. Diao and H.L. Tsai, "Modeling of Solute Redistribution in the Mushy Zone during Solidification of Aluminum-Copper Alloys", Met. Trans., vol. 24A, 1993, pp. 963-972.

48. J.R. Cahoon, "A Re-Evaluation of Inverse Segregation in the Al-Cu System", Mater. Sci. Eng., vol. 188, 1994, pp. 211-217.

49. P. Pousset, M. Rappaz, and B. Hannart, "Modeling of Inverse Segregation and Porosity Formation in Directionally Solidified Aluminum Alloys", Met. Mater. Trans., vol. 26A, 1995, pp. 2349-2358.

50. D.C.G. Lees, "Note on the Effect of Dissolved Gas on the Hot-Tearing of Aluminum Casting Alloys", J. Inst. Metals, vol. 73, 1947, p. 537.

51. E. Scheuer, S.J. Williams, and J. Wood, "Foundry Properties of Aluminum Alloys", Metal Ind., vol. 85, 1954, p. 63.

52. P. Sun and H. Yang, "A Research on the Testing Methods of Hot-Crack Tendencies of Alloys", Casting Technology (China), vol, 4. 1987, p. 23.

53. J.A. Spittle and A.A. Cushway, Metals Technology, vol. 10, no. 6, 1983. p. 895.

54. J. Campbell, "Dihedral Angle and the Equilibrium Morphology of Grain Boundary Phases", Metallography, vol. 4, 1971, pp. 269-78.

55. A. Couture and J.O. Edwards, "The Hot-Tearing of Copper-Base Casting Alloy", Trans. AFS, vol. 74, 1966, pp. 709-721.

56. S. Oya, U. Honma, T. Fujii, and M. Othaki, "Evaluation of Hot Tearing in Binary Al-Si Alloy Castings", Aluminium, vol. 60, no. 20, 1984, p. 777.

57. D. Warrington and D.G. McCartney, "Development of a New Hot-Cracking Test for Aluminum Alloys", Cast Metals, vol. 2, 1989, p. 134.

58. Y.F. Guven and J.D. Hunt, "Hot Tearing", Solidification Processing 1987, Sheffield, UK, 21-24 Sept. 1987, pp. 392-394.

59. Y.F. Guven and J.D. Hunt, "Hot Tearing in Aluminum Copper Alloys", Cast Metals, vol. 1, no. 2, 1988, p. 104.

60. H. Chadwick, "Hot Shortness in Al 4.5% Cu Alloys", Casting Metal, vol. 4, no. 1, 1991, pp. 43-49.

61. W. Patterson and S. Engler, "The Hot Shortness Tendency and Mechanical Properties of Aluminum Casting Alloys", Aluminium, vol. 35, 1959, p.124.

62. Z. Buray and E. Buray-Mihalyi, "The Effect of Small Additions on the Hot Shortness of AlZnMg Alloys of Moderate Strength", Translated from ZIS-Mitterlungen, vol. 3, 1974, pp. 259-268, Information Company of America, 2204 Walnut St., Philadelphia, PA 19103, pp. 1-15.

63. R.A. Dodd, "Hot Tearing of Castings: A Review of the Literature", Foundry Trade Journal, vol. 101, 1956. p. 321.

64. J.B. Caine, Design of Ferrous Castings, American Foundrymen's Society Inc., 1976, p. 20.

65. C.A. Aliravci, "Investigation of Quantitative Methods to Measure the Hot Tearing Tendency in Wrought Aluminum Alloys", Alcan Chair Research Report I, Université du Québec à Chicoutimi, 1995.

66. J. van Deghem and A. De Sy, "A Contribution to Understanding the Mechanism of Hot Tearing of Cast Steel", Trans. AFS, vol. 73, 1965, p. 282.

67. W. Lin, J.C. Lippold, and W.A. Baeslack, "An Evaluation of Heat-Affected Zone Liquidation Cracking Susceptibility, Part I: Development of a Method for Quantification", Welding Journal, vol. 72, no. 4, 1993, p. 135.

68. J.C. Hamaker and Wm.P. Wood, "Influence of Phosphorus on Hot Tearing Resistance of Plain and Alloy Gray Iron", Trans. AFS, vol. 60, 1952, p. 501.

69. H. Taumura, N. Kato, S. Ochiai, and Y. Katagiri, "Cracking Study of Aluminum Alloys by the Variable Tensile Strain Hot Cracking Test", Trans. Jpn. Welding Society, vol. 8, no. 2, 1977, pp. 63-69.

70. T.M. Pollock, D.R. Mumm, K. Muraleedharan, and P.L. Martin, "In-Situ Observations of Crack Initiation and Growth at Notches in Cast Ti-48Al-2Cr-2Nb", Scripta Materialia, vol. 35, No. 11, 1996, pp. 1311-1316.

71. A.L. Purvis, E. Kannatey-Asibu, and R.D. Pehlke, "Evaluation of Acoustic Emission from Sand Cast Aluminum Alloy 319 during Solidification and Formation of Casting Defects", Trans. AFS, vol. 98, 1990, pp. 1-7.

72. A.L. Purvis, E. Kannatey-Asibu, Jr., and R.D. Pehpke, "Modeling Thermal Stresses During Solidification", Modeling of Casting, Welding and Advanced Solidification Processes VI, eds. T.S. Piwonka, V. Voller, and L. Katgerman, TMS, 1993, pp. 601-608.

73. G.M. Goodwin, "Hot Cracking: Measurement, Mechanisms and Modeling", Welding Journal, vol. 69, 1990, pp. 26-31.

74. U. Chandra, "Computer Prediction of Hot Tears, Hot Cracks, Residual Stresses and Distortions in Precision Castings: Basic Concepts and Approach", Light Metals, AIME, 1995, pp. 1107-1117.

75. J. Moriceau, "Thermal Stress in Continuos DC Casting of Al Alloys Discussion of Hot Tearing Mechanisms", Light Metal, AIME, 1975, p. 119.

76. B. Hannart, F. Cialti, and R. Van Schalkwijk, "Thermal Stresses in DC Casting of Aluminum Slabs: Application of a Finite Element Model", Light Metals, AIME, 1994, pp. 879-887.

77. J. Cambell, Castings, Butterworth-Heineman Ltd., Oxford, UK, 1991, pp. 209-232.

78. U. Feurer, "Mathematisches Modell der Warmrißneigung von binären Aluminiumlegierungen", Giesserei Forschung, vol. 28, 1976, p. 75.

79. "Solidification Characteristics of Aluminium Alloys, Volume 1: Wrought Alloys", SKANALUMINIUM, Oslo, November 1986.

80. M.C. Flemings, Solidification Processing, McGraw Hill Book Company, New York, 1974.

81. ASM Handbook Volume 2, Properties and Selection Nonferrous Alloys and Special Purpose Materials, ASM, The Materials Information Society, 1990.